INVESTIGATION OF THE STRUCTURAL RESPONSE OF MASONRY SYSTEMS USING TRADITIONAL AND DATA-DRIVEN NUMERICAL TECHNIQUES

by

Siphesihle Mpho Motsa

In fulfilment of a Doctor of Philosophy in Civil Engineering

College of Agriculture, Engineering and Science, University of KwaZulu-Natal

School of Engineering

Civil Engineering

University of KwaZulu-Natal

Durban

December 2022

Supervisor:

Prof. Georgios A. Drosopoulos

PREFACE

The research contained in this thesis was completed by the candidate while based in the Department of Civil Engineering, School of the College of Agriculture, Engineering and Science, University of KwaZulu-Natal, Howard Campus, Durban, South Africa.

The contents of this work have not been submitted in any form to another university and, except where the work of others is acknowledged in the text, the results reported are due to investigations by the candidate.

Signed: ……...

Prof. Georgios A. Drosopoulos

Date:

DECLARATION 1: PLAGIARISM

Supervisor:

As the candidate's supervisor, I agree to the submission of this dissertation.

Signed: ……..…... **Prof. Georgios A. Drosopoulos** Date: ……

Candidate:

I, **Siphesihle Mpho Motsa ,** declare that

1. The research reported in this dissertation, except where otherwise indicated, is my original research.

2. This dissertation has not been submitted for any degree or examination at any other university.

3. This dissertation does not contain other persons' data, pictures, graphs or other information, unless specifically acknowledged as being sourced from other persons.

4. This dissertation does not contain other persons' writing, unless specifically acknowledged as being sourced from other researchers. Where other written sources have been quoted, then:

a. Their words have been re-written, but the general information attributed to them has been referenced.

b. Where their exact words have been used, then their writing has been placed in italics and inside quotation marks and referenced.

5. This dissertation does not contain text, graphics or tables copied and pasted from the Internet, unless specifically acknowledged, and the source being detailed in the thesis and in the References sections.

Signed:

…… ……..……

Siphesihle Mpho Motsa Date

DECLARATION 2: PUBLICATIONS

The submission of the Doctor of Philosophy in Engineering Degree is by a compendium of several peer reviewed scientific papers, published in journals accredited by the South African Department of Higher Education and Training (DHET). The research articles provided herein, constitute original work of the candidate, resulting from the structural investigation of masonry systems using traditional and Data-driven numerical techniques. Authorship contribution statements of the research articles presented in this study are presented in the Appendix section of this thesis. The list of publications are as follows:

Publications:

1. **Motsa, S.M.**, Stavroulakis, G., Drosopoulos, G. Structural response of circular masonry arches as predicted by machine learning. (Article has been submitted for publication and is currently under review).

2. Charalambidi, B., Koutsianitis, P., **Motsa, S.M.**, Tairidis, G., Kasampali, A., Drosopoulos, G., Stavroulaki, M. and Stavroulakis, G., (2022). Modelling, identification and structural damage investigation of the Neoria monument in Chania. *Developments in the Built Environment, 10*, p.100069. (https://doi.org/10.1016/j.dibe.2022.100069)

3. Tapkın, S., Tercan, E., **Motsa, S.M.**, Drosopoulos, G., Stavroulaki, M., Maravelakis, E. and Stavroulakis, G., (2022). Structural Investigation of Masonry Arch Bridges Using Various Nonlinear Finite-Element Models. *Journal of Bridge Engineering, 27(7),* p.04022053. (https://doi.org/10.1061/(ASCE)BE.1943-5592.0001870)

Conferences:

1. Charalambidi, B., Koutsianitis, P., Motsa, S.M., Drosopoulos, G., Koutsianitis, P., Kasampali, A., Stavroulaki, M. and Stavroulakis,G. (2021). Structural Damage Investigation of the Neoria Monument in Chania. *Transdisciplinary Multispectral Modeling and Cooperation for the Preservation of Cultural Heritage: Second International Conference, TMM_CH 2021, Athens, Greece, December 13–15, 2021.* (https://www.tmm-ch.com/tmm_ch2021)

2. Motsa, S.M., Drosopoulos, G., Charalambidi, B., Koutsianitis, P., Kasampali, A., Stavroulaki, M. and Stavroulakis, G., (2021). Discrete and XFEM Analysis for Crack Interpretation of the Neoria Monument in Chania. *Transdisciplinary Multispectral Modeling and Cooperation for the Preservation of Cultural Heritage: Second International Conference, TMM_CH 2021, Athens, Greece, December 13–15, 2021.* (https://www.tmm-ch.com/tmm_ch2021)

Signed:

……

Siphesihle Mpho Motsa

Page intentionally left blank

ACKNOWLEDGEMENTS

Firstly, all praise and thanks to the **Almighty** for providing me with the capacity and resources to conduct this research.

Secondly, I would like to express my sincerest grateful to my parents, family, and friends for their continued support throughout my academic career.

Thirdly, **Prof Georgios A. Drosopoulos** deserve a special vote of thanks for his supervision, guidance, discussions, and great insight in the field of structural engineering & computational mechanics. He has assisted me in more ways than he should and has gone beyond the role of a supervisor; for this, I am extremely grateful.

I would like to acknowledge **Prof Serkan Tapkin, Prof Emre Tercan** and the **General Directorate of Highways of Turkey** for providing access to the data and reports for the Dağarcık Bridge which is investigated as part of this thesis.

Special acknowledgements to **Prof Georgios E. Stavroulakis**, Technical University of Crete (TUC), and his team for providing experimental data and reports for the study of the Neoria monument in Chania which is presented as part of this thesis. A special vote of thanks for his guidance, discussions, and access to the software packages (Abaqus and MATLAB) used in the preparation of thesis.

Lastly, a special acknowledgement to the **Erasmus+ Program** within the framework of action "**International Credit Mobility**" for funding my 3-months Erasmus stay in Chania, Greece. This was facilitated through a mutual agreement between the Technical University of Crete, School of Production Engineering and Management and the University of KwaZulu-Natal, department of Civil Engineering under the Structural Engineering & Computational Mechanics (SECM) Group. Special thanks to **Prof Georgios E. Stavroulakis** for providing office space, computer facilities/equipment and collaboration-discussions during my 3-months stay in Chania.

"It takes a village to raise a child."

- African Proverb

ABSTRACT

The understanding of the structural behaviour of masonry structures is of great importance for the preservation of their structural integrity and restoration. Masonry arches are among the oldest structural systems in the world. The failure of these structures can lead to loss of the architectural inheritance and therefore, a full understanding of their structural behaviour is of paramount importance.

Over the years, several approaches have been developed for the investigation of failure of masonry structures. Emphasis is given in the heterogeneous nature of masonry (masonry blocks and mortar joints), which imposes a difficulty in simulating the response of this structural type. Continuum damage and discrete models can be adopted to simulate damage in masonry structures. Finite element analysis is one of the numerical tools, which are widely used for this task.

In this thesis, a methodology is proposed for the structural evaluation of masonry systems, such as buildings and arches, using nonlinear finite element analysis. Traditional constitutive descriptions, including non-smooth contact mechanics, as well as damage mechanics, are adopted for the investigation of the ultimate, failure response of masonry structures. Within this framework, the existing interfaces between masonry blocks, standing for potential damage surfaces, are simulated using unilateral contact and friction. To capture the compressive damage mode on the blocks, damage plasticity laws are introduced. Compressive and tensile damage plasticity laws can also be used to simulate the failure response of complex masonry systems.

A new approach is also provided in the thesis, relying on data-driven structural engineering using machine learning principles. According to this approach, artificial neural networks are adopted to replace time-consuming numerical simulations, providing a fast and computationally efficient evaluation of the failure response for masonry arches. Datasets are built for this purpose, using finite element analysis simulations. For the implementation of the parametric simulations, which are needed for the development of the datasets, programming codes in Python and Matlab are developed, in collaboration with commercial finite element models. The proposed concept can be adopted to predict the mechanical response, failure load and collapse mechanism of masonry arches and thus, it can be used for the structural health monitoring of these structures.

To provide a holistic investigation of the structural response, the thesis focuses on the evaluation of both the static structural and the dynamic response of masonry buildings. Case studies in real structural systems are included, highlighting the applicability and efficiency of the proposed methodologies. In particular, the structural response of a three-span masonry arch bridge in Turkey, as well as the response of a seven-span shipyard building in Greece, has been investigated.

Among the outcomes of this thesis, is the evaluation of the collapse mechanisms of multi-span masonry arches, as these compare to the collapse mechanisms of single-span arches. It is proved that a four-hinge failure mechanism arises when a vertical load is applied at the middle arch of a three-span masonry arch bridge, which is a typical response observed on single span masonry arches. It is also noted that a hinge-mechanism is the critical failure pattern for discrete models of multi-span masonry arches, under in-plane and out-of-plane loads.

For the structural assessment of masonry buildings, it is proved in this thesis that finite element analysis can be used to explain real and possibly undocumented structural damages experienced by the buildings, due to static and/or dynamic actions.

An effort is also made in the thesis, to propose an innovative data-driven methodology, aiming to capture the structural response and collapse mechanism of masonry arches. Thus, it is shown how machine learning can be integrated within structural analysis and used to solve the complex problem of the structural evaluation of circular masonry arches. The computational cost of this methodology is significantly reduced, comparing to conventional finite element simulations. The extension of this concept can be adopted for the structural health monitoring of masonry structures.

Table of Contents

List of Figures

Chapter 2

Chapter 3

Chapter 6

List of Tables

Chapter 2

Chapter 6

Chapter 1 – Introduction

1.1 Background

Masonry as a building material is among the oldest and widely used materials. Structures made of masonry are among the most traditional structural forms extensively used across the world, which is attributed to their affordability and availability. The use of masonry as a building material can be considered as the beginning of civil engineering (Phonphuak and Chindaprasirt, 2015). This method of construction dates back to the 7000 BCE, where masonry was in the form of sun-dried mud blocks (Murmu and Patel, 2018). This was influenced by the prevailing geological formations and conditions of surrounding areas, since natural stones were mostly used. Other factors include the durability, easy to handle, aesthetic appear and affordability.

Some of the monumental structures which are an architectural marvel are made up of masonry: the Great Wall of China, the Colosseum in Rome, the pyramids in Egypt, Chichén Itzá in Mexico, Petra in Jordan, the Taj Mahal in India, the Machu Picchu in Peru, The Pont Du Gard in France and the Mnajdra Prehistoric Temples in Malta.

Over the years, the technique of using masonry as a construction material advanced and the people's craftsmen skills improved. This led to the desire to construct structures that can enclose and/or span over areas. This method of construction constitutes a particular structural type, known as masonry arch bridge or masonry vault. The technique of building arches was first seen in the 2nd millennium BC in Mesopotamian brick architecture (Anastasio, 2020). The first arch structure was discovered by archaeologists in ruins of Babylonia and estimated it was constructed about the year 1400 B.C (Brick Industry Association, 2007).

Mansory structures have a peculiar structural behaviour due to their no-tension characteristics. Their strength lies on the geometric form of the structure, which is properly built to ensure it is mainly in compression when subjected to loads. The contact conditions between adjacent stones/blocks allow for the potential development of normal and/or tangential displacements between them, introducing a nonlinear response. Therefore, a thorough understanding of the structural behaviour of masonry structures is of crucial importance, for their restoration and preservation.

Most of the ancient masonry structures have sustained some form of damage over the decades while in service. Some of the common structural problems that they may experience, which can

lead to failure and/or collapse, are (a) deterioration of the masonry material due to thermal effects, moisture, or chemical actions; (b) damage of the arch barrel due to ring-separation, arch barrel distortion, and cracking, which is a result of longitudinal shear or tensile failure (Ford et al., 2003, Melbourne, 1991); (c) failure of the foundation, which is mainly caused by settlement of supports (Ashurst, 1992); and (d) vehicle collision, which can interact with abutments, arch barrels, or piers(Melbourne et al., 2006, Wilmers, 2012). It must be noted that some of these defects take place simultaneously. Other factors which can compromise the structural integrity of masonry structures include aging, different and/or amplified loads due to seismic activity, and increased vehicle axle loads.

A methodology is proposed in this thesis, investigating different numerical methods and techniques, adopted to overcome the challenges involved in the structural evaluations of existing masonry systems (buildings and arches). Some aspects of the proposed methodology are highlighted here: (a) analytical study of the geometry using laser scanning and MATLAB scripts, (b) destructive and non-destructive tests, and information from literature review used to provide material properties, (c) nonlinear finite element analysis and machine learning tools, including artificial neural networks, developed to assess the structural response of masonry systems, emphasizing in failure.

Case studies on various masonry systems are then investigated. These include a three-span masonry arch bridge in Turkey (Tapkın et al., 2022), a seven-span shipyard building in Greece (Charalambidi et al.), and a single span masonry arch structure. These structures were designed for different functionally, thus, they are subjected to different loading conditions. Therefore, the related study enhances the depth and understanding of the structural behaviour of various masonry systems with different geometries and load types.

1.2 Motivation for the Research

Masonry structures are part of our architectural inheritance, and their preservation is of paramount importance. They can be found in various sizes and configurations, depicting significantly varying aesthetic details. In Africa and Asia, most of the ancient masonry structures were made up of stone or earth material. In America, ceramics were mostly used as masonry (Maldonado et al., 2019). Quite often, masonry structures are integrated in modern infrastructure, for instance, the railway masonry arch bridges in UK.

The mechanical properties of masonry stones/blocks are uncertain which is attributed to the following reasons: (a) local irregularities of the geometry which is not always visible, including internal imperfections of the masonry, (b) deterioration of material changing the behaviour of the masonry structure from monolithic to discrete, (c) undocumented damage and repairs on structure, and (d) local variation of material strength and stiffness due to chemical deterioration.

The process of restoring the structural integrity of old masonry structures requires a good understanding of the structural behaviour of the system. In particular, this process includes, (a) visual assessment of the structure; (b) material testing for the constituent materials; (c) understanding of the original design and the structural capabilities by developing numerical models; and (d) implementing the actual restoration of the different elements of the structure after the previous steps have been considered.

In early years, most of the structural investigations of masonry systems were based on static stability and geometric proportions and were mostly limited to two- dimensional geometries (e.g. arches or walls). During this time, relevant studies were used for design and construction. Over the years, there has been a shift in focus, where the study of masonry structures mainly emphasizes in the preservation and structural restoration. This is not a trivial task due to the potential deterioration of the material properties over the years, as well as due to the fact that the structure might have experienced different loads due to earthquakes, settlement of supports and others, which may have caused significant damage and/or collapse.

In this thesis, a detailed study of masonry structures is undertaken using a range of numerical modelling techniques. Within nonlinear finite element analysis, several parameters related to the structural response of masonry buildings and arches are investigated, including the out-of-plane and in-plane behaviour, as well as the elastic and plastic (damage) response of masonry. The adopted modelling approaches are used to investigate the ultimate response under static and dynamic loads. Restoration of the systems under investigation can then be implemented, to ensure that the structural integrity is preserved.

1.3 Research Aims and Objectives

The aim of this study is to propose a methodology for a holistic investigation of the structural behaviour of masonry systems. To successfully achieve this aim, the following objectives are formulated:

- Developing detailed numerical models in the framework of finite element analysis (FEA) that can simulate realistically the structural response of masonry buildings and arches.
- Implementing proper constitutive descriptions, aiming to capture failure of the investigated structures.
- Developing a methodology that uses artificial intelligence and machine learning to predict the structural behaviour of masonry arches.

1.4 Technical and Scientific Contributions

The work presented in Chapters 4 and 5 includes a detailed description of different techniques of numerical modelling of masonry structures, in the framework of finite element analysis. First, an analytical study is conducted to provide the geometry of the structures using laser scanning. From the laser scanner, a point cloud describing the geometry is obtained and transformed to a solid 3-D geometry suitable for finite element modelling. In Chapter 4, discrete and continuum modelling approaches, including unilateral contract and friction laws as well as damage mechanics constitutive descriptions, are adopted to investigate the following aspects of the structural response of masonry arch bridges, (a) the opening/sliding between the stones, (b) compressive and tensile failure, (c) quasi-brittle material failure, and (d) the beneficial influence of the backfill over the arch.

In Chapter 5, static and dynamic finite element analysis models are proposed to, (a) identify the material properties and the damage patterns of a masonry building, and (b) explain the existing damage developed in the building. It should be noted that due to the large size of the building, age and damage, the material properties vary across the structure.

Among the most important contributions emerging from this research, is the introduction of machine learning elements, implementing data-driven structural engineering and used to predict the structural behaviour of masonry arches. This concept is presented in Chapter 6 of the thesis. Within machine learning, artificial neural networks used to predict the structural response of masonry arches, are trained by using datasets, generated from a parametric analysis of nonlinear finite element models.

Within the thesis, different numerical modelling techniques are adopted, focusing on the structural investigation of masonry buildings and arches with different geometries and loading types. This

provides an insight to the non-trivial structural behaviour of masonry structures which is attributed to the heterogeneous nature of the material and the contact conditions between the masonry stones.

- predict the structural behaviour of masonry arches.

1.5 Research Scope and Limitations

The scope of this study is limited to the structural behaviour of masonry structures such as buildings and arches, with emphasis on the heterogeneous nature of masonry. In this study, non-linear finite element models are used to gain a sight on the structural behaviour of masonry systems with real structural systems used as case studies to highlight the efficiency and applicability of the proposed methods. Also, an innovative data-driven methodology is proposed to capture the structural response and collapse mechanism of masonry arches. The complex structural problem is solved by using non-linear finite element models to perform a parametric study to create a dataset to be used for the machine learning.

The scope of this study is limited by the following reasons: funding and computational costs. Funding limited the number of case studies that can be considered for this study since collecting comprehensive experimental data requires a lot of expensive machinery and resources. Computational cost and computer resources limited the number of finite elements models and the complexity of the models as the more complex the models are, the more computational resources are required.

1.6 Structure of the Thesis

This thesis is organised into seven chapters, two of which are published papers derived from this investigation and presented in their original form. One (special issue article pending) chapter includes an article submitted to an international journal. An overall introduction is given in the present chapter and a summary of the findings and overall conclusions are provided in the last chapter. In particular, the content of each chapter of the thesis is provided below:

Chapter 1 provides an overall introduction and motivation of this study. The structure of the thesis is presented.

Chapter 2 provides a literature overview related to the structural response of masonry arches and buildings. The importance of masonry structures in the society is also highlighted.

Chapter 3 presents the methodology adopted on this thesis.

Chapter 4 introduces nonlinear, three-dimensional finite element models which are used to provide the ultimate response and collapse mechanism of multi-span masonry arches (published article 1).

Chapter 5 presents the framework for the structural evaluation of a partially collapsed masonry monument, using static and dynamic analysis within the finite element method. The existing damage on the structure is investigated (published article 2).

Chapter 6 presents an innovative methodology for analysing the structural response of circular masonry arches using machine learning. The proposed scheme aims to provide a tool for the computationally inexpensive and fast assessment of the structure response of masonry arches (article submitted for publication).

Chapter 7 provides a summary of the key findings and conclusions, which are derived from this study. In addition, future work and recommendation of further research are presented.

1.7 References

Anastasio, S. 2020. Building between the two rivers: an introduction to the building archaeology of ancient Mesopotamia. *Building between the Two Rivers***,** 1-220.

Ashurst, D. 1992. An assessment of repair and strengthening techniques for brick and stone masonry arch bridges.

Brick Industry Association, 2007. Technical notes 31: Brick masonry arches.

Charalambidi, B., Koutsianitis, P., Motsa, S. M., Tairidis, G., Kasampali, A., Drosopoulos, G., Stavroulaki, M. & Stavroulakis, G. Developments in the Built Environment.

Chilton, J. C. & Isler, H. 2000. *Heinz Isler: the engineer's contribution to contemporary architecture*, Telford.

Ford, T., Augarde, C. & Tuxford, S. Modelling masonry arch bridges using commercial finite element software. 9th International Conference on Civil and Structural Engineering Computing, Egmond aan Zee, The Netherlands, 2003. 2-4.

Heyman, J. 1982. *The Mansonry Arch,* Chichester, UK: Ellis Horwood.

Maldonado, N. G., Martín, P., del Solar, G. G. & Domizio, M. 2019. Historic Masonry. *Heritage.* IntechOpen.

Melbourne, C. 1991. Conservation of masonry arch bridges. *Brick and Block Masonry,* 3**,** 1563-1570.

Melbourne, C., McKibbins, L., Sawar, N. & Gaillard, C. S. 2006. Masonry arch bridges: condition appraisal and remedial treatment. *CIRIA, London*.

Murmu, A. & Patel, A. (2018). Towards Sustainable Bricks Production : An overview. Journal of Construct and Building Material. 165. 10.1016/j.conbuildmat.2018.01.038.

Phonphuak, N. & Chindaprasirt, P. 2015. Types of waste, properties, and durability of pore-forming waste-based fired masonry bricks. *Eco-efficient masonry bricks and blocks***,** 103-127.

Tapkın, S., Tercan, E., Motsa, S. M., Drosopoulos, G., Stavroulaki, M., Maravelakis, E. & Stavroulakis, G. 2022. Structural Investigation of Masonry Arch Bridges Using Various Nonlinear Finite-Element Models. *Journal of Bridge Engineering,* 27**,** 04022053.

Wilmers, W. Restoration of masonry arch bridges. Proceedings of the Institution of Civil Engineers-Bridge Engineering, 2012. Thomas Telford Ltd, 135-146.

Chapter 2 – Literature review

2.1 Introduction

The aim of this chapter is to provide and insight to the current literature which is related to the structural evaluation of masonry buildings and arches. First, a brief discussion on the general background of masonry as a building material is presented. Following that, a discussion on the structural response of masonry is presented together with information on how the mechanical properties of masonry can be obtained experimentally. Thereafter, a review of unreinforced masonry arches is presented and common techniques for analysing the structural performance of arches are explored. Finally, the background of finite element modelling for masonry structures is presented.

2.2 Description of Masonry

Masonry is a heterogeneous material, since it consists of individual units and joints. These units can be bricks, blocks, ashlars, adobes, irregular stones, and others. The cohesive layer or mortar can be any material with adhesive properties like clay, bitumen, chalk, glue, and lime-/cement-based mortar.

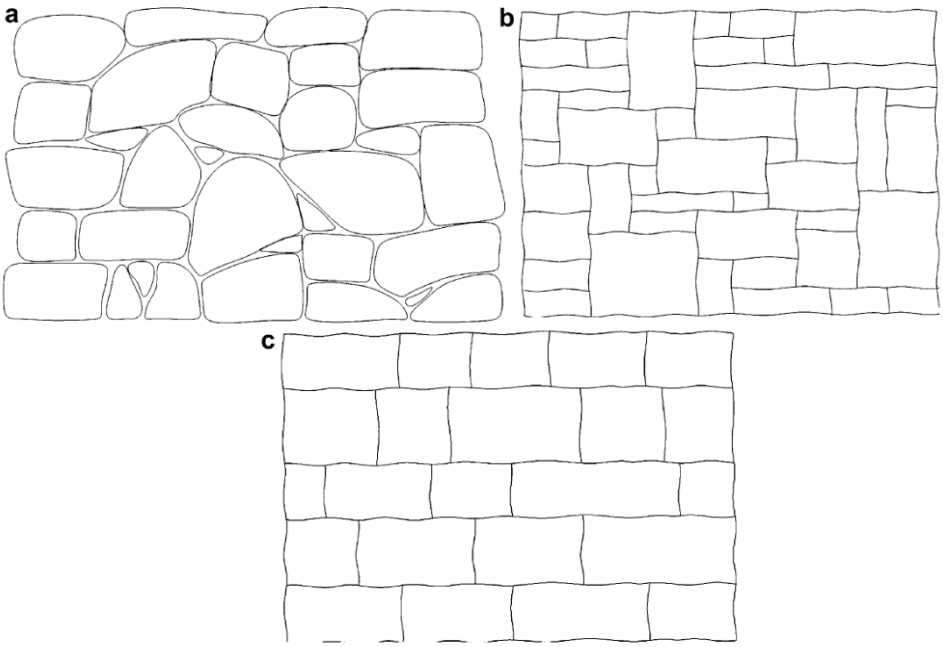

Figure 2- 1: Different types of stone masonry: (a) rubble masonry; (b) ashlar masonry; (c) coursed ashlar masonry (Lourenço, 2014).

Stone was the first known material to be used for the masonry blocks. The use of stone can be in different configurations to achieve various geometries. Figure 2-1 shows some of the possible configurations of using stone as a building material. Over the years, different masonry materials have been developed, due to the developments/improvements of the construction technique, craftsmanship, the local culture and wealth, knowledge of materials, architectural reasons, and lastly the availability of materials.

The construction of ancient masonry structures was very complex. The separation of architectural features and structural elements was not always clear. When the walls of the structures where needed to be very thick, typically two/three layers of different types of stones would be used: the outer layer would be ashlars, the inside layer/layers would be an infill of rubbles and/or irregular small stones. A typical section of a thick masonry wall is shown in Figure 2-2. This kind of complex arrangement of masonry makes it cumbersome to fully analyse the behaviour of these structures/systems.

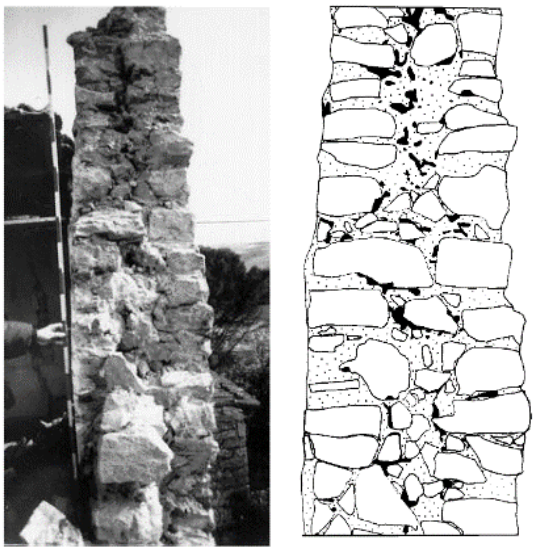

Figure 2- 2: Section of a thick masonry wall: (a) photograph of wall and (b) schematic drawing of the masonry wall (Binda, et al, 1999).

2.3 Material behaviour of masonry

In ancient and modern masonry structures, there is a wide variation of materials, techniques and craftsmanship skills making the task of understanding the structural response and performing structural analysis of such systems complex. With all these variations, masonry as a building material can be classified into two types, based on its structural behaviour, namely, reinforced and unreinforced. In a reinforced masonry building or arch, a type of reinforcement, like for instance fibre reinforced polymer (FRP) strips or steel reinforcement in the form of bars/ties, is provided on the masonry to increase the tensile strength and enhance the structural behaviour. |This usage of reinforcement in the masonry, makes the nonlinear behaviour, which arises due to the interfaces between the discrete masonry blocks/units, less critical.

On the other hand, unreinforced masonry has a very low tensile strength and the nonlinear behaviour due to the discrete masonry blocks/units can be critical. Due to this potential damage along the interfaces of masonry blocks, which may also lead to out-of-plane failure, masonry structures are more vulnerable to seismic loads (Chieffo et al., 2019, Standard, 2005). In Eurocode 6 and in general engineering practise, the tensile strength of masonry is approximated to be one tenth of the compressive strength (Standard, 2005).

2.4 Computational Mechanics for masonry elements

When modelling the complex material behaviour of masonry by introducing either analytical or numerical approaches, three techniques can be adopted, (a) the detailed micro-modelling, (b) the simplified micro-modelling and (c) the macro-modelling.

In the detailed micro-modelling, units and mortar in the joints are represented by continuum elements, whereas the unit-mortar interface is represented by discontinuous elements. Within the simplified micro-modelling approach, expanded units are represented by continuum elements, whereas the behaviour of the mortar joints and unit-mortar interface is lumped in discontinuous elements. These interface elements represent the potential crack location where tensile and shear cracking may occur. In the macro-modelling approach, units, mortar, and unit-mortar interface are lumped into a homogeneous continuum (Lourenço, 2002). Schematically, these models are shown in Figure 2-3 below.

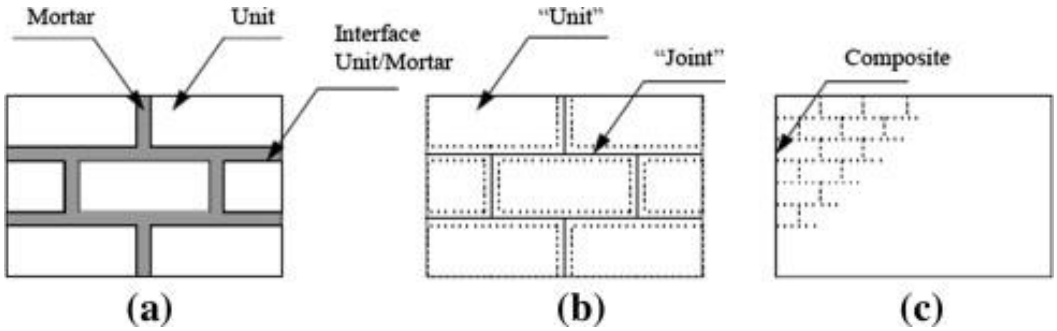

Figure 2- 3:Modeling techniques for masonry structures: (a) detailed micro-modelling; (b) simplified micro-modelling; (c) macro-modelling (Lourenço,2002).

In macro modelling, the overall geometry of the structure is approximated, which allows for more complex loading conditions to be applied, for instance, focusing on the nonlinear seismic response. This approach also allows for the simulation of the nonlinear behaviour of the material, with relatively low computational cost. It is also noted, that for the accurate modelling of masonry, comprehensive experimental data may be needed. The strength of the material is usually tested while deformation characteristics, like the inelastic strain response may or may not be found.

2.5 Experimental data for masonry

When investigating the stress and strain distribution in structures or structural components, one of the critical factors to be considered is the material properties. The mechanical material properties can be obtained from conducting destructive and non- destructive experimental tests.

Destructive testing is the process whereby the material is broken down in order to obtain its mechanical properties like strength, toughness and hardness. This form of testing is not preferable for important and protected monumental structures since it alters and/or destroys the material. However, this form of testing often provides the most critical characteristics of the material. Some of the widely used destructive testing techniques are presented in Table 2-1 below.

Table 2- 1: Commonly used destructive test techniques.

Technique	Capabilities	Limitation
Tensile test	Tensile strength	Test sample is destroyed or damaged in the process of testing.
Compression test	Compressive strength	
Bending test	Flexure strength	
Torsion test	Torsion/Twisting strength	
Hardness test	Deformation/ impact strength	

On the contrary, non-destructive testing is used when the material properties can be determined without destroying and/or altering the material. This form of testing is preferable for monumental structures. Some of the commonly used non-destructive testing techniques are presented in Table 2-2 below. It is noted that the visual inspection is generally the easiest and cheapest non-destructive testing approach, provided the structure is accessible.

Table 2- 2: Commonly used non-destructive test techniques (Vyas and Kazys, 2018).

Technique	Capabilities	Limitation
Visual Inspection	Macroscopic surface flaws	Small flaws are difficult to detect, no subsurface flaws.
Microscopy	Small surface flaws	Not applicable to larger structures, no subsurface flaws.
Radiography	Subsurface flaws	Smallest defect detectable is 2% of the thickness, radiation protection. No subsurface flaws not for porous materials.
Dye penetrant	Surface flaws	No subsurface flaws, not for porous materials.
Ultrasonic	Subsurface flaws	Material must be good conductor of sound.
Magnetic Particle	Surface / near surface and layer flaws	Limited subsurface capability, only for ferromagnetic materials.
Acoustic emission	Can analyse entire structure	Difficult to interpret, and expensive equipment required.

2.6 Masonry to mortar bond

Masonry structures derive their strength from the individual masonry units which have a high compressive strength and low tensile strength. This enables them to perform well under compressive loads and poorly when subjected to tension loads. The interface between the units is

the weakest point of this assembly, due to the low tensile resistance of the mortar joints, leading to potential cracking.

To accurately model the behaviour of the interfaces, their failure modes under different loading conditions need to be fully understood. The two main failure modes are tensile failure and shear failure. These are known as mode I and mode II failure type, respectively (Lourenço, 2021). In Figure 2-4, schematic diagrams of these failure types are shown. A secondary mode of failure may appear when mode I and II failures take place concurrently. This secondary mode is known as mixed mode failure.

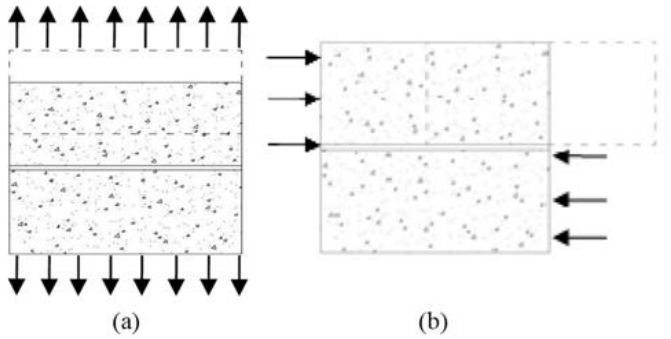

Figure 2- 4: The main failure modes of mortar in masonry structures (a) Tensile failure and (b) shear failure (Thamboo and Dhanasekar, 2016).

The contact conditions of adjacent masonry blocks/stones can be modelled using two modelling techniques, namely, the detailed micro-modelling and the simplified micro-modelling technique. In the detailed micro-modelling approach, the mortar layer and the discrete masonry units are simulated using their real geometry and their distinct properties are explicitly incorporated (Adam et al., 2010, Vyas and Venkatarama Reddy, 2010, Shieh-Beygi and Pietruszczak, 2008, Zucchini and Lourenço, 2007, Brencich and Gambarotta, 2005). In the simplified micro-modelling approach, the mortar layer is modelled by defining a contact mechanics law, between the interfaces of the discrete masonry units (da Porto et al., 2010, Orduña and Lourenço, 2003, Berto et al., 2002, Zhuge et al., 1998, Dhanasekar, 1985).

2.7 Vaults and Arches

Over the years, the construction techniques on masonry systems have been improved in such a way that unique architectural buildings were constructed to match the aesthetic appeal of the environment. A new construction method was developed to enclose and/or span over areas using

masonry. This technique of construction was first observed in Mesopotamian architecture, dating back to the 2nd Millennium BC (Anastasio, 2020). This was the birth of vaults and arches as a method of construction.

Arches and vaults are efficient load-bearing structures. They distribute applied loads through compression along adjacent masonry stones. The arch as a method of construction is directly linked to the material behaviour of the masonry. There exists a harmonic relation between the masonry stones/blocks and the shape of the arch to ensure the structure is mainly under compression. Compression failure of masonry arches is generally unlikely to take place, thus, the typical failure mode of arches is tensile (Grillanda et al., 2021).

2.7.1 Structural theory for arches and vaults

The structural design of ancient masonry arches was based on engineering practice developed at that time, which was mainly focused on three structural criteria: strength, stiffness and stability (Dahmen and Ochsendorfs, 2012, Heyman, 1996). Stability was probably the most critical condition in the design of masonry arches since the compressive strength of unreinforced masonry is often adequate to support the applied loads. On the other hand, vaults and unreinforced arches may not be able to support seismic actions or settlement of supports, since these conditions can lead to instability.

To evaluate the stability of masonry arches, the concept of the thrust line was introduced. In particular, a thrust line is a line passing through the centres of the internal pressure, which is developed at the sections of an arch. It is used to represent the path of the resultant compressive forces (Méry, 1840, Moseley, 1856).

The stability of unreinforced masonry arches is achieved when the thrust line is maintained within the cross-section of adjacent masonry units, which ensures that the structure is under compression. Figure 2-5a shows a typical arch with a thrust line maintained within the cross-section of the masonry units. To ensure stability, the designer needs to properly define the geometry of the structure in such a way that it remains mainly in compression under any loading conditions. In the event, the thrust line falls at the boundary of the section of the masonry, a hinge is formed which can lead to damage and/or partial collapse of the structure (Figure 2-5b). This problem of finding a suitable geometry for masonry arches, was first explained by (Hooke, 1676) using the ‘hanging chain’ principle.

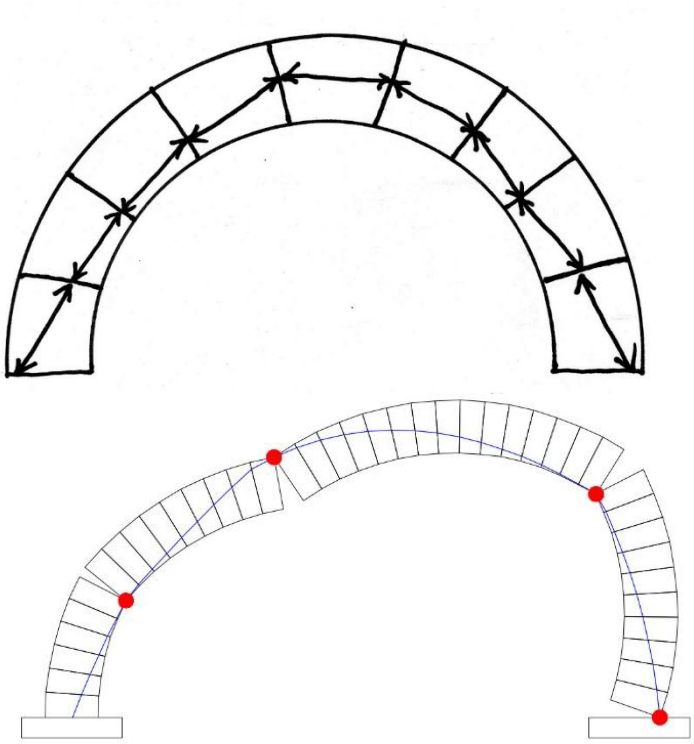

Figure 2- 5: (a) An arch with thrust lines within sections, (b) an arch with thrust lines outside the sections (Pulatsu et al., 2019).

2.7.2 Robert Hooke's 'hanging chain' Principle

Several researchers and engineers have made efforts to understand the structural response of masonry arches. Robert Hooke (Hooke, 1676) has been pioneer for first describing the stability of masonry arches under their self-weight by proposing a rational rule to sizing masonry arches. This rule is based on the analogy of a hanging chain forming catenary in tension under its self-weight. Then, it is concluded that the inverted chain, representing an arch, stands rigid in compression (Heyman, 1982, Heyman, 1998, O'Dwyer, 1999, Block et al., 2006).

In (Hooke, 1676), it was concluded that both the chain and the arch will be in equilibrium, the chain under tension and the arch under compression (Figure 2-6a). This principle led to the concept of the funicular polygon which states that, the shape made by a string or chain under certain loads, if inverted, is the ideal geometry to support the same set of loads. This method has successfully been used to produce the line of thrust along the masonry arch structures.

In 1748, (Poleni) used Hooke's hanging chain principle to assess the safety of the cracked dome of St. Peter's in Rome. Figure 2-6b shows Hooke's hanging chain principle as applied to the

analysis of St. Peter's dome. Recently, this technique was used by (Gáspár et al., 2022), in a study which relates the optimal geometry of a masonry arch and the number of concurrent hinges under self-weight, at a limit state quantified by minimum thickness.

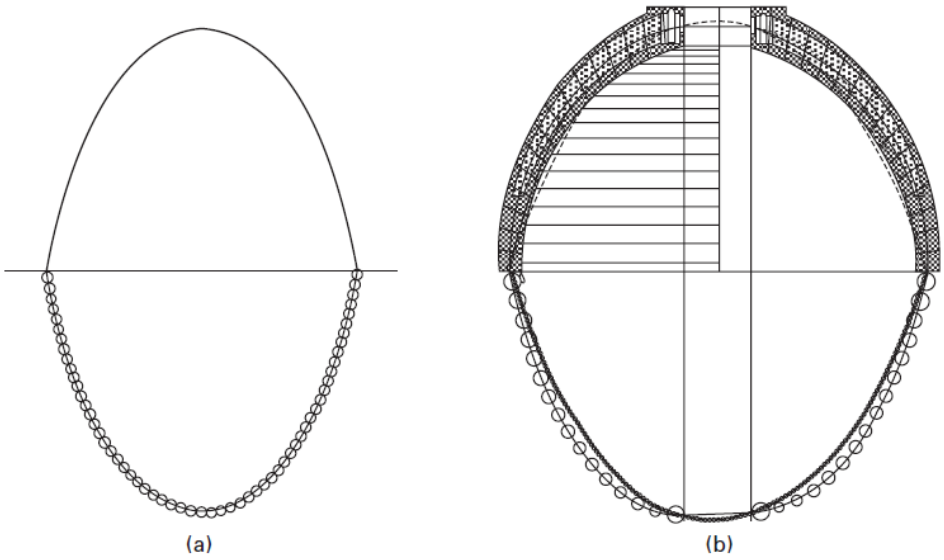

Figure 2- 6: (a) Hooke's hanging chain in tension with the corresponding inverted arch in compression; (b) the safety of the cracked dome of St Peter's in Rome demonstrated by Hooke's principle (Block et al.,2006)

2.7.3 Classical mechanics on unreinforced masonry arches

A few decades later, a new technique of analysing arch structures was presented, known as the *classical collapse mechanism*. This technique uses the funicular polygon as the fundamental tool for analysing arches and is based on the estimation of the thrust line. The classical collapse mechanism theory as presented by (Heyman, 1982), has been widely used for determining the load-bearing capacity of masonry arches. This concept has been used as the building block for other analytical methods aiming to estimate the thrust line in masonry arches. In (Heyman, 1982), it was concluded that, for arches to be fully under compression, the thrust line must lie within the core (middle third) of the section.

Unreinforced masonry arches form a plastic hinge when the thrust line is tangent to the extrados and/or intrados of the ring. The introduction of three hinges changes the determinacy of a fixed support arch from statically indeterminate to statically determinate. The addition of a fourth hinge triggers a kinematic collapse mechanism classically known as the four-hinge collapse mechanism (Heyman, 1967). This four-hinge collapse mechanism is generally the common cause of structural failure on arches.

In the classical studies presented by (Heyman, 1982), the structural behaviour of unreinforced masonry arches under settlement of supports is also explored. It was mentioned in these studies that if the abutments spread for a reason, ‘‘the arch could accommodate itself to the increased span by forming three hinges, one at the crown in the extrados, and one at each abutment in the intrados’’. In the same studies it was also claimed that if the abutments are too close, ‘‘three hinges have again been formed to accommodate the decreased span, one at the crown in the intrados and one at each abutment in the extrados”. In a study conducted by (Drosopoulos et al., 2008), these conclusions were verified using nonlinear finite element models, in single span, two-dimensional arches. In Chapter 4 of the thesis, the possibility for a three-hinge mechanism to appear due to settlement of supports in multi-span arches, using three-dimensional finite element analysis, is investigated.

2.8 The main elements of a masonry arch bridge and their functionality

A masonry arch bridge, like any other structure, consists of different structural elements which contribute to the overall structural integrity and load bearing capacity. The main structural elements of a masonry arch bridge are shown in Figure 2-7.

The main structural element is the arch barrel, which is found in different geometries, such as for instance, semi-circle, semi-ellipse and parabolic. The arch barrel is generally a ring of large stones which transfer the applied loads to the supports, through compression in the masonry sections. The fill material (compacted fill soil) is placed above the arch barrel, to provide a level formation for the road carriageway or railway surface. The fill material distributes the load from the road carriageway or railway surface over a larger area, to reduce the load intensity on the arch barrel. This has a beneficial contribution to the load-carrying capacity of the arch bridge, by reducing the load intensity experienced by the arch barrel. Furthermore, the self-weight of the fill material introduces an overall compressive load to the arch barrel, which further enhances the structural response of the arch.

The spandrel walls are built on the side of the arch barrel and may extend to the wing walls beyond the abutments, to ensure the fill material does not spill out. Damage or collapse of the spandrel walls can lead to the loss of the fill material over the arch barrel rendering the bridge unfit for use. The wing walls and parapets do not have a direct influence on the structural integrity of the arch bridge. The wing walls are mainly used to contain the fill material beyond the abutment wall and to minimise settlement on the road carriageway or railway surface. Parapets are used to protect users from falling into the watercourse-way, road track, railway track or lower ground since most masonry arch bridges are at an elevated height relative to the surrounding area.

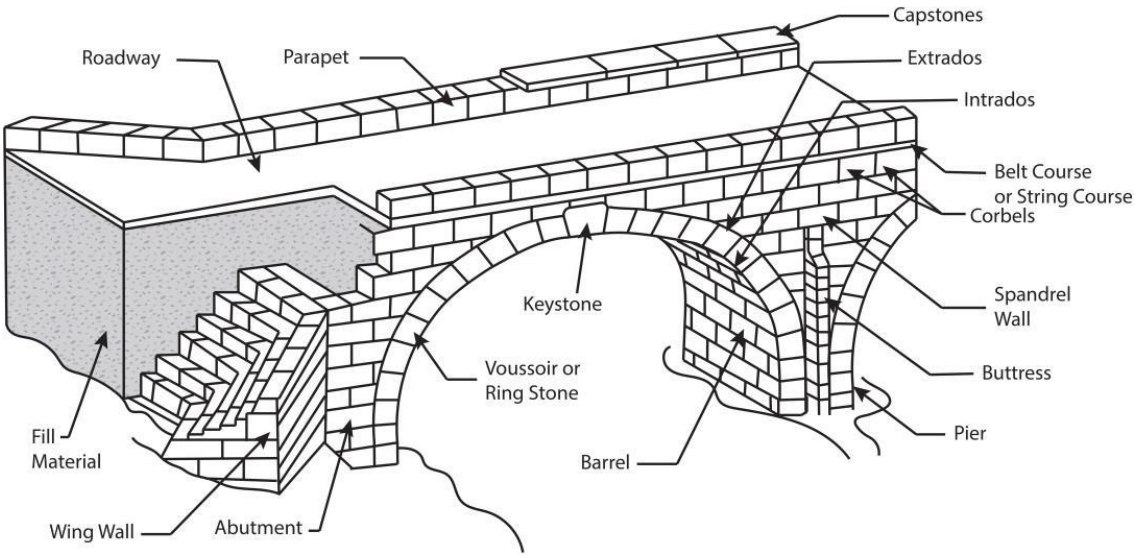

Figure 2- 7: Elements of a masonry arch bridge (Pipinato, 2022).

2.9 Methods used to investigate the structural response of masonry arches

In recent years, several studies have been conducted to evaluate the structural behaviour of masonry arches and improve their ultimate strength. Some of the recognized methods include (a) the military engineering experimental establishment method, (b) the collapse mechanism method, (c) the finite-element method (FEM) and (d) the limit analysis method. Another recent and innovative approach is to adopt machine learning principles in order to evaluate the structural response of masonry arches. In Chapter 6 of the thesis, a methodology is proposed, elaborating this concept.

2.9.1 Military engineering experimental establishment (MEXE) method

The military engineering experimental establishment (MEXE) method is a semi-empirical method based on elastic analysis that only considers the independent strength of the arch barrel (Hughes et al., 1997). This method is derived from Pippard's elastic method (Pippard et al., 1936) with a point load applied at mid span of the arch (Wang et al., 2013). Empirical formulas with modifying factors referring to the geometry and material conditions of the structure are used to calculate the load capacity (Pippard et al., 1936). These modifying factors are obtained from visual inspection of the structure.

Due to its simplicity and quickness, this method has been widely adopted in Europe for the assessment of railway and highway masonry arches (Orbán, 2004). Advancement in research and experience has demonstrated that this method is very conservative and seriously underestimates the load capacity of the structure (Code, 2011). In contrary, (Wang et al., 2013) has shown that in some cases, the MEXE method is non-conservative and the lack of transparency in the method makes it difficult to fully understand the influence of the assumptions made.

2.9.2 Collapse mechanism method

The collapse mechanism method uses simple equilibrium calculations based on the assumption that the collapse of an unreinforced masonry arch takes place due to the formation of a four-hinge mechanism (Hughes et al., 2002, Page, 1993). The research done by (Pippard et al., 1936, Pippard and Baker, 1968), formulates the foundation of this method. In this research, it was developed a tabular procedure of determining the ultimate load of unreinforced voussoir arches. It was assumed that a structural instability would occur when the thrust line is tangent to the intrados and/or extrados at four points of the arch, which will result in the formation of four hinges.

In later years, (Heyman et al., 1980) presented a solution which uses equilibrium equations to determine the ultimate load for unreinforced masonry arches. This was called the 'geometric factor of safety' solution, which is also known as the mechanism approach. In this solution, the following assumptions were made: (a) masonry stones have no tensile strength, (b) the compressive strength of each stone is infinite, (c) sliding between stones cannot occur, and (d) the masonry blocks/stones are rigid. It was also concluded that the ultimate load was obtained when the point load was applied at the quarter span of the arch, with hinges forming at the springings and crown of the masonry arch (Heyman et al., 1980). This four-hinge failure mechanism is shown in Figure 2-8.

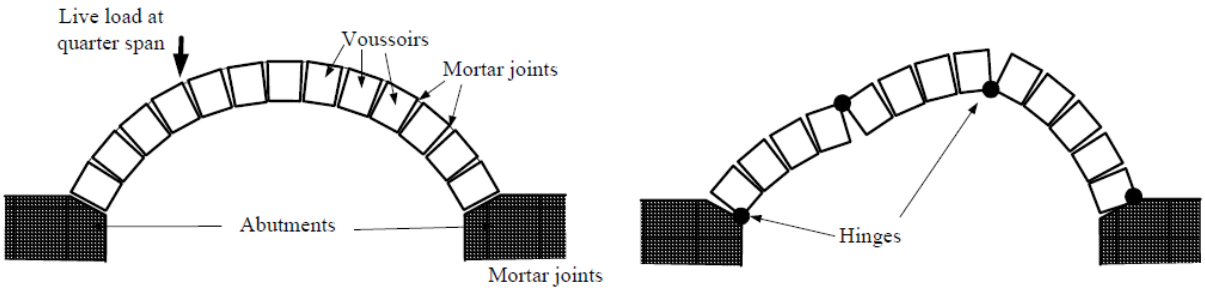

Figure 2- 8: Collapse of a voussoir arch with four-hinge mechanism (Ford et al., 2003).

A few years later, after the development of the mechanism approach, (Crisfield and Packham, 1987) developed a computational technique to obtain the ultimate load of unreinforced masonry arches by solving the equations of equilibrium. In this improvement, the following aspects of the masonry arch were incorporated: (a) the compressive strength of masonry, (b) the dispersion of load through the fill over the arch barrel, and (c) the lateral earth pressure exerted on the arch barrel by the fill.

In (Boothby, 1995), further development to the mechanism analysis was made, by introducing the possibility of sliding failure in arches. In his study, it was concluded that a collapse mechanism is most likely to occur in unreinforced masonry arches with low-rise-to-span ratios and thick arch barrel.

2.9.3 Limit analysis method

Limit analysis method is a modern implementation of the classical collapse mechanism method based on linear programming (Gilbert and Melbourne, 1994, Melbourne and Gilbert, 1995). This method is adopted by the Ring software (LimitState:RING, 2020). In this method, the structure is simulated as a schematic assembly of rigid, no-tesion blocks, introducing also frictional sliding in-between the interfaces of the blocks (Caporale and Luciano, 2012). The blocks are modelled as rigid bodies of infinite compressive strength, such that crushing cannot occur. Instead, hinges can be developed at the interfaces.

In (Foraboschi, 2004, Caporale et al., 2006), it was concluded that in some instances, reinforced masorny arches can experience compressive failure, indicating that crushing of the bricks and/or the mortar joints should also be considered in the analysis. In (Orduña and Lourenço, 2003), a modification of the limit analysis method was proposed, to incorporate compressive failure of unreinforced mansory arches. This novel procedure was also proposed by (Orduña and Lourenço, 2005b, Orduña and Lourenço, 2005a), by adopting a limit for the compressive strenght of the mansory. Frictional sliding and torsion failure modes at the interfaces were also included in these descriptions.

This method has been used in (Moreira et al., 2016), to assess the reliability of five mansory arch railway bridges located in Portugal. These mansory arch bridges were modelled as rigid units separated by contact interfaces along masonry joints, with a rigid-plastic constitutive behaviour. In this study (Moreira et al., 2016), it was conlcuded that the structural response of the mansory arch railway bridges, becomes less predictable with increase in span length. In (Costa et al., 2015),

the limit analysis method was adopted to evaluate the ultimate load-carrying capacity of São Lázaro bridge, which is a mansory arch bridge located in Portugal with two unequal arch spans. The RING software (LimitState:RING, 2020) was utilised to perform the structural assessment of the bridge, considering the action of the dead load and incremental static loading simulating the vehicle load as recommned on the national design standards.

2.9.4 Investigation of the structural response of masonry arches using the finite element method (FEM)

The finite element method (FEM) is a numerical procedure which can be used to solve equations governing a physical system (Oñate, 2009). In particular, the method is used to solve partial differential equations, describing the mechanical response of structural systems. Within the FEM method, a weak formulation is usually adopted, such as the Principle of Virtual Work, converting the systems of differential equations to integral expressions (Drosopoulos and Stavroulakis, 2022).
Finite elements are introduced to discretize the overall geometry, interconnected at discrete points (nodes). The finite element method can be used to predict the structural response of complex structural systems, which would not be solved by traditional analytical approaches.

During the last years, the finite element method is widely used in research focusing on the structural evaluation of masonry buildings and arches. Referring to masonry arches, the finite-element method relies on the development of a computational, structural model that considers the influence of each element of the bridge (arch barrel, spandrel walls, wing walls, fill, and parapets) (Crisfield, 1985b, Towler, 1985).

In the study of the structural behaviour of masonry arches, the finite element method was first used by (Towler and Sawko, 1982) and (Crisfield, 1985b) to compare against experimental models of masonry arch structures. In the early models adopting the finite element method, the effects of the fill material above the arch barrel were not considered and the arch was modelled as a two-dimensional structure.

In later work, (Crisfield, 1985a, Crisfield and Wills, 1986, Crisfield and Packham, 1987) noticed the importance of the fill material for the estimation of the ultimate load, and the fact that arches depicted very low collapse loads when the positive influence of the fill was ignored. As mentioned above in the thesis, the presence of the fill over the arch barrel reduces the load intensity on the

arch, thus, increasing the ultimate load. In the modelling of the fill material above the arch, the Mohr-Coulomb yield criterion, as presented by (Crisfield, 1987), was adopted. To ensure convergence to a solution and stability of the analysis, an incremental-iterative procedure called Newton-Raphson, was used.

In the framework of finite element analysis, different computational strategies have been used to simulate the structural response of masonry buildings and arches, including: (a) the micro-modelling, (b) the macro-modelling, (c) the multi-scale and (d) the continuum approach. In the following lines of this section, a brief literature review, emphasizing in these methods, is provided.

2.9.4.1 Micro-modelling approach

The micro-modelling approach is a comprehensive analysis of masonry structures, which is ideal for small structural elements since it is computationally expensive. In this modelling strategy, the masonry units are modelled as continuum elements and the mortar interfaces are represented by discontinuous elements. This approach was first developed by (Cundall, 1971) to model joint failure in sliding rock masses. For the structural assessment of masonry arch bridges, this approach has been used in (Tapkın et al., 2022, Costa et al., 2015, Thavalingam et al., 2001, Ng et al., 1999).

2.9.4.2 Macro-modelling approach

The macro-modelling approach is a simplified and efficient approach used to evaluate the overall response of masonry structures. In this approach, the individual masonry units and joints are not explicitly simulated. Instead, the collapse mechanism is smeared out in the continuum using damage mechanics models. The material is regarded as anisotropic composite and a relation is established between average masonry strains and stresses. In (Anthoine, 1992, Lourenço, 1996), it is proposed that there are few orthotropic material models which can be used to evaluate the behaviour of masonry structures (Laurenco et al., 1995). In (Zampieri et al., 2015, Pelà et al., 2013, Pelà et al., 2009), the macro-modelling approach has been adopted to investigate the structural behaviour of masonry arch bridges under seismic loading. The same approach has also been used in (Pulatsu et al., 2019,Conde et al., 2017, Fanning and Boothby, 2001).

2.9.4.3 Multi-scale methods

The multi-scale modelling approach is a strategy adopted to model the heterogeneous nature of masonry, where the constitutive behaviour on the macroscopic level is represented by the effective behaviour of a corresponding Representative Volume Element (RVE) (Sorić et al., 2018). In (Ainsworth and Mihai, 2009), an adaptive multi-scale approach for modelling large masonry structures is proposed. This approach combines simplified structural level and detailed micro-scale modelling by reducing the contact constraints without significantly changing the behaviour of the structure. In (Mihai and Ainsworth, 2009), adaptive multi-scale approach was adopted to simulate a three-span arch masonry arch bridge in Cambridge, UK. In (Drosopoulos and Stavroulakis, 2018), a multi-scale computational homogenization approach is used to investigate localization of damage in masonry walls. The Extended Finite Element method (XFEM) is used to capture crack propagation in the macroscopic level.

2.9.4.4 Continuum models

Continuum models, such as for instance damage mechanics laws, are used to simulate the material behaviour in finite element models, focusing on tensile and compressive damage, as well as irreversible (plastic) strains (Toti et al., 2013). When adopting continuum models, diagonal tension cracking on the masonry units and masonry crushing, can be observed. Different continuum models can be used to capture failure for masonry structures, including: (a) Mohr-Coulomb plasticity law (b) Drucker- Prager law, and (c) Concrete smeared crack model.

The Mohr-Coulomb law describes the shear and normal stress response and is commonly used for materials depicting greater compressive strength than tensile strength, like for instance the fill material (soil). This model uses the conservation of energy principle to describe the linear relationship between shear and normal stresses (or minimum and maximum principal stresses) at failure (Labuz & Zang, 2012).

The Drucker-Prager law describes the pressure-dependent failure mode, when a material has failed or experienced plastic yielding (Campbell & Durán, 2017). This model is commonly used to describe the mechanical failure of rock, soil, concrete, and other pressure dependent materials (Jiang et al., 2011). It is comprehensive in describing the isotropic hardening or softening of a material and uses linear, exponential or hyperbolic functions to describe yield surfaces.

The concrete smeared crack model describes the nonlinear behaviour of cement-based materials subjected to different loading paths. This model simulates the crack initiation and propagation by using a multidirectional fixed smeared crack approach (Edalat Behbahani et al., 2015). The inelastic behaviour of the material is incorporated by combining plasticity and damage theories using a yield function.

2.9.5 Machine learning methods

Machine learning is a branch of artificial intelligence which uses datasets and algorithms to make predictions of the response of systems. In the past, machine learning was not commonly used in structural engineering due to limitations on machine learning algorithms and computing power (Reich, 1997). Over the years, there has been development and improvement of the machine learning algorithms and computational power. These improvements have resulted in the significant increase of using machine learning tools, to solve complex structural engineering problems (Thai, 2022).

In (Jing et al., 2022), an artificial neural network called *BridgeNet* is proposed for automating the segmentation of masonry arch bridge elements from a large-scale masonry point cloud. In (Melchiorre et al., 2021), machine learning algorithms are used to structurally optimize the cross-section of a circular arch by calculating the internal stresses and comparing them against the yield stresses of the material. In (Civera et al., 2022), artificial intelligence and machine learning algorithms are used for structural health monitoring, to interpret operational modal analysis mode shapes, which is normally a labour-intensive task. The vibrational modes predicted by the machine learning algorithms were compared against experimental cases.

In Chapter 6 of this thesis, a data-driven machine learning approach, for the structural evaluation of masonry arches is proposed. It must be noted, that during the time of writing this thesis, no relevant work was found.

2.10 Investigation of the structural response building using the finite-element method (FEM)

The finite-element method has been widely used to evaluate the structural response of masonry buildings, due to its flexibility in modelling structural elements. In (Rosenhaupt and Sokal, 1965, Saw, 1974), the behaviour of masonry building elements were assumed to be isotropic elastic to simplify the problem and the influence of mortar joints was ignored. In (Dhanasekar et al., 1984), a simplified 'nonlinear' finite element model was proposed, were material properties of masonry and joints were averaged following numerous biaxial tests on bricks of masonry. In this approach, the structure was modelled as a continuum, ignoring local effects. Other researchers (Smith and Carter, 1970, Stafford Smith and Rahman, 1972, Ali and Page, 1985), refined this procedure to incorporate a discrete modelling of masonry blocks and mortar.

In (Lourenco and Rots, 1993, Laurenco et al., 1995), the two approaches (Micro- and macro-modelling) for modelling masonry building was presented. In (Lourenço et al., 2007), finite element models were used to assess the structural integrity and safety of a Monastery of Jerónimos in Lisbon, Portugal. This monumental structure was assessed for static and dynamic conditions. In (Beskos, 1993, Sánchez-Beitia and Brebbia, 1997, Tzamtzis and Asteris, 2004, Milani et al., 2007, De Villiers et al., 2021), static analysis for masonry building under their self-weight have been developed under the framework of finite element modelling.

Dynamic loads induced by seismic actions is generally critical in large-scale monumental structures. In (Acary and Jean, 1998, Jean et al., 2001, Caliò et al., 2012, Cescatti et al., 2020, Clementi, 2021), the seismic response of masonry buildings is investigated using finite element analysis. This method has been widely recognized as an efficient and effective approach that can be adopted for the structural assessment of old masonry structures (Armesto et al., 2010, Sevim et al., 2011, Domede et al., 2013, Ataei et al., 2016). In (Shabani et al., 2022), finite element models were used to investigate the soil-structure interaction on a stone masonry tower in Tønsberg, Norway. Non-destructive testes were used to calibrate digital-twin models to evaulate the risk of resonance effect due to siesmic actions in zones of low seismicity activity. In (Pirchio et al., 2021), unreinforced mansory churches in Italy were investigated using finite element models to understand the global behavior of the churches and to identify the most critical local mechanisms for collapse potential.

2.11 References

Acary, V. & Jean, M. Numerical simulation of monuments by the contact dynamics method. Monument-98, Workshop on seismic perfomance of monuments, 1998. 69-78.

Adam, J. M., Brencich, A., Hughes, T. G. & Jefferson, T. 2010. Micromodelling of eccentrically loaded brickwork: Study of masonry wallettes. *Engineering Structures,* 32**,** 1244-1251.

Ainsworth, M. & Mihai, L. A. 2009. An adaptive multi-scale approach to the modelling of masonry structures. *International journal for numerical methods in engineering,* 78**,** 1135-1163.

Ali, S. & Page, A. 1985. An elastic analysis of concentrated loads on brickwork. *MASONRY INT. Masonry Int.***,** 9.

Anastasio, S. 2020. Building between the two rivers: an introduction to the building archaeology of ancient Mesopotamia. *Building between the Two Rivers***,** 1-220.

Anthoine, A. 1992. In-plane behaviour of masonry(a literature review). *EUR(Luxembourg).*

Armesto, J., Roca-Pardiñas, J., Lorenzo, H. & Arias, P. 2010. Modelling masonry arches shape using terrestrial laser scanning data and nonparametric methods. *Engineering Structures,* 32**,** 607-615.

Ashurst, D. 1992. An assessment of repair and strengthening techniques for brick and stone masonry arch bridges.

Ataei, S., Jahangiri Alikamar, M. & Kazemiashtiani, V. 2016. Evaluation of axle load increasing on a monumental masonry arch bridge based on field load testing. *Construction and Building Materials,* 116**,** 413-421.

Berto, L., Saetta, A., Scotta, R. & Vitaliani, R. 2002. An orthotropic damage model for masonry structures. *International Journal for Numerical Methods in Engineering,* 55**,** 127-157.

Beskos, D. 1993. Use of finite and boundary elements in the analysis of monuments and special structures. *Bulletin of the association of civil engineers of Greece*.

Binda, L.,Gambarotta, L.,& Lagomarsino, S. & Modena, C. (1999). A multilevel approach to the damage assessment and seismic improvement of masonry buildings in Italy. Seismic Damage to Masonry Buildings, A. Bernardini Ed., Balkema, Rotterdam.

Block, P., DeJong, M. & Ochsendorf, J. 2006. As Hangs the Flexible Line: Equilibrium of Masonry Arches. *Nexus Network Journal,* 8**,** 13-24.

Boothby, T. E. 1995. Collapse modes of masonry arch bridges. *Masonry International,* 9**,** 62-69.

Brencich, A. & Gambarotta, L. 2005. Mechanical response of solid clay brickwork under eccentric loading. Part I: Unreinforced masonry. *Materials and structures,* 38**,** 257-266.

Caliò, I., Marletta, M. & Pantò, B. 2012. A new discrete element model for the evaluation of the seismic behaviour of unreinforced masonry buildings. *Engineering Structures,* 40**,** 327-338.

Campbell, J. & Durán, M., 2017. Numerical model for nonlinear analysis of masonry walls.*Numerical Model for Nonlinear Analysis of Masonry Walls*, 16(2), 189-201.

Caporale, A. & Luciano, R. 2012. Limit analysis of masonry arches with finite compressive strength and externally bonded reinforcement. *Composites Part B: Engineering,* 43**,** 3131-3145.

Caporale, A., Luciano, R. & Rosati, L. 2006. Limit analysis of masonry arches with externally bonded FRP reinforcements. *Computer methods in applied mechanics and engineering,* 196**,** 247-260.

Cescatti, E., Salzano, P., Casapulla, C., Ceroni, F., da Porto, F. & Prota, A. 2020. Damages to masonry churches after 2016–2017 Central Italy seismic sequence and definition of fragility curves. *Bulletin of Earthquake Engineering,* 18**,** 297-329.

Charalambidi, B., Koutsianitis, P., Motsa, S. M., Tairidis, G., Kasampali, A., Drosopoulos, G., Stavroulaki, M. & Stavroulakis, G. 2022. Modelling, identification and structural damage investigation of the Neoria monument in Chania. *Developments in the Built Environment,* 10**,** 100069.

Chieffo, N., Clementi, F., Formisano, A. & Lenci, S. 2019. Comparative fragility methods for seismic assessment of masonry buildings located in Muccia (Italy). *Journal of Building Engineering,* 25**,** 100813.

Civera, M., Mugnaini, V. & Zanotti Fragonara, L. 2022. Machine learning-based automatic operational modal analysis: A structural health monitoring application to masonry arch bridges. *Structural Control and Health Monitoring,* 29**,** e3028.

Clementi, F. 2021. Failure analysis of apennine masonry churches severely damaged during the 2016 central Italy seismic sequence. *Buildings,* 11**,** 58.

Code, U. 2011. 778-3R, Recommendations for the inspection, assessment and maintenance of masonry arch bridges. *UIC International Union of Railways*.

Conde, B., Ramos, L. F., Oliveira, D. V., Riveiro, B. & Solla, M. 2017. Structural assessment of masonry arch bridges by combination of non-destructive testing techniques and three-dimensional numerical modelling: Application to Vilanova bridge. *Engineering Structures,* 148**,** 621-638.

Costa, C., Arêde, A., Morais, M. & Aníbal, A. 2015. Detailed FE and DE Modelling of Stone Masonry Arch Bridges for the Assessment of Load-carrying Capacity. *Procedia Engineering,* 114**,** 854-861.

Crisfield, M. & Packham, A. 1987. A mechanism program for computing the strength of masonry arch bridges. *Research report-Transport and Road Research Laboratory*.

Crisfield, M. A. Computer methods for the analysis of masonry arches. 1985 1985a. Civil-Comp 85, Proceedings.

Crisfield, M. A. 1985b. FINITE ELEMENT AND MECHANISM METHODS FOR THE ANALYSIS OF MASONRY AND BRICKWORK ARCHES. RESEARCH REPORT.

Crisfield, M. A. 1987. Plasticity computations using the Mohr—Coulomb yield criterion. *Engineering Computations,* 4**,** 300-308.

Crisfield, M. A. & Wills, J. 1986. Nonlinear analysis of concrete and masonry structures. *Finite element methods for nonlinear problems, Bergan, ed., Springer-Verlag, Berlin***,** 639-652.

Cundall, P. A. A computer model for simulating progressive, large-scale movement in blocky rock system. *Proceedings of the International Symposium on Rock Mechanics*, 1971, 1971.

da Porto, F., Guidi, G., Garbin, E. & Modena, C. 2010. In-plane behavior of clay masonry walls: experimental testing and finite-element modeling. *Journal of structural engineering,* 136**,** 1379-1392.

Dahmen, J. F. D. & Ochsendorfs, J. A. 2012. Earth masonry structures: arches, vaults and domes. *Modern Earth Buildings.* Elsevier.

De Villiers, W. I., Van Zijl, G. P. A. G. & Boshoff, W. P. 2021. Finite element analysis of single-storey unreinforced alternative masonry walls. *Advances in Structural Engineering,* 24**,** 2011-2026.

Dhanasekar, M. 1985. The performance of brick masonry subjected to in-plane loading.

Dhanasekar, M., Page, A. & Kleeman, P. A finite element model for the in-plane behavior of brick masonry. Proc. 9th Australasian Conference on Mechanisms of Structures, 1984. 262-267.

Domede, N., Sellier, A. & Stablon, T. 2013. Structural analysis of a multi-span railway masonry bridge combining in situ observations, laboratory tests and damage modelling. *Engineering Structures,* 56**,** 837-849.

Drosopoulos G, Stavroulakis G. *Nonlinear Mechanics for Composite Heterogeneous Structures*, CRC Press, Taylor & Francis, 2022.

Drosopoulos, G. A. & Stavroulakis, G. E. 2018. A computational homogenization approach for the study of localization of masonry structures using the XFEM. *Archive of Applied Mechanics, 1-18.*

Drosopoulos, G., Stavroulakis, G. & Massalas, C. 2008. Influence of the geometry and the abutments movement on the collapse of stone arch bridges. *Construction and Building Materials,* 22**,** 200-210.

Edalat Behbahani, A., Barros, J. A. O. & Ventura-Gouveia, A. 2015. Plastic-damage smeared crack model to simulate the behaviour of structures made by cement based materials. *International Journal of Solids and Structures,* 73-74**,** 20-40.

Fanning, P. J. & Boothby, T. E. 2001. Three-dimensional modelling and full-scale testing of stone arch bridges. *Computers & Structures,* 79**,** 2645-2662.

Foraboschi, P. 2004. Strengthening of masonry arches with fiber-reinforced polymer strips. *Journal of composites for construction,* 8**,** 191-202.

Ford, T., Augarde, C. & Tuxford, S. 2003. Modelling masonry arch bridges using commercial finite element software. 9th International Conference on Civil and Structural Engineering Computing, Egmond aan Zee, The Netherlands, 2003. 2-4.

Gáspár, O., Sajtos, I. & Sipos, A. A. 2022. Multi-Hinge Failure Mechanisms of Masonry Arches Subject to Self-Weight as Derived from Minimum Thickness Analysis. *International Journal of Architectural Heritage***,** 1-29.

Gilbert, M. & Melbourne, C. 1994. Rigid-block analysis of masonry structures. *Structural engineer,* 72.

Grillanda, N., Milani, G., Ghosh, S., Halani, B. & Varma, M. 2021. SHM of a severely cracked masonry arch bridge in India: Experimental campaign and adaptive NURBS limit analysis numerical investigation. *Construction and Building Materials,* 280**,** 122490.

Heyman, J. 1967. On shell solutions for masonry domes. *International Journal of Solids and Structures,* 3**,** 227-241.

Heyman, J. 1982. *The Mansonry Arch,* Chichester, UK: Ellis Horwood.

Heyman, J. 1996. The stone skeleton: structural engineering of masonry architecture. 1996. Cambridge University Press, 133A.

Heyman, J. 1998. *Structural analysis: a historical approach,* Cambridge University Press.

Heyman, J., Pippard, A. & MEXE. 1980. THE ESTIMATION OF THE STRENGTH OF MASONRY ARCHES. *Proceedings of the Institution of Civil Engineers,* 69**,** 921-937.

Hooke, R. 1676. *A description of helioscopes, and some other instruments,* London, printed by T.R. for John Martyn.

Hughes, T. G., Blackler, M. J. & MEXE. 1997. A review of the UK masonry arch assessment methods. *Proceedings of the Institution of Civil Engineers-Structures and Buildings,* 122**,** 305-315.

Hughes, T. G., Hee, S. C. & Soms, E. 2002. Mechanism analysis of single span masonry arch bridges using a spreadsheet. *Proceedings of the Institution of Civil Engineers-Structures and Buildings,* 152**,** 341-350.

Jean, M., Acary, V. & Monerie, Y. 2001. Non-smooth contact dynamics approach of cohesive materials. *Philosophical Transactions of the Royal Society of London. Series A: Mathematical, Physical and Engineering Sciences*, 359**,** 2497-2518.

Jing, Y., Sheil, B. & Acikgoz, S. 2022. Segmentation of large-scale masonry arch bridge point clouds with a synthetic simulator and the BridgeNet neural network. *Automation in Construction*, 142**,** 104459.

Jiang, J., Wu, Y. & Zhao, X. 2011. Application of Drucker-Prager Plasticity Model for Stress-Strain Modeling of FRP Confined Concrete Columns. *Procedia Engineering*, 14**,** 687-694.

Labuz, J. F. & Zang, A., 2012. Mohr–Coulomb Failure Criterion. *Rock Mech Rock Eng*, 45(3), 975-979.

Laurenco, P., Rots, J. G. & Blaauwendraad, J. 1995. Two approaches for the analysis of masonry structures: micro and macro-modeling. *HERON, 40 (4), 1995*.

LimitState, LimitState:RING Manual, Version 3.2.c edition (2020). http://www.limitstate.com/ring. Accessed 30 November 2022.

Lourenco, P. & Rots, J. 1993. On the use of micro-models for the analysis of masonry shear walls. *Computer methods in structural masonry-2. Swansea***,** 14-26.

Lourenço, P. B., Krakowiak, K. J., Fernandes, F. M. & Ramos, L. F. 2007. Failure analysis of Monastery of Jerónimos, Lisbon: How to learn from sophisticated numerical models. *Engineering Failure Analysis*, 14**,** 280-300.

Lourenço, P. 1996. Computational strategies for masonry structures [thesis]. *The Netherlands: Delft University of Technology*.

Lourenço, P. B. 2002. Computations on historic masonry structures. *Progress in Structural Engineering and Materials*, 4**,** 301-319.

Lourenço, P.B. 2014. Masonry Structures, Overview. In: Beer, M., Kougioumtzoglou, I., Patelli, E., Au, IK. (eds) Encyclopedia of Earthquake Engineering. Springer, Berlin, Heidelberg. https://doi.org/10.1007/978-3-642-36197-5_111-1

Lourenço, P. B. 2021. Masonry Structures, Overview. *In:* BEER, M., KOUGIOUMTZOGLOU, I. A., PATELLI, E. & AU, I. S.-K. (eds.) *Encyclopedia of Earthquake Engineering.* Berlin, Heidelberg: Springer Berlin Heidelberg.

Melbourne, C. 1991. Conservation of masonry arch bridges. *Brick and Block Masonry*, 3**,** 1563-1570.

Melchiorre, J., Manuello, A. & Marano, G. 2021. Application of a Machine Learning Algorithm for the Structural Optimization of Circular Arches with Different Cross-Sections. *Journal of Applied Mathematics and Physics*, 09**,** 1159-1170.

Mihai, L. A. & Ainsworth, M. 2009. An adaptive multi-scale computational modelling of Clare College Bridge. *Computer Methods in Applied Mechanics and Engineering,* 198**,** 1839-1847.

Milani, G., Lourenço, P. & Tralli, A. 2007. 3D homogenized limit analysis of masonry buildings under horizontal loads. *Engineering Structures,* 29**,** 3134-3148.

Gilbert, M. & Melbourne, C. 1994. Rigid-block analysis of masonry structures. *Structural engineer,* 72.

Méry, E., 1840. Sur l'équilibre des voûtes en berceau. In *Annales des ponts et chaussées* (Vol. 19, pp. 50-70).

Moreira, V. N., Fernandes, J., Matos, J. C. & Oliveira, D. V. 2016. Reliability-based assessment of existing masonry arch railway bridges. *Construction and Building Materials,* 115**,** 544-554.

Moseley, H., 1856. *THE MECHANICAL PRINCIPLES OF ENGINEERING AND ARCHITECTURE*. New York, Wiley & Halstead

Ng, K., Fairfield, C., Sibbald, A. & LUSAS 1999. Finite-element analysis of masonry arch bridges. *Proceedings of the Institution of Civil Engineers-Structures and Buildings,* 134**,** 119-127.

Motsa, S. M., Drosopoulos, G. A., Stavroulaki, M. E., Maravelakis, E., Borg, R. P., Galea, P., d'Amico, S. & Stavroulakis, G. E. 2020. Structural investigation of Mnajdra megalithic monument in Malta. *Journal of Cultural Heritage,* 41**,** 96-105.

O'Dwyer, D. 1999. Funicular analysis of masonry vaults. *Computers & Structures,* 73**,** 187-197.

Oñate, E. 2009. Introduction to the Finite Element Method for Structural Analysis. *In:* OÑATE, E. (ed.) *Structural Analysis with the Finite Element Method: Linear Statics.* Dordrecht: Springer Netherlands.

Orbán, Z. 2004. Assessment, reliability and maintenance of masonry arch railway bridges in Europe. *Arch Bridges IV–Advances in Assessment, Structural Design and Construction. Eds: P. Roca and C. Molins, Barcelona,* 2004**,** 152-161.

Orduña, A. & Lourenço, P. 2005a. Three-dimensional limit analysis of rigid blocks assemblages. Part II: Load-path following solution procedure and validation. *International journal of solids and structures,* 42**,** 5161-5180.

Orduña, A. & Lourenço, P. B. 2005b. Three-dimensional limit analysis of rigid blocks assemblages. Part I: Torsion failure on frictional interfaces and limit analysis formulation. *International Journal of Solids and Structures,* 42**,** 5140-5160.

Orduña, A. ı. n. & Lourenço, P. B. 2003. Cap model for limit analysis and strengthening of masonry structures. *Journal of Structural Engineering,* 129**,** 1367-1375.

Page, J. 1993. Masonry Arch Bridges. London: London Transport Research Laboratory. HMSO.

Pelà, L., Aprile, A. & Benedetti, A. 2009. Seismic assessment of masonry arch bridges. *Engineering Structures,* 31**,** 1777-1788.

Pelà, L., Aprile, A. & Benedetti, A. 2013. Comparison of seismic assessment procedures for masonry arch bridges. *Construction and Building Materials,* 38**,** 381-394.

Phonphuak, N. & Chindaprasirt, P. 2015. Types of waste, properties, and durability of pore-forming waste-based fired masonry bricks. *Eco-efficient masonry bricks and blocks***,** 103-127.

Pippard, A. J. S. & Baker, J. F. 1968. *The analysis of engineering structures*, Edward Arnold London.

Pippard, A. J. S., Tranter, E. & Chitty, L. 1936. THE MECHANICS OF THE VOUSSOIR ARCH.(INCLUDES APPENDIX). *Journal of the Institution of Civil Engineers*, 4**,** 281-306.

Pirchio, D., Walsh, K. Q., Kerr, E., Giongo, I., Giaretton, M., Weldon, B. D., Ciocci, L. & Sorrentino, L. 2021. Integrated framework to structurally model unreinforced masonry Italian medieval churches from photogrammetry to finite element model analysis through heritage building information modeling. Engineering Structures, 241, 112439.

Poleni, G. 1748. *Memorie istoriche della Gran Cupola del Tempio Vaticano*, Padua: Nella Stamperia del seminario.

Pulatsu, B., Erdogmus, E., & Lourenço, P.B. 2019. Comparison of in-plane and out-of-plane failure modes of masonry arch bridges using discontinuum analysis. *Engineering Structures,* 178**,** 24-36.

Reich, Y. 1997. Machine learning techniques for civil engineering problems. *Computer-Aided Civil and Infrastructure Engineering,* 12**,** 295-310.

Rosenhaupt, S. & Sokal, Y. 1965. Masonry walls on continuous beams. *Journal of the Structural Division,* 91**,** 155-171.

Sánchez-Beitia, S. & Brebbia, C. 1997. *Structural studies, repairs, and maintenance of historical buildings.*

Saw, C. 1974. Linear elastic finite element analysis of masonry walls on beams. *Building Science,* 9**,** 299-307.

Sevim, B., Bayraktar, A., Altunişik, A. C., Atamtürktür, S. & Birinci, F. 2011. Assessment of nonlinear seismic performance of a restored historical arch bridge using ambient vibrations. Nonlinear Dynamics, 63, 755-770.

Shabani, A., Feyzabadi, M. & Kioumarsi, M. 2022. Model updating of a masonry tower based on operational modal analysis: The role of soil-structure interaction. Case Studies in Construction Materials, 16, e00957.

Shieh-Beygi, B. & Pietruszczak, S. 2008. Numerical analysis of structural masonry: mesoscale approach. *Computers & Structures,* 86**,** 1958-1973.

Smith, B. S. & Carter, C. Distribution of Stresses in Masonry Walls subjected to Vertical Loading'. Proc. 2nd Int. Brick Masonry Conference, 1970. 119-124.

Stafford Smith, B. & Rahman, K. 1972. THE VARIATIONS OF STRESS IN VERTICALLY LOADED BRICKWORK WALLS. *Proceedings of the Institution of Civil Engineers,* 51**,** 689-700.

Standard, B. 2005. Eurocode 6—Design of masonry structures—. *British Standard Institution. London*.

Sorić, J., Wriggers, P. & Allix, O. 2018. *Multiscale Modeling of Heterogeneous Structures*.

Tapkın, S., Tercan, E., Motsa, S. M., Drosopoulos, G., Stavroulaki, M., Maravelakis, E. & Stavroulakis, G. 2022. Structural Investigation of Masonry Arch Bridges Using Various Nonlinear Finite-Element Models. *Journal of Bridge Engineering,* 27**,** 04022053.

Thai, H.-T. 2022. Machine learning for structural engineering: A state-of-the-art review. *Structures,* 38**,** 448-491.

Thamboo, J. & Dhanasekar, M. 2016. Nonlinear finite element modelling of high bond thin-layer mortared concrete masonry. International Journal of Masonry Research and Innovation. 1. 5. 10.1504/IJMRI.2016.074727.

Thavalingam, A., Bicanic, N., Robinson, J. & Ponniah, D. 2001. Computational framework for discontinuous modelling of masonry arch bridges. *Computers & structures,* 79**,** 1821-1830.

Toti, J., Marfia, S. & Sacco, E. 2013. Coupled body-interface nonlocal damage model for FRP detachment. *Computer Methods in Applied Mechanics and Engineering,* 260**,** 1-23.

Towler, K. & Sawko, F. 1985. Limit state behaviour of brickwork arches. Sesto congresso internazionale sulle murature in mattoni. Roma, 16-19 maggio 1982. Sixth international brick masonry conference. Rome, 16th-19th may, 1982, 1982. 422-429.

Towler, K. D. S. 1985. Applications of non-linear finite element codes to masonry arches. *In:* TOPPING, B. H. V., ed. 2nd Int. Conf. on Civil and Structural Engineering Computing, 1985 Edinburgh. 197–202.

Tzamtzis, A. & Asteris, P. 2004. FE Analysis of Complex Discontinuous and Jointed Structural Systems: Part 2: Application of the Method – Development of a 3D Model for the Analysis of Unreinforced Masonry Walls. *Electronic Journal of Structural Engineering,* 4**,** 93-107.

Vyas, J. & Kazys, R. 2018. A Review on Nondestructive Techniques and Characteristics of Composite Materials for the Aerospace System. *MATEC Web of Conferences,* 233**,** 00003.

Vyas, U. & Venkatarama Reddy, B. V. 2010. Prediction of solid block masonry prism compressive strength using FE model. *Materials and structures,* 43**,** 719-735.

Wang, J., Haynes, B. J. & Melbourne, C. 2013. A comparison between the MEXE and Pippard's methods of assessing the load carrying capacity of masonry arch bridges.SECON-CSSE, Zagred, Croatia., 589-596.

Zampieri, P., Zanini, M. A. & Modena, C. 2015. Simplified seismic assessment of multi-span masonry arch bridges. *Bulletin of Earthquake Engineering,* 13**,** 2629-2646.

Zhuge, Y., Thambiratnam, D. & Corderoy, J. 1998. Nonlinear dynamic analysis of unreinforced masonry. *Journal of structural engineering,* 124**,** 270-277.

Zucchini, A. & Lourenço, P. B. 2007. Mechanics of masonry in compression: Results from a homogenisation approach. *Computers & structures,* 85**,** 193-204.

Chapter 3 – Methodology

3.1 Introduction

Chapter 3 outlines the methods and procedures applied in the thesis, to achieve the aims and objectives provided in Chapter 1. The main aim of this study is to investigate the structural response of masonry systems, such as buildings and arches, using nonlinear finite element analysis. To achieve this, a methodology is proposed in the thesis, investigating different numerical methods and techniques, adopted to overcome the challenges involved in the structural evaluation of existing masonry systems. Aspects of the proposed methodology include: (a) analytical study of the geometry of the structures under investigation using laser scanning and MATLAB scripts, (b) information from literature or evaluation of old destructive/non-destructive tests, used to provide the material properties, and (c) nonlinear finite element analysis and machine learning tools, including artificial neural networks, developed to assess the structural response of masonry systems, emphasizing in failure.

3.2 Details of the adopted finite element models

To holistically investigate the response of masonry systems (arches and building), both discrete and continuum approaches are adopted in the thesis. In particular, traditional constitutive descriptions, incorporating principles of non-smooth contact mechanics, as well as damage mechanics laws, are adopted for the investigation of the ultimate, failure response of masonry structures.

3.2.1 Discrete constitutive description

Within the discrete approach, unilateral contact–friction interfaces are introduced between the masonry stones, to simulate the response between the stone blocks, in the mortar joints. Potential damage like the hinge-mechanism is represented by the opening and/or sliding of those interfaces. Figure 3-1(a) shows an example of a unilateral contact–friction interface, introduced to evaluate potential damage on a multi-span masonry arch bridge. This investigation is conducted using nonlinear finite element analysis, as presented in Chapter 4 of the thesis.

To simulate the contact conditions between the masonry blocks, principles taken from contact mechanics have been adopted. Figure 3-1(b) shows a schematic representation of the contact conditions between two adjacent blocks. The mathematical formulation of the contact-friction laws, which are introduced in the interfaces between the masonry blocks, is provided by equations (1)-(5) (Panagiotopoulos, 1985, Drosopoulos et al., 2006).

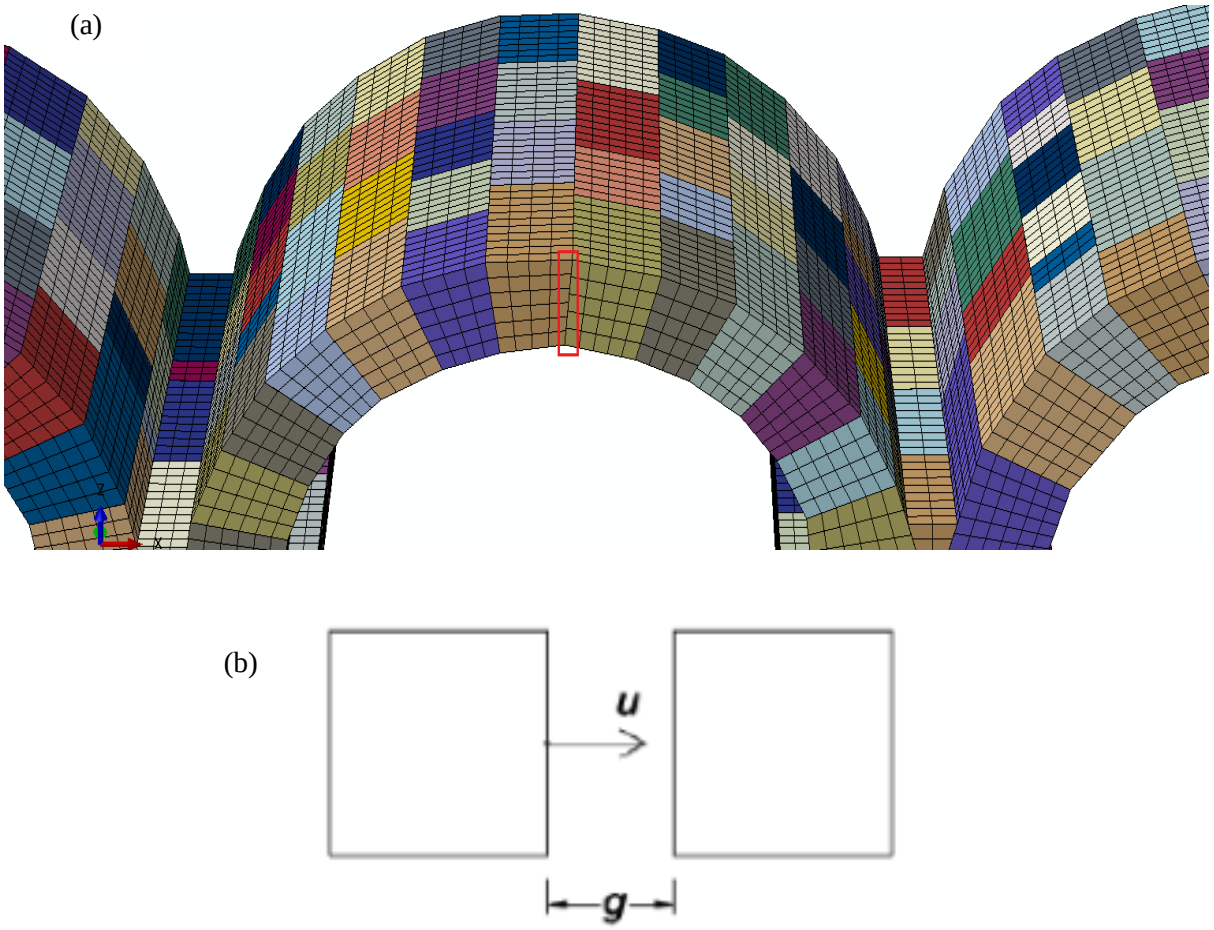

Figure 3-1: (a) A unilateral contact interface (marked in red) assigned on an arch bridge finite element model, and (b) schematic representation of the contact conditions between two stones.

In particular, u is a single degree of freedom and g represents the initial opening between the contacting bodies, as shown in Figure 3-1(b). Inequality (1) expresses the non-penetration condition between adjacent blocks. Inequality two states that only a compressive force (pressure) t^n, and no tensile forces, can be developed in the interfaces. Equation (3) provides the

complementarity condition, stating that either contact occurs, with non-zero compressive forces in the interface, or separation takes place, resulting in zero interface forces.

$$h = u - g \leq 0 \Longrightarrow h \leq 0 \qquad (1)$$

$$-t^n \geq 0 \qquad (2)$$

$$t^n(u - g) = 0 \qquad (3)$$

The behaviour in the tangential direction between the interfaces, is defined by a static version of the Coulomb friction model. Two contacting surfaces start sliding when the shear stress in the interface reaches a critical value equal to:

$$t^t = \tau_{cr} = \pm\mu|t^n| \qquad (4)$$

where t^t and t^n are the shear stress and the contact pressure at a given point of the contacting surfaces, respectively, and μ is the friction coefficient. There are two possible directions of sliding along an interface, so t^t can be positive or negative depending on that direction. Furthermore, there is no sliding if $|t^t| < \mu|t^n|$ (stick conditions). The sliding rule can be summarized by the following relations, where u_t is the displacement (sliding) in the tangential direction of an interface:

$$|t^t| < \mu|t^n| \longrightarrow u_t = 0 \ (no\ sliding) \qquad (5a)$$

$$t^t = \mu|t^n| \longrightarrow u_t \geq 0 \ (sliding\ in\ one\ diretion) \qquad (5b)$$

$$t^t = -\mu|t^n| \longrightarrow u_t \leq 0 \ (sliding\ in\ the\ opposite\ direction) \qquad (5c)$$

The unilateral contact-friction problem is strongly nonlinear, due to the mentioned conditions applied at the interfaces between the stones. Thus, the nonlinearity is caused by the opening–closure and sticking–slipping response along these interfaces. The overall nonlinear problem is solved using the Newton-Raphson incremental-iterative procedure. The same contact mechanics law has been adopted to simulate (and explain) the cracks on the vault roof of the masonry building investigated in Chapter 5 (Figure 3-2).

Figure 3- 4: Seven-span shipyard masonry building in Greece, with vaulted roof (Providakis, 2021).

3.2.2 Continuum models

To simulate the material behaviour in the framework of finite element analysis, continuum models incorporating damage mechanics laws are adopted. In Chapter 4, a smear crack and a damage plasticity law are used to represent failure on a masonry arch bridge. Both compressive and tensile failure types can be observed, when applying these damage mechanics constitutive descriptions.

3.2.2.1 Smear crack damage model

The smeared crack damage law is adopted to simulate the brittle nature of masonry by incorporating the uniaxial tensile and compression behaviour. Within this model, cracking is assumed to occur when the stress reaches a critical failure surface, given by the relationship between the equivalent pressure stress, p, and the Mises equivalent deviatoric stress q, as shown Figure 3-3b. The compressive response is defined within elastic-plastic theory, using a simple form of yield surfaces written in terms of the equivalent pressure stress p, and the Mises equivalent deviatoric stress q (Figure 3-3b). The post-failure behaviour of the damaged material is modelled with a tension stiffening law and the stress–displacement diagram shown in Figure 3-3c.

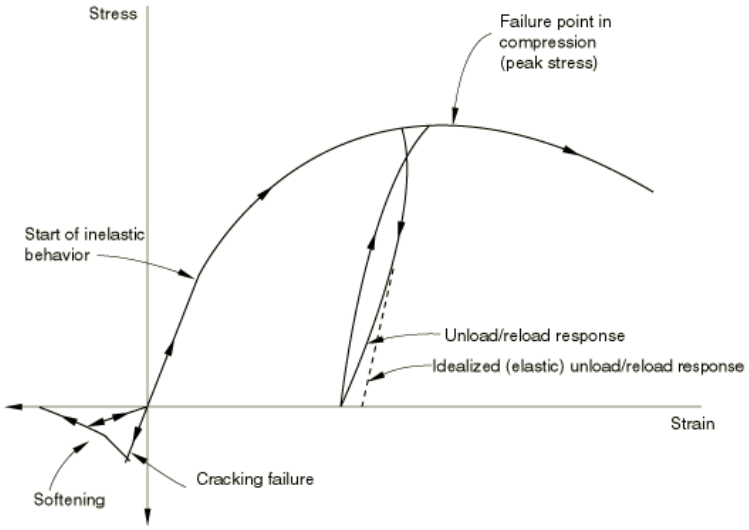

Figure 3- 3:(a) Uniaxial stress–strain law of the smeared crack damage model (Simulia, 2016).

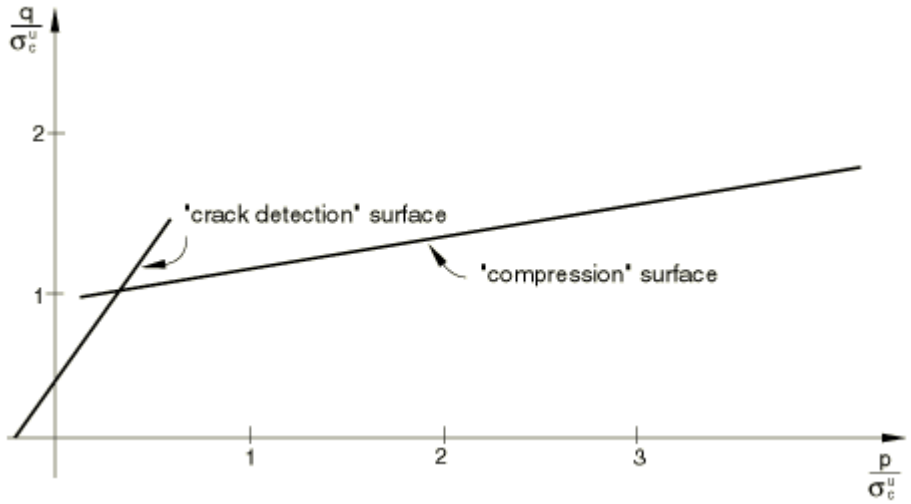

Figure 3- 5:(b) Failure surfaces of the smeared crack damage model (Simulia, 2016).

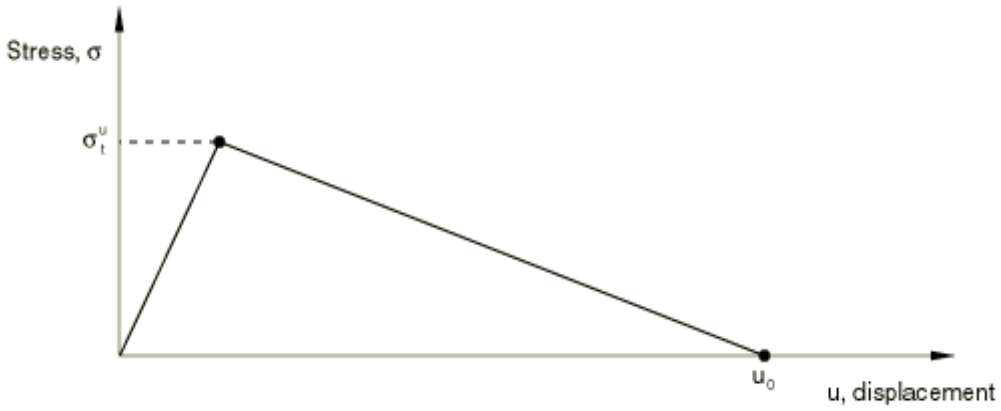

Figure 3- 3:(c) Stress–displacement law of the smeared crack damage model representing tension softening (Simulia, 2016).

3.2.2.2 Damage plasticity law

A damage plasticity, continuum constitutive description is adopted to simulate the failure behaviour for quasi-brittle structures, like masonry and concrete, subjected to monotonic or cyclic actions. The main two failure mechanisms, which can be depicted by this law, are tensile cracking and compressive crushing. During unloading the elastic stiffness of the material is considered damaged. This is depicted using two damage variables, one for tension and another for compression, both introduced in the model as functions of the plastic strains. These damage variables take values from zero, representing the undamaged material, to one, depicting total loss of strength. If the initial elastic stiffness of the material is E_0, d_t and d_c are the tensile and compressive damage variables, respectively, then the stress-strain relations under uniaxial tension and compression loading are provided by the following equations (Simulia, 2016):

$$\sigma_t = (1 - d_t)E_0\left(\varepsilon^t - \varepsilon_{pl}^t\right) \quad (6)$$

$$\sigma_c = (1 - d_c)E_0\left(\varepsilon^c - \varepsilon_{pl}^c\right) \quad (7)$$

3.2.3 Geometric modelling

To obtain the geometry of the masonry structures studied in Chapters 4 and 5 of the thesis, terrestrial laser scanning was used to obtain a point cloud, describing the geometry. Analysis is then conducted, to convert the point cloud to an appropriate three-dimension solid geometric format, to be used by the structural analysis software. In addition, other resources, like existing drawings and reports were used to enrich the geometric details. Figure 3-4(a) shows a photo of the masonry arch studied in Chapter 4, taken during the collection of the point cloud using terrestrial laser scanning. Figure 3-4(b) shows an image of the masonry building investigated in Chapter 5, during analytical processing of the point cloud to a three-dimension geometry by using triangulation of the data collected.

(a)

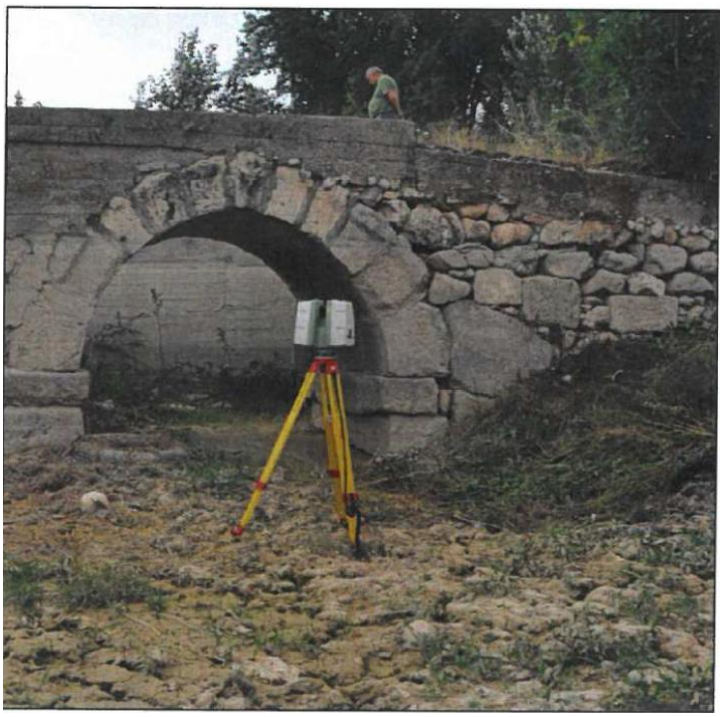

(b)

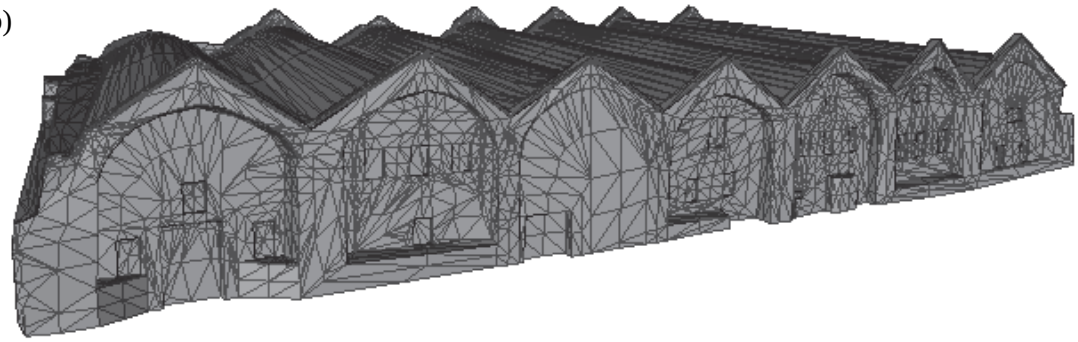

Figure 3- 4:(a) 3D scanning of the masonry arch bridge using terrestrial laser scanner, and (b) analytical processing by triangulation of point cloud to 3D geometry.

3.2.4 Modal analysis and damage identification

To determine the natural dynamic characteristics of masonry structures, modal analysis can be used, in the framework of finite element analysis. In modal analysis, natural frequencies, damping factors and mode shapes of the structure are obtained to formulate a mathematical model which describes its dynamic behaviour. The vibration response of a structure is expressed as a linear combination of a set of simple harmonic motions called the natural modes of vibration or mode

shapes. In this thesis, modal analysis simulations are implemented in Chapter 5, to identify existing damage on a large masonry building.

The determination of structural and material properties of a partially collapsed monument and the evaluation of existing damages is not a trivial task. The complexity of this task is amplified by the size of the structure. The modal analysis is assisted by micro-tremor measurements which experimentally measure the natural frequencies of the structure due to ambient vibrations. The numerically calculated eigenvalues are compared to experimentally measured quantities. The correlation between numerical and experimental measurements, provides an insight of the structural response. A least square technique is adopted for the modal assurance criterion, by driving the model from a Python script. Standard design codes for structural investigation, recommend that the modal analysis used should have as many eigenvectors as possible in order to activate 75% of the total mass of the structure. All the details of this research, are provided in Chapter 5 of the thesis.

3.2.5 Extended finite element method (XFEM)

To investigate the initiation and propagation of cracks in the masonry building studied in Chapter 5, the extended finite element method is adopted. The method is an extension of the conventional finite element analysis, introducing cracks crossing finite elements and contact interfaces, allowing them to propagate in an arbitrary path. The main concept of this method is to use the partition of unity property and properly enrich the nodal displacement approximation enrichment functions, as shown in equation (8) (Simulia, 2016). For the enrichment of the split elements, the Heaviside function H is used as given in equation (8). The domain of a crack crossing an element is shown in Figure 3-5. This numerical method was applied in Chapter 5, in an attempt to explain the transverse cracks on the vaulted roof of the masonry building.

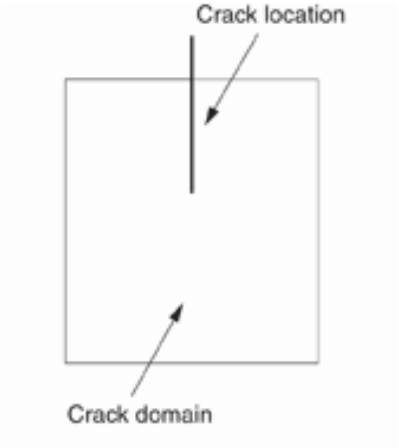

Figure 3- 5: Definition of a crack and crack domain for XFEM (Simulia, 2016).

$$u = \sum_{I=1}^{N} N_I(x)\left[u_I + H(x)a_I + \sum_{a=1}^{4} F_a(x)b_I^a\right] \quad (8)$$

3.3 Machine learning

An innovate procedure for the investigation of the structural response of circular masonry arches using machine learning is proposed in Chapter 6 of this thesis. A data-driven analysis of circular masonry arches is proposed, to evaluate the mechanical response of arches considering different arch shapes (span and thickness of the stones that make up the arch).

The first step of this investigation is to conduct parametric simulations, in order to develop a dataset with input and output geometric and structural parameters of the masonry arch. The parametric simulations were driven by MATLAB and Python scripts to build nonlinear finite element models with unilateral contact/friction laws used to simulate the response between masonry blocks. The dataset obtained was then used to train the artificial neural network.

To train the artificial neural networks, the Levenberg-Marquardt algorithm is adopted due to its fastest training algorithms. It uses the Jacobian matrix to compute the solution and assumes that the performance function is the mean or sum of square errors. Equations (9) to (11) show the

principle that the Levenberg-Marquardt algorithm is based on (MathLab, 2021). The Hessian matrix is approximated by equation (9) when the performance function is provided by the sum of squares errors and the gradient can be computed as Jacobian matrix multiplied by the vector of network errors, see equation (10). Equation (11) shows how the Levenberg-Marquardt algorithms approximate the Hessian matrix by combining the Gradient Descent and Newton-Raphson method.

$$H = J^T J \tag{9}$$

$$g = J^T e \tag{10}$$

$$x_{k+1} = x_k - [J^T J + \mu I]^{-1} J^T e \tag{11}$$

Three artificial neural networks are trained in this study to predict different structural responses: (a) deformation due to self-weight only, (b) deformation due to self-weight and a vertical point load applied at ¼ span of the arche, and (c) the ultimate load.

3.4 References

Drosopoulos, G., Stavroulakis, G. & Massalas, C. 2006. Limit analysis of a single span masonry bridge with unilateral frictional contact interfaces. *Engineering Structures,* 28**,** 1864-1873.

MathLab 2021. release R2021a. *Natick, Massachusetts: The MathWorks Inc*.

Panagiotopoulos, P. D. 1985. *Inequality Problems in Mechanics and Applications: Convex and nonconvex energy functions*, Springer Science & Business Media.

Providakis, C. 2021. March 2021. Experimental investigation of eigenmodal characteristics. *Research Investigation for the Restoration of Neoria, Technical University of Crete, Municipality of Chania, Ephorate of Antiquities. Chania*.

Simulia, D. S. 2016. ABAQUS analysis user's manual (version 6.14). *Providence, RI: Dassault Systèmes Simulia.*

Chapter 4 – Structural Investigation of Masonry Arch Bridges Using Various Nonlinear Finite-Element Models

Date:	01-23-2022
To:	"Siphesihle Mpho Motsa" motsampho@gmail.com;214580281@stu.ukzn.ac.za
cc:	"Serkan Tapkın" serkantapkin@bayburt.edu.tr, "Emre Tercan" etercan87@gmail.com, "Georgios Drosopoulos" gdrosopoulos@uclan.ac.uk, "Maria Stavroulaki" mstavr@mred.tuc.gr, "Emmanuel Maravelakis" marvel@hmu.gr, "Georgios Stavroulakis" gestavr@dpem.tuc.gr
From:	"Journal of Bridge Engineering" editorial.coordinator@asce.kwfco.com
Subject:	Decision on Manuscript MS BEENG-5402R2

Ref.: Ms. No. BEENG-5402R2

Structural investigation of masonry arch bridges using various non-linear finite element models

Serkan Tapkın; Emre Tercan; Siphesihle Mpho Motsa; Georgios Drosopoulos; Maria Stavroulaki; Emmanuel Maravelakis; Georgios Stavroulakis

Dear Mr Siphesihle Mpho Motsa,

Congratulations! Your Technical Paper has been accepted for publication in ASCE's Journal of Bridge Engineering. Your manuscript will now be forwarded to a Production Editor who will prepare it for publication and you will be notified of a publication date once your Technical Paper has been scheduled for an issue.

Our editors have requested that all accepted authors serve as reviewers for the Journal of Bridge Engineering. If you are not already a reviewer for the journal and are willing to serve as one, please reply to this email and let me know.

Also, please be sure to read the following important info for newly accepted authors:

- ASCE authors can make their paper open access for a one-time fee. Read more here.
- Your accepted paper is fully citable using its DOI. The DOI for your accepted paper can be found in the "Submissions in Production" folder in your Editorial Manager account. Note that this DOI will not be activated until the paper is published online in the ASCE Library. The paper may be cited before publication as: [Authors]. Forthcoming. "[Article title]." [Journal Name]. [DOI].
- Following your article: Please note that registered users to the ASCE Library can sign up for a citation alert for any paper. This alert will send you an email anytime your manuscript is cited by another journal in the CrossRef indexed publications. These citations will also appear on the abstract page for your article.
- Authors who are ASCE younger members are encouraged to apply for the Collingwood Prize. Authors may nominate their own paper, and nominations are accepted on a rolling basis.

Your paper is now being transferred to ASCE's Production department. Production staff will perform a quality check upon receipt of your paper, and may contact you to resolve queries or address any issues with files or format before copyediting and page composition begins. Please be aware that your paper will be withdrawn if production queries are not addressed and page proofs are not reviewed and returned in a timely manner.

Thank you so much for submitting your work to ASCE's Journal of Bridge Engineering and please let us know if you have any further questions.

Sincerely,

Monica Leigh

Editorial Coordinator

ASCE

Structural Investigation of Masonry Arch Bridges Using Various Nonlinear Finite-Element Models

Serkan Tapkın[1]; Emre Tercan[2]; Siphesihle Mpho Motsa[3]; Georgios Drosopoulos[4]; Maria Stavroulaki[5]; Emmanuel Maravelakis[6]; and Georgios Stavroulakis[7]

Abstract: This article presents an investigation of the structural behavior of a masonry arch bridge in Turkey. An analytical study has been conducted to provide the geometry of the structure, using laser scanning. A point cloud describing the geometry was obtained and properly transformed into a format that is appropriate for structural analysis software (CAE). Then, nonlinear finite-element models were developed to simulate structural responses of the bridge. The goal of the article is to highlight the influence of both continuum and discrete approaches and related constitutive laws on the responses of the bridge. Thus, continuum damage laws and a discrete model consisting of unilateral contact–friction interfaces were developed. Different load cases were tested and a comparison between the results obtained from the different approaches was considered. The failure mechanisms and the ultimate strengths were derived, and core points of the models were highlighted. The output of this work shows how the different failure models predict the behavior of the masonry arches. It also shows that the three-hinge mechanism, which has been depicted in classical studies for single-span arch masonry bridges under a horizontal settlement of supports, may also be obtained for multiarch bridges. Similarly, downward, vertical settlement of supports may result in the development of two hinges, as in single-span arches. Finally, the beneficial influence of the backfill in limiting the failure in the arch is addressed. **DOI: 10.1061/(ASCE)BE.1943-5592.0001870**.

Author keywords: Masonry arch bridge; Terrestrial laser scanning; Unilateral contact–friction; Continuum damage model; Discrete-element method.

Introduction

Masonry arch bridges are among the oldest manmade structures, many of which have survived for thousands of years (Sevim et al. 2011). They are found in various sizes and configurations and their aesthetic details vary significantly (Catalan and Aldea 2007). Masonry arch bridges play a vital role in the cultural heritage of several countries, highlighting the need for preservation. Research conducted by Van Beek (1987) and Campbell and Tutton (2013) in Lower Egypt, Iran, the Eastern Mediterranean region, and Mesopotamia showed that the earliest masonry arch structures (about 5,000 years old) were made up of sun-dried mud bricks.

A thorough understanding of the structural behavior of masonry arch bridges is of crucial importance, in terms of their restoration and preservation. Aging and different loads due to earthquakes, settlement of supports, and vehicles have an increased impact on their structural condition, causing significant damage and/or collapse of these structures. Hence, their conservation and preservation are of paramount importance. The process of structural restoration includes (a) visual assessment of the structure; (b) material testing by adopting, for instance, nondestructive tests for the constituent materials; (c) understanding of the original design and the structural capabilities by developing numerical models; and (d) implementing the actual restoration of the different elements of the structure after the previous steps have been considered.

Most of the old masonry arch bridges have sustained some form of damage over the decades while in service. Some of the common structural problems that they experience, which can lead to failure and collapse, are (a) deterioration of the masonry material due to thermal effects, moisture, or chemical actions; (b) damage of the arch barrel due to ring-separation, arch barrel distortion, and cracking, which is a result of longitudinal shear or tensile failure (Ford et al. 2003; Melbourne 1991); (c) failure of the foundation, which is mainly caused by settlement of supports (Ashurst 1992); and (d) vehicle collision, which can interact with abutments, arch barrels, or piers (Melbourne et al. 2006; Wilmers 2012). Note that some of these defects take place simultaneously.

[1]Professor, Faculty of Engineering, Dept. of Civil Engineering, Bayburt Univ., Bayburt 69010, Turkey. ORCID: https://orcid.org/0000-0003-1417-9972. Email: serkantapkin@bayburt.edu.tr

[2]Associate Professor, General Directorate of Highways, 13th Region, Dept. of Survey, Project and Environment, Antalya 07090, Turkey. ORCID: https://orcid.org/0000-0001-6309-1083. Email: etercan87@gmail.com

[3]Dept. of Civil Engineering, Structural Engineering and Computational Mechanics Group, Univ. of KwaZulu-Natal, Durban 4001, South Africa (corresponding author). ORCID: https://orcid.org/0000-0003-4990-5225. Email: 214580281@stu.ukzn.ac.za

[4]Lecturer, Dept. of Civil Engineering, School of Engineering, Univ. of Central Lancashire, Preston PR1 2HE, UK; Honorary Associate Professor, Dept. of Civil Engineering, Structural Engineering and Computational Mechanics Group, Univ. of KwaZulu-Natal, Durban 4001, South Africa. Email: gdrosopoulos@uclan.ac.uk

[5]Associate Professor, Faculty of Architecture, Applied Mechanics Laboratory, Technical Univ. of Crete, Chania GR-73100, Greece. Email: mstavr@mred.tuc.gr

[6]Associate Professor, Dept. of Electronic Engineering, Hellenic Mediterranean Univ., Chania GR-73100, Greece. Email: marvel@hmu.gr

[7]Professor, School of Production Engineering and Management, Institute of Computational Mechanics and Optimization, Technical Univ. of Crete, Chania GR-73100, Greece. ORCID: https://orcid.org/0000-0001-9199-2110. Email: gestavr@dpem.tuc.gr

Note. This manuscript was submitted on August 17, 2021; approved on January 23, 2022; published online on May 6, 2022. Discussion period open until October 6, 2022; separate discussions must be submitted for individual papers. This paper is part of the ***Journal of Bridge Engineering***, © ASCE, ISSN 1084-0702.

In recent years, several studies have been conducted to evaluate the structural behavior of masonry arch bridges and improve their ultimate strength. Some of the recognized techniques used in the assessment of masonry arch bridges include (a) the military engineering experimental establishment (MEXE), a semiempirical method based on elastic analysis that only considers the independent strength of the arch barrel (Hughes and Blackler 1997); (b) the collapse mechanism method, which uses simple equilibrium calculations based on the assumption that the collapse of the arch barrel takes place due to the formation of a four-hinge mechanism (Hughes et al. 2002; Page 1993); and (c) the finite-element method (FEM), which relies on the development of a computational, structural model that considers the influence of each element of the bridge (arch barrel, spandrel walls, wing walls, fill, and parapets) (Crisfield 1985; Towler 1985). This method has been widely recognized as an efficient and effective approach that can be adopted for the structural assessment of old masonry structures (Armesto et al. 2010; Ataei et al. 2016; Conde et al. 2017; Domede et al. 2013; Lubowiecka et al. 2009; Sevim et al. 2011).

In the structural investigation of masonry arches, it has been noted that the geometry of the structure plays a vital role on its structural integrity, and a change of the geometry in respect to the original one can result in excessive deformation, leading to collapse (Guastavino and Moreno 2006). Armesto et al. (2010) and Conde et al. (2017) developed FEMs of masonry arch bridges, using terrestrial laser scanning technology to obtain the real, exact geometry of the structure. In particular, Armesto et al. (2010) performed a deformation analysis of the Segura Roman Bridge in Portugal by creating a three-dimensional (3D) geometry from unstructured point clouds, collected from six different positions around the bridge. A nonparametric algorithm was also proposed, which generated a smooth 3D surface based on a local bivariate kernel smoother, allowing for the estimation of cross sections without the need for any prior parametric shape. Conde et al. (2017) developed a 3D FEM of the Vilanova masonry arch bridge in Spain based on a comprehensive field survey that was conducted by adopting fully nondestructive testing techniques, such as laser scanning, ground penetration radar, sonic tests, and ambient vibration tests. As part of the study, a two-dimensional (2D) limit state analysis was performed on one of the arches of the bridge to depict the effect of the live load and to determine the impact of the four-hinge failure mechanism, which was initially presented in Heyman (1982), on the structural response of the arch.

Ataei et al. (2016) conducted a load-capacity assessment on an 80-year-old masonry arch bridge consisting of 10 arch spans. Finite-element analysis (FEA) and limit analysis models using the RING software (RING 2021) were developed for the arch of the main span of the bridge, with a length of 40 m and height of 30 m. Continuum numerical models have been used, allowing for the estimation of deformations with a high precision (0.01 mm). The study showed that the bridge can still be in service even when the axle load is increased from 200 to 250 kN.

Lubowiecka et al. (2009) and Sevim et al. (2011) studied masonry arch bridges by introducing modal analysis to calibrate the developed nonlinear FEMs. In particular, Lubowiecka et al. (2009) observed that the value of the Young's modulus is vital for the natural frequencies of the structure, noticing that a similar observation is derived in Motsa et al. (2020). Sevim et al. (2011) applied a time-history ground motion acceleration of a 0.515 g on the calibrated FEM, resulting in acceptable stress limits for the masonry stones, and a maximum displacement of 8.2 mm developed at the middle region of the span.

Domede et al. (2013) developed a 3D FEM for a three-span masonry arch bridge. In an effort to reproduce the failure cracks present on the structure, a settlement of the middle support was assigned. On the damaged model of the bridge, an increasing train load was applied, resulting in a failure load of 25 MN. The results of the study show that the safety margin between failure load and service load is quite high.

More recent articles have highlighted significant aspects of the structural response of masonry arches. Sarhosis et al. (2016) provided a literature review on experimental investigations and assessment methods for masonry arch bridges. Pulatsu et al. (2019) developed masonry arch bridge models using a mixed discrete–continuum approach. The aim of this study was to depict the influence of the soil backfill and of the spandrel walls on the mechanical response. Casapulla et al. (2019) and Mousavian and Casapulla (2020) proposed a digital tool for the design of stable semicircular masonry arches consisting of interlocking blocks. To increase the sliding resistance between the blocks compared with conventional blocks, they introduced interlocking connectors in the analysis. Zampieri et al. (2015) developed a kinematic analysis process to address the transverse seismic capacity and provide the limit horizontal load of multispan masonry bridges with slender piers. Gönen and Soyöz (2021) investigated different numerical methods, including nonlinear static and dynamic FEMS, to evaluate the seismic response of masonry arch bridges.

This paper presents the structural investigation of the Dağarcık bridge, a masonry arch bridge in Turkey. By using two types of computational models into a three-span arch bridge, adopting both a discrete and a continuum mechanical description to study the development of failure patterns that have been previously derived in single-span arches. These patterns involve the development of hinges representing cross-section failure, when settlement of supports, both horizontal and vertical, arise. Since this loading type can result in the total collapse of masonry arches, the investigation of the phenomenon for multispan arches provides an innovative aspect to the current investigation. The study actually proves that hinge mechanisms of single-span arches due to settlement of supports may also arise in multispan arches.

The present work also provides an insight on two types of constitutive descriptions, focusing on both a discrete and continuum approach. Both concepts have been used in previous and current research on masonry arches. Hence, it appears there is a need for a holistic investigation of their ultimate mechanical response, using the two approaches individually as well as in combination. This study provides details of the parameters used within the two descriptions, and important points are introduced that highlight the advantages and disadvantages of these approaches.

First, 3D laser scanning is used to represent the geometry of the bridge, in the form of a point cloud. This is converted into a 3D solid geometry using AutoCAD. Then, a series of nondestructive tests are conducted on the masonry stones of the bridge, to provide their mechanical properties. Finally, a number of nonlinear FEMs are developed, adopting both discrete and continuum mechanical laws. The discrete models incorporate unilateral contact–friction interfaces between the masonry stones. The continuum models include a smear crack and a damage plasticity law applied on the masonry arch to represent failure. The soil backfill that is found above the arches is also introduced in some of the models, and its influence on the mechanical response of the structure is highlighted. The developed numerical models are used to evaluate the structural response of the masonry bridge under various load cases.

Research Aim

The goal of this study was to investigate the structural behavior of a masonry arch bridge and provide further insight on mechanical

laws that can be used for the task. The developed numerical models were applied to the Dağarcık bridge, located in Turkey. The structural investigation of this historically and architecturally important monument was conducted by considering a combination of nondestructive tests and numerical FEA.

First, a 3D laser scan of the masonry structure is implemented, where 91,360,850 cloud points are collected from nine scanning position stations around the bridge. Then, nonlinear FEA takes place, adopting either a discrete or a continuum approach. With the discrete approach, unilateral contact–friction interfaces are introduced between the masonry stones, to simulate the mortar joints. Opening and/or sliding of those interfaces indicates damage. With the continuum approach, two failure laws initially adopted for concrete are applied to the arch. Discrete models incorporating the continuum laws are also developed, to offer a further insight to the mechanical response. Opening or sliding of the interfaces and compressive failure of the arch can be depicted by this combination of discrete and continuum laws. The mechanical properties of the masonry stones are obtained from nondestructive tests and the literature.

Figs. 1(a and b) show some of the inherited features of the bridge under investigation, which have been simulated by the numerical models through the use of the point cloud. The developed numerical models also simulate further defects, such as the slight settlement of the supports, which are sometimes difficult to be identified by a physical inspection. Note that the overall concept presented in this study, adopting laser scanning of a masonry arch and structural analysis using various nonlinear FEMs with different constitutive descriptions, can also be applied for other masonry structures.

Description of Dağarcık Bridge

The Dağarcık Bridge is located in the Onaç River, found within the boundaries of Dağarcık village, located 22 km southeast of Burdur city center and 11 km northwest of the Bucak District in Turkey. There is no inscription on the Dağarcık Bridge indicating the date of construction or renovation. This masonry arch bridge is of great historical and architectural importance, since it is believed that it was built during the Roman era. The bridge has been registered as "Real Estate Cultural Asset required to be protected" by the decision of the Antalya Cultural and Natural Assets Protection Regional Board on January 23, 2015 (GDH 2021).

The Dağarcık Bridge consists of three masonry arches. Details of the geometry of the bridge are found in Fig. 2(a). In particular, from the downstream views of the structure shown in Figs. 2(a and b) and the upstream view shown in Fig. 2(c), it is obtained that the first (left) arch has a length of 3.28 m and a height of 2.44 m, and it consists of five stone sequences up to the keystone. The middle arch has a length of 3.20 m and a height of 2.67 m, and it consists of six stone sequences up to the keystone. The last arch has a length of 2.93 m and a height of 2.54 m, and it consists of five stone sequences up to the keystone (GDH 2021).

The masonry stones of the arch are made of travertine. Their mechanical properties were obtained from experimental investigation of the material in situ and literature studies presented in GDH (2021). In this article, due to its poor condition, the mortar between the stones has not been considered.

Proposed Structural Models

Adopted Constitutive Descriptions

Six nonlinear FEMs have been developed in this study to provide a holistic insight of the structural response for the considered masonry arch bridge, emphasizing potential collapse mechanisms. The first is a discrete model consisting of unilateral contact–friction interfaces used to simulate potential failure due to opening/sliding between the stones of the arch. Due to the presence of the contact laws assigned between the stones, the model is nonlinear. Linear elastic material properties are also considered for the stones.

The second model uses a continuum smeared cracking constitutive law to simulate compressive and tensile failure of the arch. This law is appropriate for monotonic loading, at low confining pressures.

An alternative, concrete damage plasticity, continuum constitutive description is considered in a third model. This is appropriate for the simulation of failure on quasi-brittle materials and may also be used when cyclic loads are considered. Damage variables are introduced in the material law to capture failure under tension and compression.

The fourth model uses the discrete approach with the unilateral contact–friction interfaces, but it is also enriched with the continuum concrete smeared crack model.

The fifth model adopts the discrete approach, enriched by the damage plasticity model.

(a) (b)

Fig. 1. Features of bridge under investigation: (a) view of middle span showing some damage on masonry stones at support; and (b) the keystone of the third arch. (Images reproduced from GDH 2021.)

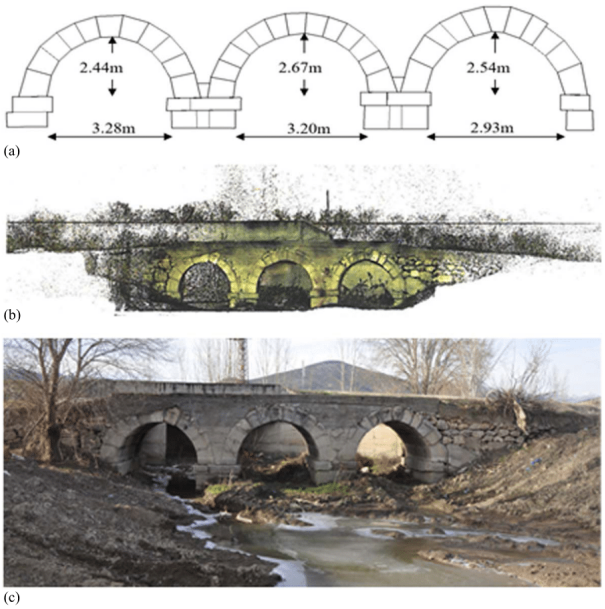

Fig. 2. Details of the geometry of the bridge: (a) schematic representation of the dimensions of the Dağarcık Bridge; (b) 3D point cloud of the Dağarcık Bridge; and (c) upstream view of the Dağarcık Bridge. [Images (b and c) reproduced from GDH 2021.]

Table 1. List of models developed

Model no.	Model description
1	Pure discrete
2	Continuum with concrete smeared cracking law
3	Continuum with concrete damage plasticity law
4	Discrete with concrete smeared cracking law
5	Discrete with concrete damage plasticity law
6	Continuum model for the arch and the fill, adopting the Mohr–Coulomb failure criterion for the fill and the concrete damage plasticity law for the arch

A final, sixth model is developed, incorporating the backfill, soil material above the arch, in the analysis. A Mohr–Coulomb failure law is adopted for the fill. The arch in this case is simulated using the continuum concrete damage plasticity law.

Note that the discrete models are useful in representing hinged failure mechanisms, after opening of the interfaces occurs. The continuum models can depict the type of failure experienced by the structure, either compressive or tensile. Combining the discrete and the continuum description in one model may lead to both opening of the interfaces (hinges) and compressive (or tensile) failure of the material (if any). Table 1 provides a list of the developed models.

General Description of Model

A FARO Focus3D X130 terrestrial laser scanner was used to create an accurate 3D model of a point cloud representing the geometry of the arch bridge. User requirements for the level of detail, the color, the selection of the coordinate system of reference and the type of the 3D product (Maravelakis et al. 2013) were defined during the initial planning of the project. The produced point cloud was then processed in AutoCAD, and a total of 200 individual building blocks of the arch bridge were manually extracted using selected points and profiles from the point cloud.

The geometry created was exported as a STEP file and was imported on Abaqus 6.12-3 (Hibbitt et al. 2012) for the creation of the FEMs. To simulate the different loading cases that the bridge may experience, both fixed supports and settlement of supports have been considered as the boundary conditions at the bottom side of the structure.

The developed models consist of 58,320 3D finite elements used to simulate the three arches [Fig. 3(a)]. Fig. 3(b) provides a closer view of the mesh density. The finite elements are eight-node solid elements (hexahedrons), with three displacement degrees of freedom at each node. In Figs. 3(c and d), the mesh of the structure is provided when the backfill soil material above the arch is included in the simulation.

Hinge Mechanism

The classical collapse mechanism of arch bridges, which was presented in Heyman (1982), has been adopted for the determination of the load-carrying capacity of stone arch bridges in previous studies, for instance in (Drosopoulos et al. 2008). This technique uses the funicular polygon as the fundamental tool of analyzing arches and is based on the estimation of the thrust line carrying the load on the arches. For a rectangular section of stones (voussoirs), the

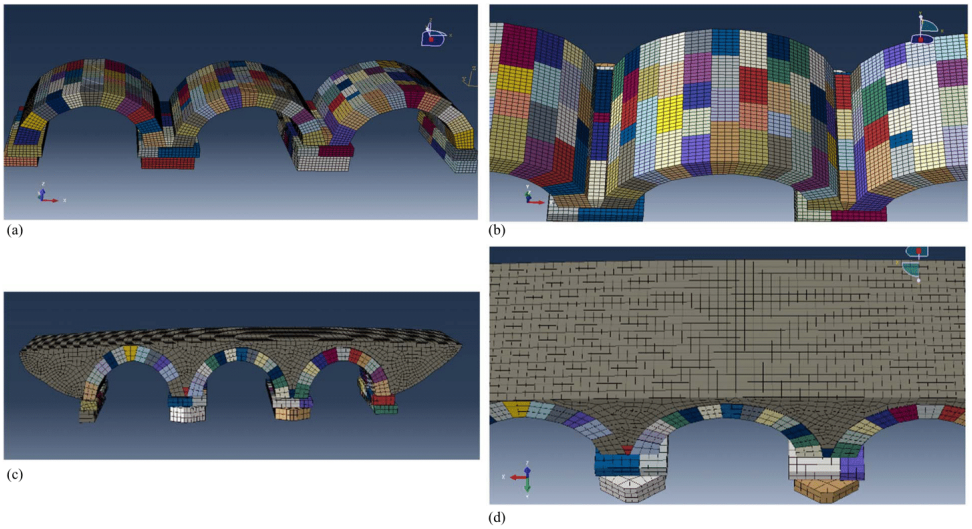

Fig. 3. Mesh of the used FEMs: (a) full view of bridge with masonry stones only; (b) closer view of bridge with masonry stones only; (c) full view of bridge with masonry stones and backfill; and (d) closer view of bridge with masonry stones and backfill.

thrust line lies within the middle third "core" of the section (Heyman 1982).

A hinge is formed when the thrust line in a cross section is adjacent to the ring of the arch, at an eccentricity e of the normal force P, from the center line of the arch. The resultant bending moment M is equal to Pe and is developed around the center line of the arch, assuming the arch is unreinforced and, therefore, does not develop any tensile strength. A single-span arch with two fixed supports has a determinacy degree of three. When three hinges are developed, the structure becomes statically determinate. Then, the development of a fourth hinge will turn the structure into a mechanism, leading to collapse. This collapse mechanism is common in unreinforced masonry arch bridges, with a vertical load acting at one-quarter of the span of the arch. According to Heyman (1982), this is the worst load position, resulting in the lowest resistance.

In the present study, a vertical load is applied at one-quarter of one of the spans of the bridge, acting together with the self-weight of the structure. According to Heyman (1982), compressive failure is not usually expected since the developed compressive stresses are generally low. However, the continuum laws that have been used can also capture this failure type.

Another outcome of the classical studies presented in Heyman (1982) is the description of the structural response of arches when settlement of supports takes place. These studies mentioned that if the abutments spread for a reason, "the arch could accommodate itself to the increased span by forming three hinges, one at the crown in the extrados, and one at each abutment in the intrados." The same studies also claimed that if the abutments are too close, "three hinges have again been formed to accommodate the decreased span, one at the crown in the intrados and one at each abutment in the extrados." In Drosopoulos et al. (2008), these conclusions were verified using nonlinear FEMs, in single-span, 2D arches. One of the aims of the present study is to highlight the validity of these conclusions for multispan arches.

Ultimate Behavior and Collapse Prediction within FEA

In the framework of FEA for masonry arch bridges, the ultimate strength of the bridge is defined as the point preceding collapse of the structure. When the structure is close to reaching its ultimate strength, the analysis becomes unstable due to the introduction of at least one zero eigenvalue on the tangential stiffness matrix. When the ultimate strength of the structure is finally reached, the analysis is terminated.

In the framework of FEA, the force–displacement diagram obtained at the end of the simulation is used to determine when the structure is close to collapse, as depicted by the end of the graph.

Material Properties Using the Concrete Smeared Crack and Damage Plasticity Model

A smeared crack concrete damage model and a concrete damage plasticity model are adopted in the study to consider the compressive and tensile failure of the masonry arch. The smeared crack model allows for the simulation of brittle materials, such as concrete and masonry, by incorporating the uniaxial tensile and compression behavior. According to this model, cracking is assumed to occur when the stress reaches a critical failure surface, provided by the relationship between the equivalent pressure stress and the Mises equivalent deviatoric stress.

In the framework of this model, no individual macrocracks are developed. In addition, the compressive response of the material is modeled by an elastoplastic theory. The post-failure behavior of the damaged material is modeled using a tension stiffening law and the corresponding stress–displacement diagram.

The second continuum approach introduces the concrete damage plasticity law. This is appropriate for quasi-brittle structures, for instance masonry and concrete, subjected to monotonic or cyclic actions. The main two failure mechanisms that can be depicted

Table 2. Concrete smeared cracking law parameters for the stones used in the arch bridge

Yield stress (MPa)	Compressive stress (MPa)	Ratio of uniaxial tension to compression failure stress	Ratio of biaxial to uniaxial compression failure stress
28	70	0.1	1.16

Table 3. Concrete damage plasticity model parameters for the stones used in the arch bridge

Dilation angle	Flow potential eccentricity	Ratio of biaxial to uniaxial compression failure stress	Ratio of second stress invariant of the tensile meridian to the compression meridian	Viscosity parameter
35	0.1	1.16	0.67	0

by this law are tensile cracking and compressive crushing. During unloading, the elastic stiffness of the material is considered damaged. This is depicted using two damage variables, one for tension and another for compression, both introduced in the model as functions of the plastic strains. These damage variables take values from zero, representing the undamaged material, to one, depicting total loss of strength of the material. If the initial elastic stiffness of the material is E_0, and d_t and d_c are the tensile and compressive damage variables, respectively, then the stress–strain relations under uniaxial tension and compression loading are provided by

$$\sigma_t = (1 - d_t)E_0(\varepsilon^t - \varepsilon^t_{pl}) \tag{1}$$

$$\sigma_c = (1 - d_c)E_0(\varepsilon^c - \varepsilon^c_{pl}) \tag{2}$$

Tables 2–6 and Figs. 4 and 5 provide all the material parameters used in these two constitutive descriptions. In addition, for all material laws, Young's modulus, Poisson's ratio, and the density values given in Table 6 are adopted. These correspond to the building material used to make the arch bridge, which is travertine (Erdoğan 2011; GDH 2021). The compressive strength of the travertine stone is 70 MPa and the tensile strength is approximately 10% of the compressive strength, 7 MPa. This is mentioned in *TS EN 1996-1-1+A1 Eurocode 6*, which is one of the codes to design arch bridges (CEN 2005; GDH 2021).

For the models that incorporate the backfill soil material found above the arch, a Mohr–Coulomb failure law is used to simulate damage on the fill. Table 7 lists the adopted parameters for this law.

Discrete Model for Arches

To simulate the contact conditions between each stone, principles taken from contact mechanics have been adopted. For a discrete structure, these relations are written for every point of a unilateral boundary or interface:

$$h = u - g \leq 0 \Rightarrow h \leq 0 \tag{3}$$

$$-t^n \geq 0 \tag{4}$$

$$t^n(u - g) = 0 \tag{5}$$

where u = single degree of freedom; and g = initial opening between the contacting bodies. The behavior in the tangential direction between the stone interfaces is defined by a static version of

Table 4. Compression behavior parameters for the concrete damage plasticity model for the stones used in the arch bridge

Yield stress (MPa)	Compressive strength (MPa)	$\varepsilon c0$ (strain at maximum compressive strength)	εccu (maximum strain)	εcpl (final plastic strain)
28	70	0.00887199	0.01774398	0.00177440

Table 5. Tension behavior parameters concrete damage plasticity model for the stones used in the arch bridge

Yield stress (MPa)	εtcr (strain at the tensile yield stress)	εtpl (final plastic strain)
7	0.00044360	0.00443599

Table 6. Mechanical properties for the stones used in the arch bridge

Material	Young's modulus E (GPa)	Density (kg/m^3)	Poisson's ratio
Travertine	15.780	2300	0.3

Source: Data from GDH (2021).

Table 7. Mechanical properties for fill used in the arch bridge

Young's modulus, E (GPa)	Poisson's ratio	Density (kg/m^3)	Angle of internal friction (degrees)	Cohesion (KPa)	Dilation angle (degrees)
0.3	0.3	2000	37	10	24

Source: Data from GDH (2021).

the Coulomb friction model. Two contacting surfaces start sliding when the shear stress in the interface reaches a critical value equal to:

$$t^t = \tau_{cr} = \pm\mu|t^n| \tag{6}$$

where t^t and t^n = shear stress and the contact pressure at a given point of the contacting surfaces, respectively; and μ = friction coefficient. There are two possible directions of sliding along an interface, so t^t can be positive or negative, depending on that direction. Furthermore, there is no sliding if $|t^t| < \mu|t^n|$ (stick conditions). The sliding rule can be summarized by the following relations:

$$|t^t| < \mu|t^n| \rightarrow u_t = 0 \text{ (no sliding)} \tag{7a}$$

$$t^t = \mu|t^n| \rightarrow u_t \geq 0 \text{ (sliding in one direction)} \tag{7b}$$

$$t^t = -\mu|t^n| \rightarrow u_t \leq 0 \text{(sliding in the opposite direction)} \tag{7c}$$

where u_t = displacement (sliding) in the tangential direction of an interface.

The Lagrange multiplier method is used to incorporate in the equilibrium equations, the unilateral contact–friction equations. Moreover, a friction coefficient equal to 0.5 is adopted in this study (Melbourne and Gilbert 1995). For the continuum models, a tie-constraint condition is considered for the interfaces between the masonry stones. This prevents sliding and opening at the interfaces, in all directions.

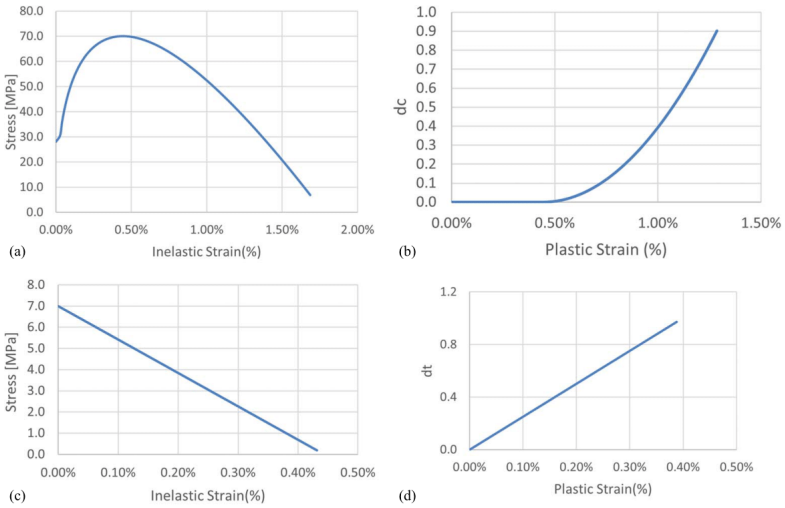

Fig. 4. Material response adopted within the concrete damage plasticity model: (a) compressive stress–inelastic strain; (b) compressive damage variable–inelastic strain; (c) tensile stress–inelastic strain; and (d) tensile damage variable–inelastic strain according to Lubliner et al. (1989) and Hognestad (1951).

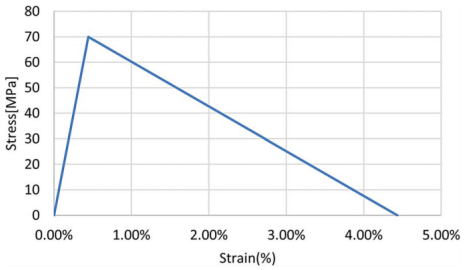

Fig. 5. Stress–displacement law adopted for the smeared cracking model according to Belarbi and Hsu (1994) and Lubliner et al. (1989).

Results and Discussions

Load Cases

In the present study, the structural behavior of a masonry arch bridge is investigated using different load types and adopting different numerical models to predict the structural response.

The different load types that are implemented are based on critical load cases that the bridge is likely to experience in situ. These load cases include loads applied as forces and displacements in the plane, as well as in the out-of-plane direction of the bridge, in different positions. In particular, the following load cases are considered: (a) a vertical load applied at about one-quarter of the middle span of the bridge, to determine the ultimate strength; (b) a horizontal, outward displacement of 100 mm in the plane of the bridge, on both outer supports, representing settlement of supports; (c) a horizontal inward displacement of 100 mm in the plane of the bridge on both supports; (d) 100 mm horizontal displacement of the two internal supports in the direction of the water flow, perpendicular to the plane of the bridge; (e) a vertical load applied at about

Table 8. List of load cases considered in the study

Load case no.	Load case description
(a)	Vertical load applied at about one-quarter of the middle span of the bridge.
(b)	Horizontal, outward displacement of 100 mm in the plane of the bridge, on both outer supports.
(c)	Horizontal inward displacement of 100 mm in the plane of the bridge on both outer supports.
(d)	100-mm horizontal displacement of the two internal supports in the direction of the water flow, perpendicular to the plane of the bridge.
(e)	Vertical load applied at about one-quarter span of the middle span of the bridge with 20-mm displacement of the two internal supports in the direction of the water flow perpendicular to the plane of the bridge.
(f)	100-mm downward displacement of the two internal supports.
(g)	Vertical load applied at about one-quarter span of the middle span of the bridge with 20-mm downward displacement of the two internal supports.
(h)	Incorporation of backfill; horizontal, outward displacement of 100 mm in the plane of the bridge, on both outer supports.
(i)	Incorporation of backfill; horizontal inward displacement of 100 mm in the plane of the bridge on both outer supports.
(j)	Incorporation of backfill;100-mm horizontal displacement of the two internal supports in the direction of the water flow, perpendicular to the plane of the bridge.
(k)	Incorporation of backfill; vertical load applied at about one-quarter of the middle span of the bridge.

one-quarter span of the middle span of the bridge with 20 mm displacement of the two internal supports in the direction of the water flow perpendicular to the plane of the bridge; (f) 100 mm vertical displacement of the two internal supports in the downward direction; and (g) a vertical load applied at about one-quarter span of the middle span of the bridge with 20 mm vertical displacement of the two internal supports in the downward direction. The first four load cases are also considered for the model with backfill above the arch. Note that the vertical load is equally distributed into five points along the width of the bridge, to minimize the effects of localized failure. Table 8 lists all load cases.

In the developed numerical models, two steps are considered. The first is a dynamic implicit analysis step, in a quasistatic framework that introduces a gravity load (self-weight of the structure) of 9.81 m/s^2. When a general static analysis was considered in the first step, numerical singularities did not allow the model to reach convergence, due to the extensive number of unilateral contact–friction interfaces that are used to simulate the contact conditions between each stone. This numerical instability was attributed to multiple micro openings/closures between stone interfaces, resulting in unstable stiffness matrices. To overcome this problem, a dynamic implicit analysis in a quasistatic framework was used. This introduced the mass stiffness in the equilibrium equations, resulting in a more stable stiffness matrix. Then, a second step is applied, with the particular loading already described.

Discrete Models with and without Concrete Plasticity Laws

This section presents results of the three discrete models with the linear elastic, smeared cracking, and damage plasticity constitutive description for the different load cases. Within the first load case, a

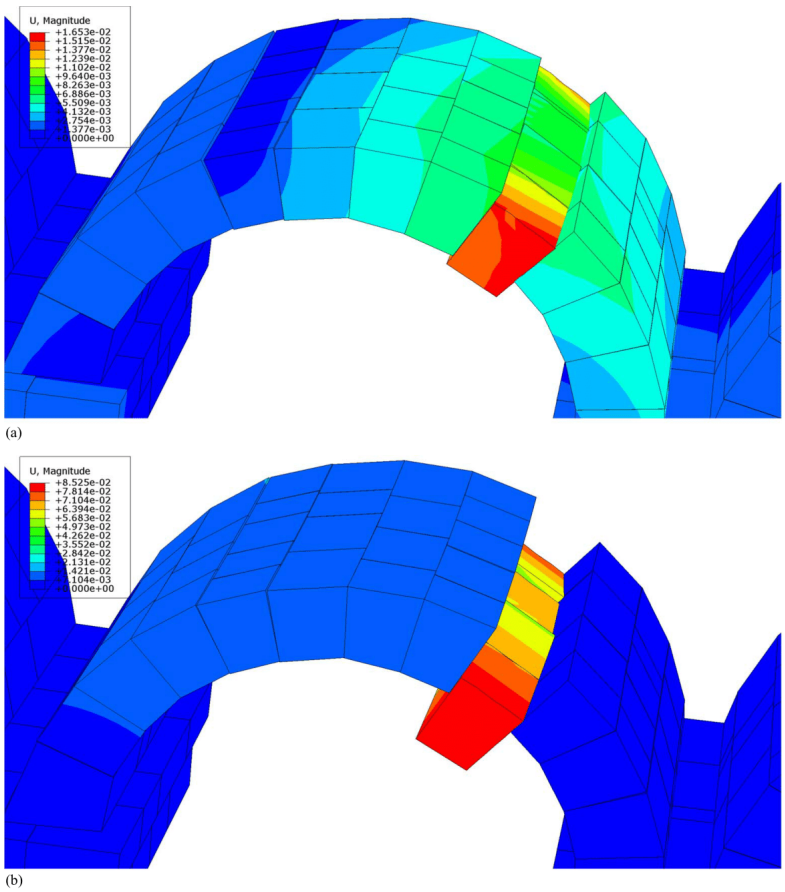

Fig. 6. Displacement (m) due to a vertical load obtained from the pure discrete model: (a) at an intermediate load step (Scale factor 10); and (b) at the final load step (Scale factor 5).

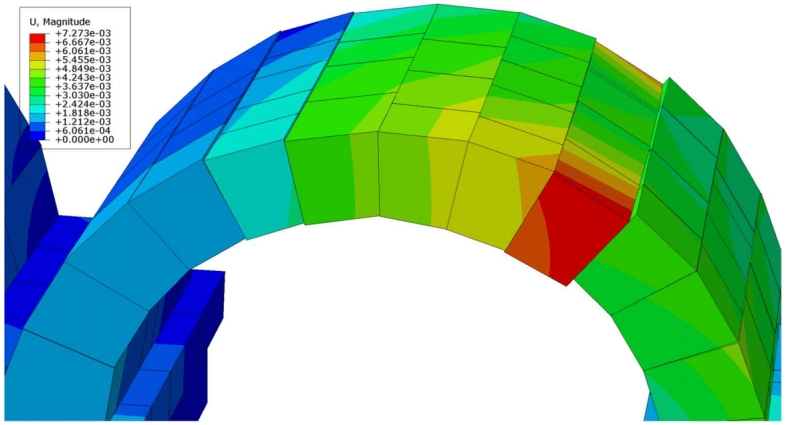

Fig. 7. Displacement (m) due to a vertical load obtained from the discrete model with the concrete damage plasticity law at the final load step (Scale factor 10).

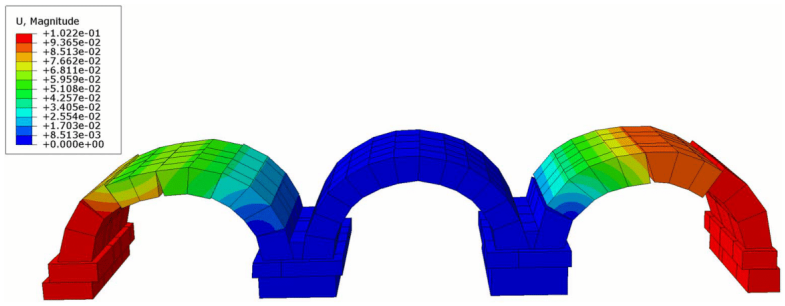

Fig. 8. Displacement (m) for outward horizontal settlements of the two outer supports (Scale factor 3) for the pure discrete model.

vertical load is applied at about one-quarter of the middle span, to determine the ultimate strength of the structure. Results indicate that a local sliding of the stones near the point of application of the vertical force is obtained from the three discrete models. In addition, although the four-hinge mechanism does not clearly appear, two more hinges arise to the left and right of the point force (extrados opening). The fourth hinge, which would normally appear close to the left support of the loaded arch in the classical four-hinge mechanism, only slightly emerges in the present models, but cannot be depicted in the image.

This is shown for the pure discrete model in Figs. 6(a and b), where a scale factor has been used to magnify the obtained displacements and better highlight the hinges. A similar result is obtained from the discrete models that use the plasticity laws, as depicted in Fig. 7, noting that for these models a local failure of the material near the point of application of the vertical load also arises.

These figures show that the pure discrete model results in higher displacements [Fig. 6(b)], compared with the ones that use plasticity laws (Fig. 7). This observation, highlighting a more brittle behavior due to usage of the plasticity laws, is also derived for the majority of the presented results.

Next, horizontal, outward, in-plane settlements of the supports of the outer arches have been applied to the three discrete models. Fig. 8 shows the plot of the final displacements for outward settlement of 100 mm in both outer supports, which could arise due to erosion of the riverbed and riverbank, and the soil in the vicinity of the supports. This figure clearly shows that the three-hinge mechanism described in the classical studies of Heyman (1982) for similar settlement of supports also arises here for the three-span arch. In particular, similar to Heyman (1982), one hinge appears at the crown at the extrados of the arches (opening at the intrados) and one at each support in the intrados (opening at the extrados). For the right outer arch, a sliding instead of an opening arises at the position where the right hinge would appear. Note that the same mechanism appears for the three discrete models, without any material failure (except the hinges).

Fig. 9 shows the plot of the final displacements of the structure when an inward movement of 100 mm is considered for the outer supports. According to this figure, sliding arises in this case at

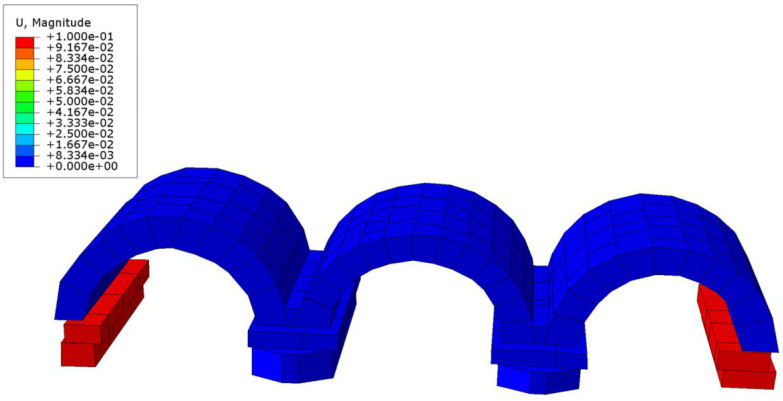

Fig. 9. Displacement (m) for inward horizontal settlements of the two outer supports (Scale factor 3) for the discrete model with the concrete damage plasticity law.

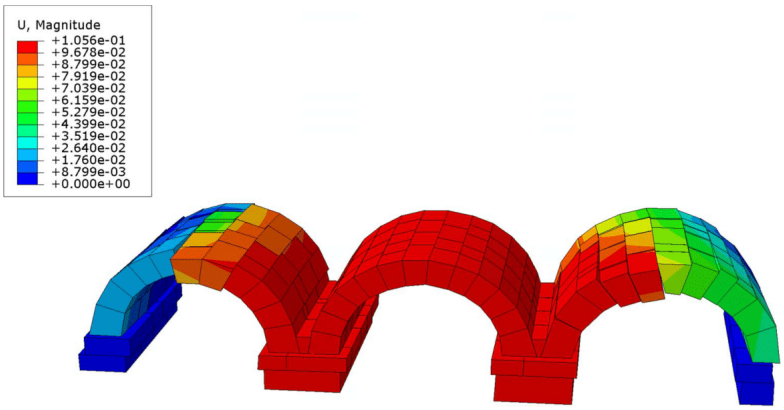

Fig. 10. Displacements (m) for out of plane settlements of the two inner supports (Scale factor 5) for the discrete model.

the two supports of the bridge. Thus, contrary to the case of outward settlement of supports, where a three-hinge mechanism appeared, for inward settlement the mechanism changes to sliding failure. For the discrete models with the plasticity laws, no failure on the material arises.

Fig. 10 shows the plot of the final displacements of the bridge when an out-of-plane settlement of 100 mm occurs on the two internal supports in the direction of the water flow. Since the outer supports are fixed, the structure develops an out-of-plane bending response, resulting in the opening of hinges at the two outer arches (Fig. 10). These hinges develop at the top of the two outer arches as well as at the supports of the right arch. The middle arch does not develop any particular damage.

An additional analysis has been conducted, combining the out of plane settlement of the inner supports and the vertical point force at one-quarter of the span of the middle arch. Results in this case resemble the ones presented in Figs. 6 and 7, and thus they mainly involve the hinge opening at the middle arch, where the vertical load is applied.

The plot of the maximum principal stresses is provided in Fig. 11, when a downward settlement of 100 mm of the two internal supports is considered. According to this figure, two hinges open in the outer arches, one closer to each inner support (opening intrados) and another closer to the outer support (opening extrados). It is also noted that the position of the hinge closer to the inner support is different in the two outer arches. A similar hinge-mechanism for downward settlement of supports is derived in Drosopoulos et al. (2008) for 2D, single-arch bridges.

The plot of the maximum principal stresses is shown in Fig. 12, for a final load case of a vertical load equal to 100 kN applied at about one-quarter of the span of the middle span of the bridge together with a 20 mm downward movement of the two internal

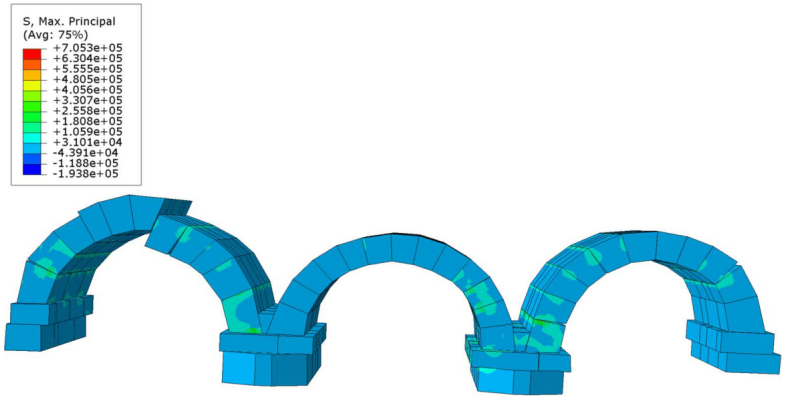

Fig. 11. Principal stresses (Pa) for downward settlements of the two inner supports (Scale factor 5) for the discrete model.

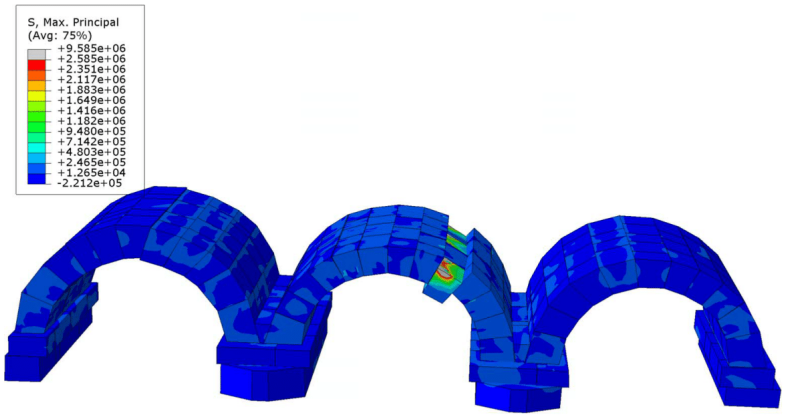

Fig. 12. Principal stresses (Pa) for downward settlements of the two inner supports (Scale factor 5) accompanied by a vertical force at the middle arch, for the discrete model.

supports. Contrary to the case of downward settlement of support without any vertical load shown in Fig. 11, the two hinges are not developed in the outer arches. Instead, only one hinge is developed in the outer left arch, while no hinge appears in the outer right arch, as depicted in Fig. 12. Hinges arise in the middle arch due to the vertical point force.

Continuum Models

This section shows the failure of the bridge by using the plastic strain distribution, arising when different load cases are applied. Within the continuum models, no opening or sliding between the masonry bricks can be depicted. Instead, material failure may be derived due to compressive or tensile response.

Within the first load case, a downward vertical force is applied to one-quarter of the span of the middle arch. The model with the smeared cracking constitutive description did not provide any failure mechanism, except local failure near the points of applications of the load. Conversely, the model with the concrete damage plasticity law resulted in the failure response shown in Fig. 13. Thus, failure appears in four regions of the arch. It is noted that the same mechanism arises in single-span arches, according to classical studies (Heyman 1982).

For the outward displacement of the two outer supports, the simulation with the smeared cracking continuum model terminated early, due to convergence issues, arising from the brittle response that is depicted in this constitutive law. Conversely, the concrete damage plasticity model provided a much-improved convergence response, allowing for the representation of damage. The three-hinge mechanism, which is derived in the classical studies of Heyman (1982) and is also obtained from the discrete models of the previous section, appears in this case too, as shown in Fig. 14.

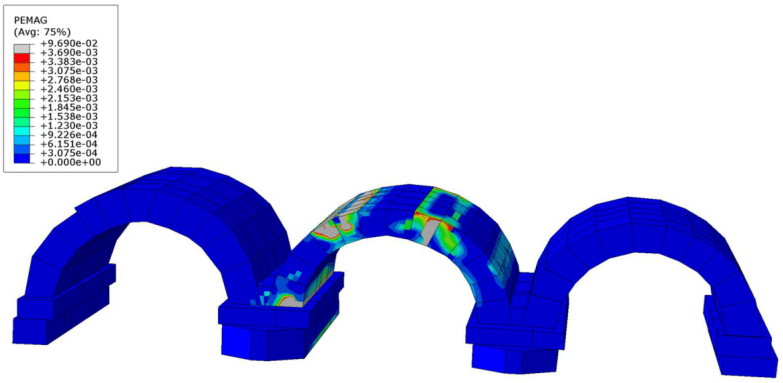

Fig. 13. Plastic strain distribution developed in the concrete damage plasticity continuum model, for a vertical load applied at the one-quarter span of the middle arch.

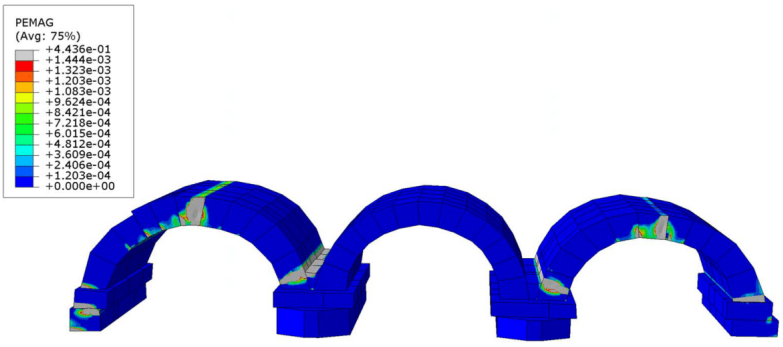

Fig. 14. Plastic strain distribution developed in the concrete damage plasticity continuum model, for outward horizontal settlement of the two outer supports.

According to this figure, the hinge at the crown is in the same position as the one derived from the discrete model in Fig. 8. However, the two remaining hinges at the supports appear lower (toward the ground), compared with the discrete models shown in Fig. 8.

When an inward settlement of the outer supports by 100 mm is applied on the continuum smeared cracking model, analysis terminates early due to convergence issues, and no plastic strain arises. On the contrary, the simulation with the concrete damage plasticity model proceeds and allows the representation of a three-hinge mechanism, as shown in Fig. 15. Note that the discrete approach presented in the previous section resulted in sliding failure mode at the supports.

For an out-of-plane settlement of the two internal supports of the bridge, tensile failure takes place at the outer arches, as shown in Fig. 16 for the continuum damage plasticity model. This is attributed to the out-of-plane bending response of the structure. Failure in this case is mainly developed at the top of these arches as well as at the supports. A similar failure mode is obtained from the discrete model shown in Fig. 10. For the same load case, a limited compressive failure also appears in the opposite face of the structure, as shown in Fig. 17.

When an out-of-plane settlement of 20 mm on the two internal supports of the bridge is combined with a vertical load of 100 kN applied at one-quarter of the span of the middle arch, plastic strain is experienced on the outer side of the middle supports. Note that a similar failure behavior was obtained (Fig. 16) for the case out-of-plane settlement of the inner supports (without vertical point load), indicating that the out-of-plane movement is the critical loading.

For a downward settlement of the two internal supports, the plastic strain distribution shown in Fig. 18 is obtained from the concrete damage plasticity model. As depicted in the figure, for each outer arch, two hinges are developed, one close to the internal support and another close to the external one. A similar hinge-pattern is also derived in Drosopoulos et al. (2008). Moreover, the discrete model's response given in Fig. 11 results in a similar hinge-mechanism, but the position of the hinge in the proximity of the internal support of the left outer arch is different compared with the corresponding hinge shown in Fig. 18.

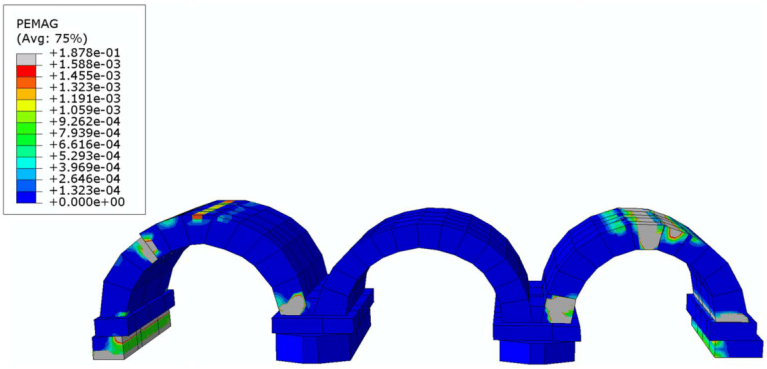

Fig. 15. Plastic strain distribution developed in the concrete damage plasticity continuum model, for inward horizontal settlement of the two outer supports.

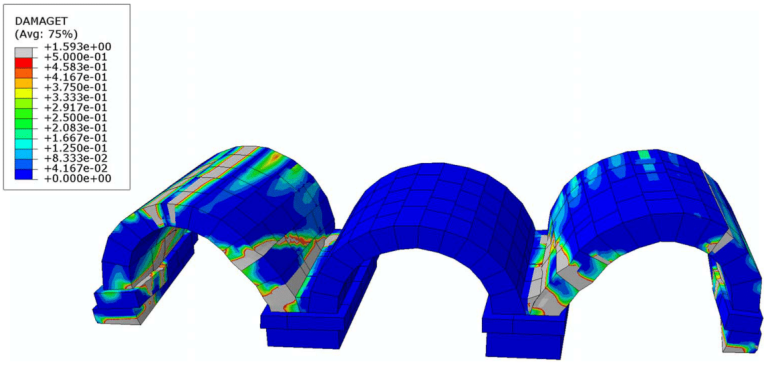

Fig. 16. Plastic strain distribution highlighting tensile damage developed in the concrete damage plasticity continuum model, for out-of-plane settlement of the two inner supports.

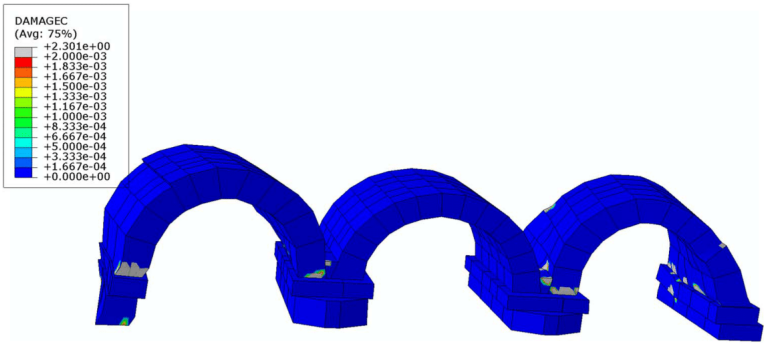

Fig. 17. Plastic strain distribution highlighting compressive damage developed in the concrete damage plasticity continuum model, for out-of-plane settlement of the two inner supports.

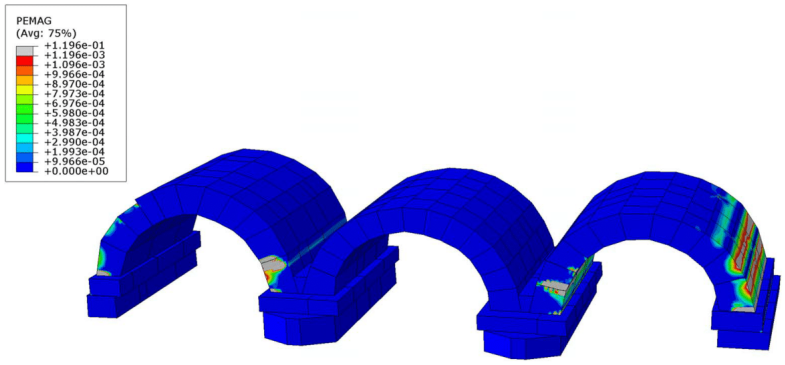

Fig. 18. Plastic strain distribution developed in the concrete damage plasticity continuum model, for downward settlement of the two inner supports.

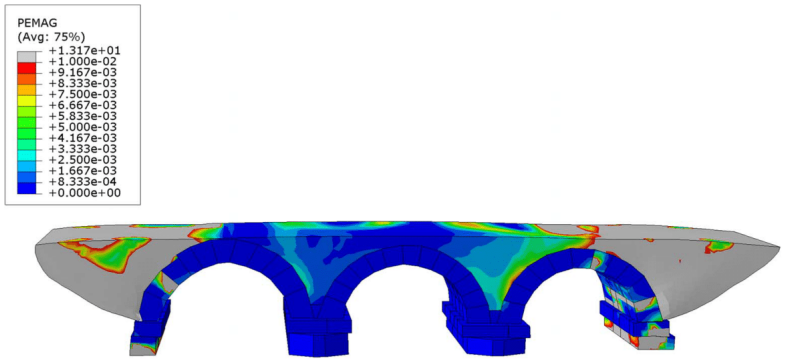

Fig. 19. Plastic strain distribution developed in the concrete damage plasticity continuum model with the backfill, for outward horizontal settlement of the two outer supports.

For a final load case, a vertical load of 100 kN is applied at about one-quarter of the span of the middle span of the bridge, together with a 20-mm downward movement of the two internal supports. Results indicate a similar failure pattern with the one depicted in Fig. 18, where downward settlement of the middle supports is considered, without any vertical load.

Influence of Backfill on Structural Response

The presence of soil backfill above the arch provides a better load distribution through the body of the backfill toward the arch, which is the main structural component. It also increases the compression above the arch. To highlight the influence of the backfill material on the overall response, a new model is developed, where backfill is simulated using 3D finite elements [Figs. 3(c and d)]. For the arch, the continuum concrete damage plasticity law has been considered. The goal of this investigation is to discuss the influence of the backfill on the response by conducting a comparison with the corresponding results when no backfill was considered.

Four load cases have been implemented in this case, namely the horizontal, outward, and inward settlement of the outer supports, the out-of-plane settlement of the middle supports, and the vertical downward force.

Fig. 19 shows the plastic strain distribution for outward settlement of the outer supports. It is clear that a quite significant failure on the backfill is observed, which is attributed to the low-quality material properties that have been assigned to it. However, note that concerning the response of the arch, although some failure is developed, this is limited compared with the results obtained from the same load case without the backfill (Fig. 14). In particular, three hinges were developed in the outer arches: one in the crown and two in the supports. According to Fig. 19, the hinges close to the internal support of each outer arch are not developed. In addition, in the left arch, the top hinge is not developed exactly in the middle of the span but toward the left side. Both comments indicate a change in the hinge-mechanism of the arch compared with the analysis without the backfill.

For the case of inward settlement of the two outer supports, Fig. 20 indicates that three hinges arise in the arch. Their position

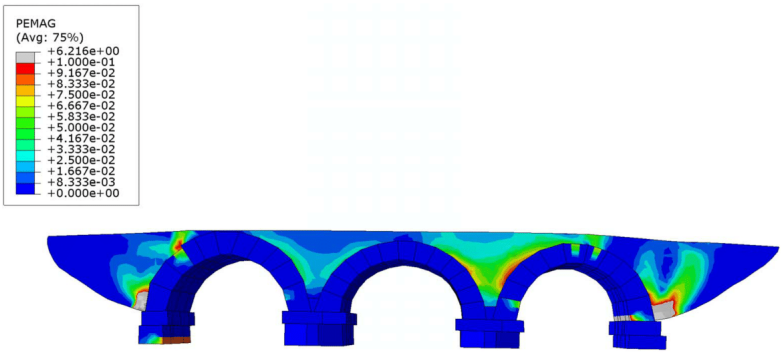

Fig. 20. Plastic strain distribution developed in the concrete damage plasticity continuum model with the backfill, for inward horizontal settlement of the two outer supports.

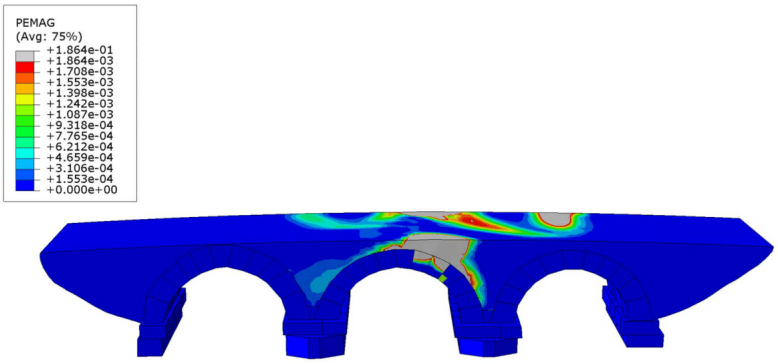

Fig. 21. Plastic strain distribution developed in the concrete damage plasticity continuum model with the backfill, for a vertical downward force applied on the backfill, in the position of one-quarter span of the middle arch.

is the same with the position of the hinges in the model without the backfill (Fig. 15), however their distribution in the arch is limited, compared with Fig. 15.

The load case with the out-of-plane settlement of the two inner supports results in a similar plastic strain distribution in the body of the arch, compared with the one received from the model without the backfill (Figs. 16 and 17).

For the last load case, where a vertical downward force is applied on the backfill, in a position near one-quarter of the middle span, the plastic strain distribution shown in Fig. 21 arises. According to this figure, failure on the arch is mainly developed near the point of the load application. Conversely, when the backfill was not considered (Fig. 13), failure on the arch developed in four points, resembling the traditional, four-hinge mechanism.

Force–Displacement Diagrams

Within FEA, force–displacement diagrams can be used to determine the point of failure of a structure. Fig. 22 shows the force–displacement diagrams obtained from the different numerical models, which were subject to a vertical load and to a combination of vertical load plus settlement of supports. Note that the continuum models lead to a stiffer response for (pure) vertical loading, compared with the discrete models.

In addition, the hinge formation mechanism is the most likely cause of failure compared with material failure in compression, since compressive failure was observed only in one case (limited compressive failure for out-of-plane settlement of support; Fig. 17). The numerical models with out-of-plane settlement of supports and with vertical settlement of internal supports combined with a vertical load are highly unstable. For these load cases, the smeared cracking models resulted in a very low ultimate load, compared with the discrete models. This is due to the brittle response of the smeared cracking law when tensile failure arises. Conversely, the discrete model allows for activation (opening–sliding) of the interfaces, which then leads to redistribution of forces until a collapse mechanism arises, resulting in a higher ultimate load compared with the continuum model.

The concrete damage plasticity models provided the capacity to properly describe the quasistatic response of masonry arches. For

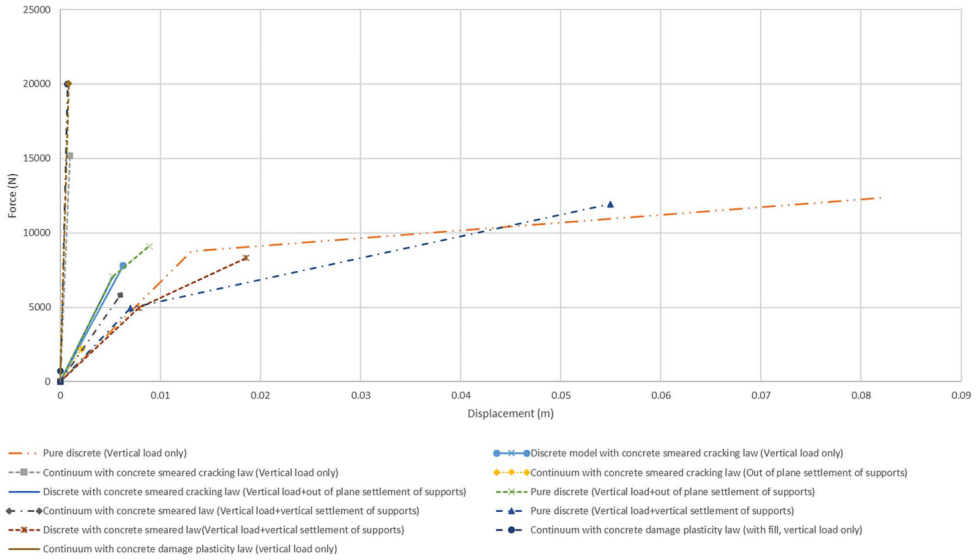

Fig. 22. Force–displacement diagrams for the discrete and the continuum models assigned a vertical downward load.

the same initial load considered in the previous simulations, this constitutive description leads to a stiff response. For a significantly higher initial load, the force–displacement graph becomes nonlinear, and the four-hinge mechanism shown in Fig. 13 arises.

Conclusions and Further Recommendations

This study used nonlinear FEMs to investigate the structural behavior of a masonry arch bridge. Various loading cases which can be experienced by the structure were considered, including settlement of supports. This type of loading may appear due to erosion and heavy water flow. The numerical models used for the structural analysis were developed based on in situ survey of the existing geometry. The 3D geometry used for the investigation was obtained on AutoCAD, using a cloud of points of the bridge collected by researchers in Turkey. A terrestrial laser scanner was used to obtain these points. The geometry was then imported in Abaqus, which is a commercial finite-element package.

Two modeling approaches were considered: adopting a discrete and a continuum constitutive description. According to the first approach, unilateral frictional contact interfaces were used to simulate the real contact conditions between the stones. Within the second approach, continuum constitutive descriptions were used, relying on a smeared cracking formulation and on a concrete damage plasticity law. The developed models were strongly nonlinear due to the presence of the interfaces and of the nonlinear material description. The Newton–Raphson incremental–iterative process was used to solve the numerical problem.

From the different FEMs presented in this study, different failure modes of the masonry arch were observed for the various load cases.

The following conclusions can be drawn from this study:

- The critical failure pattern obtained from the discrete models is the formation of hinge-mechanisms, which can be developed both in plane and out of plane, for corresponding loads. It is observed that the three hinge-mechanisms obtained in published research for horizontal, outward, and inward settlement of supports of single-arch bridges also arises from the discrete approach, adopted in this article for multispan arches. Similarly, when a vertical, downward settlement of the supports takes place, two hinges are developed in the affected arches. The same conclusion has been derived in past studies for single-span arches. A four-hinge failure mechanism arises for a vertical load at the middle arch.
- The numerical models that compute the out-of-plane loads are computationally expensive and highly unstable; hence, the corresponding simulations terminate before the full load is assigned.
- The contribution of the backfill soil material, which is found above the arch, may significantly influence the structural response. It is shown in this study that the presence of backfill may alter the failure pattern in the arch, leading to limited damage.
- The difference in the mechanical response, which is derived from discrete and continuum laws, is highlighted in the article. The discrete approach allows for the formation of hinges and sliding failure modes, resulting in a more flexible approximation of the structural response. Conversely, the continuum approach leads to a stiffer response. In addition, the discrete approach may lead to numerical instabilities and increased computational cost due to the presence of multiple unilateral contact–friction interfaces.
- The continuum approach results in easy modeling. Tensile plastic strain distribution is the dominant failure pattern depicted by this approach. Numerical instabilities may arise when point forces are considered, due to local failure near the points of

the load application. From the two continuum constitutive descriptions, the smeared cracking law results in convergence difficulties attributed to the brittle nature of this description. The concrete damage plasticity law, making use of damage variables, better describes the quasi-brittle response of the masonry arch. The failure patterns that are obtained from the continuum concrete damage plasticity law are similar to the ones derived from the discrete approach and the results found in published research.

Future research may include the investigation of the influence of the spandrel walls on the mechanical response of masonry arch bridges. Finally, the incorporation of other advanced numerical tools in the study of arches, such as the cohesive zone modeling approach, is also left for future investigation.

Acknowledgments

The authors thank the General Directorate of Highways of Turkey for providing access to the data of the presented monument.

Data Availability Statement

All data, models, and code generated or used during the study appear in the published article.

References

Armesto, J., J. Roca-Pardiñas, H. Lorenzo, and P. Arias. 2010. "Modelling masonry arches shape using terrestrial laser scanning data and nonparametric methods." *Eng. Struct.* 32 (2): 607–615. https://doi.org/10.1016/j.engstruct.2009.11.007.

Ashurst, D. 1992. *An assessment of repair and strengthening techniques for brick and stone masonry arch bridges*. Richmond, UK: The National Archives.

Ataei, S., M. Jahangiri Alikamar, and V. Kazemiashtiani. 2016. "Evaluation of axle load increasing on a monumental masonry arch bridge based on field load testing." *Constr. Build. Mater.* 116: 413–421. https://doi.org/10.1016/j.conbuildmat.2016.04.126.

Belarbi, A., and T. T. Hsu. 1994. "Constitutive laws of concrete in tension and reinforcing bars stiffened by concrete." *Struct. J.* 91 (4): 465–474.

Campbell, J. W., and M. Tutton. 2013. *Staircases: History, repair and conservation*. London: Routledge.

Casapulla, C., E. Mousavian, and M. Zarghani. 2019. "A digital tool to design structurally feasible semi-circular masonry arches composed of interlocking blocks." *Comput. Structu.* 221: 111–126. https://doi.org/10.1016/j.compstruc.2019.05.001.

Catalan, R., and L. Aldea. 2007. "New tendencies on repair and strengthening on masonry arch bridges." In *Proc., 5th Int. Conf. on Arch Bridges*, 12–14. Braga, Portugal: Universidade do Minho.

CEN (European Committee for Standardization). 2005. *Design of masonry structures. Part 1-1: General rules for reinforced and unreinforced masonry structures*. Eurocode 6. Brussels, Belgium: CEN.

Conde, B., L. F. Ramos, D. V. Oliveira, B. Riveiro, and M. Solla. 2017. "Structural assessment of masonry arch bridges by combination of nondestructive testing techniques and three-dimensional numerical modelling: Application to Vilanova bridge." *Eng. Struct.* 148: 621–638. https://doi.org/10.1016/j.engstruct.2017.07.011.

Crisfield, M. 1985. *Finite element and mechanism methods for the analysis of masonry and brickwork arches*. Research Rep. Berkshire, UK: Transport and Road Research Laboratory.

Domede, N., A. Sellier, and T. Stablon. 2013. "Structural analysis of a multispan railway masonry bridge combining in situ observations, laboratory tests and damage modelling." *Eng. Struct.* 56: 837–849. https://doi.org/10.1016/j.engstruct.2013.05.052.

Drosopoulos, G. A., G. E. Stavroulakis, and C. V. Massalas. 2008. "Influence of the geometry and the abutments movement on the collapse of stone arch bridges." *Constr. Build. Mater.* 22 (3): 200–210. https://doi.org/10.1016/j.conbuildmat.2006.09.001.

Erdoğan, Y. 2011. "Engineering properties of Turkish travertines." *Sci. Res. Essays* 6 (21): 4551–4566. https://doi.org/10.5897/SRE11.795.

Ford, T., C. Augarde, and S. Tuxford. 2003. "Modelling masonry arch bridges using commercial finite element software." In *Proc., 9th Int. Conf. on Civil and Structural Engineering Computing*, edited by B. H. V. Topping, 161–203. Stirlingshire, UK: Civil-Comp Press.

GDH (General Directorate of Highways). 2021. *Burdur province, Bucak district, Dağarcık bridge*. [In Turkish.] Technical Rep. Ankara, Turkey: GDH.

Gönen, S., and S. Soyöz. 2021. "Seismic analysis of a masonry arch bridge using multiple methodologies." *Eng. Struct.* 226: 111354. https://doi.org/10.1016/j.engstruct.2020.111354.

Guastavino, R., and R. G. Moreno. 2006. *Escritos sobre la construcción cohesiva y su función en la arquitectura*. Barcelona, España: Reverte.

Heyman, J. 1982. *The masonry arch*. Chichester, UK: Ellis Horwood.

Hibbitt, D., B. Karlsson, and P. Sorensen. 2012. *Abaqus 6.12. 3 manual*. Providence, RI: SIMULIA.

Hognestad, E. 1951. *Study of combined bending and axial load in reinforced concrete members*. Urbana, IL: Univ. of Illinois at Urbana Champaign, College of Engineering.

Hughes, T., and M. Blackler. 1997. "A review of the UK masonry arch assessment methods." *Proc. Inst. Civ. Eng. Struct. Build.* 122 (3): 305–315. https://doi.org/10.1680/istbu.1997.29801.

Hughes, T. G., S. C. Hee, and E. Soms. 2002. "Mechanism analysis of single span masonry arch bridges using a spreadsheet." *Proc. Inst. Civ. Eng. Struct. Build.* 152 (4): 341–350. https://doi.org/10.1680/stbu.2002.152.4.341.

Lubliner, J., J. Oliver, S. Oller, and E. Oñate. 1989. "A plastic-damage model for concrete." *Int. J. Solids Struct.* 25 (3): 299–326. https://doi.org/10.1016/0020-7683(89)90050-4.

Lubowiecka, I., J. Armesto, P. Arias, and H. Lorenzo. 2009. "Historic bridge modelling using laser scanning, ground penetrating radar and finite element methods in the context of structural dynamics." *Eng. Struct.* 31 (11): 2667–2676. https://doi.org/10.1016/j.engstruct.2009.06.018.

Maravelakis, E., A. Konstantaras, A. Kritsotaki, D. Angelakis, and M. Xinogalos. 2013. "Analysing user needs for a unified 3D metadata recording and exploitation of cultural heritage monuments system." In *9th Int. Symp. Visual Computing*, 138–147. Berlin: Springer.

Melbourne, C. 1991. "Conservation of masonry arches." In *Proc., 9th Int. Brick/Block Masonry Conf.*, 1563–1570. Berlin: Deutsche Gesellschaft für Maurerwerksbau e.V.

Melbourne, C., and M. Gilbert. 1995. "The behavior of multiring brickwork arch bridges." *Struct. Eng.* 73 (3): 39–47.

Melbourne, C., L. McKibbins, N. Sawar, and C. Sicilia Gaillard. 2006. *Masonry arch bridges: condition appraisal and remedial treatment*. London: CIRIA.

Motsa, S. M., G. A. Drosopoulos, M. E. Stavroulaki, E. Maravelakis, R. P. Borg, P. Galea, S. d'Amico, and G. E. Stavroulakis. 2020. "Structural investigation of Mnajdra megalithic monument in Malta." *J. Cult. Heritage* 41: 96–105. https://doi.org/10.1016/j.culher.2019.07.004.

Mousavian, E., and C. Casapulla. 2020. "Quantifiable feasibility check of masonry assemblages composed of interlocking blocks." *Adv. Eng. Software* 149: 102898. https://doi.org/10.1016/j.advengsoft.2020.102898.

Page, J. 1993. *Masonry arch bridges*. Transport Research Laboratory. London: HMSO.

Pulatsu, B., E. Erdogmus, and P. B. Lourenço. 2019. "Comparison of in-plane and out-of-plane failure modes of masonry arch bridges using discontinuum analysis." *Eng. Struct.* 178: 24–36. https://doi.org/10.1016/j.engstruct.2018.10.016.

RING. 2021. "LimitState:RING - Powerful masonry arch analysis software." Accessed February 3, 2021. https://www.limitstate.com/ring.

Sarhosis, V., S. De Santis, and G. de Felice. 2016. "A review of experimental investigations and assessment methods for masonry arch bridges." *Struct. Infrastruct. Eng.* 12 (11): 1439–1464.

Sevim, B., A. Bayraktar, A. Altunişik, S. Atamturktur, and F. Birinci. 2011. "Assessment of nonlinear seismic performance of a restored historical arch bridge using ambient vibrations." *Nonlinear Dyn.* 63: 755–770. https://doi.org/10.1007/s11071-010-9835-y.

Towler, K. D. S. 1985. "Applications of non-linear finite element codes to masonry arches." In *Proc., 2nd Int. Conf. on Civil and Structural Engineering Computing*, edited by B. H. V. Topping, 197–202. Edinburgh, UK: Civil-Comp Press.

Van Beek, G. W. 1987. "Arches and vaults in the ancient Near East." *Sci. Am.* 257 (1): 96–103. https://doi.org/10.1038/scientificamerican0787-96.

Wilmers, W. 2012. "Restoration of masonry arch bridges." *Proc. Inst. Civ. Eng. Bridge Eng.* 165: 135–146.

Zampieri, P., G. Tecchio, F. Da Porto, and C. Modena. 2015. "Limit analysis of transverse seismic capacity of multispan masonry arch bridges." *Bull. Earthquake Eng.* 13 (5): 1557–1579. https://doi.org/10.1007/s10518-014-9664-3.

Chapter 5 – Modelling, identification and structural damage investigation of the Neoria monument in Chania

In this section, the identification and evaluation of the structural damage of the Neoria monument in Chania is investigated and the findings are published in *Developments in the Built Environment*, Received: 9 November 2021; Received in revised form 31 January 2022; Accepted 17 February 2022 /Available online 24 February 2022

Developments in the Built Environment 10 (2022) 100069

Contents lists available at ScienceDirect

Developments in the Built Environment

journal homepage: www.sciencedirect.com/journal/developments-in-the-built-environment

Modelling, identification and structural damage investigation of the Neoria monument in Chania

Barbara Charalambidi [a,1], Panagiotis Koutsianitis [a,1], Siphesihle Mpho Motsa [b], Georgios Tairidis [a], Amalia Kasampali [a,1], Georgios Drosopoulos [b,c], Maria Stavroulaki [a,1], Georgios Stavroulakis [a,1,*]

[a] Technical University of Crete, Chania, 73100, Greece
[b] University of Kwazulu-Natal, Durban, South Africa
[c] University of Central Lancashire, Preston, United Kingdom

ARTICLE INFO

Keywords:
Finite element analysis
Monuments
Modal assurance criterion
Pushover analysis
Damage evaluation
Performance prediction

ABSTRACT

The structural behavior of Neoria masonry monument is studied here. The determination of structural and material properties of a partially collapsed monument and the evaluation of existing damages and their importance for further restoration studies are not trivial tasks. The investigation has been based on detailed geometric data, collected from sources and in-situ measurements. For the mechanical analysis, finite element models have been created with different level of detail, including simplified description of documented damages. Modal analysis is assisted by micro-tremor measurements. Comparison of the predictions with the experimentally measured quantities, allows the determination of material parameters with higher accuracy. A least square technique assisted by the modal assurance criterion has been used, by driving the model from a Python script. A comparison of collapse predictions based on modified pushover analysis, with classical modal analysis has been performed. An explanation of existing damages is attempted, based on the numerical models.

1. Introduction

Masonry arches are among the oldest structural systems in the world. The technique of building masonry arches was first seen in the 2nd millennium BC in Mesopotamian brick architecture (Anastasio, 2020). Arches develop their strength by transferring the applied load into compressive forces, in a thrust line along adjacent masonry blocks (Chilton and Isler, 2020). When the thrust line is found out of the section of the masonry blocks, opening of the interfaces between the blocks takes place which can result in a hinge collapse mechanism (Heyman, 1982). Furthermore, compressive failure is unlikely on masonry arch structures. Masonry structures in general have a peculiar mechanical behavior due to their no-tension material characteristics. Form of the structure and mechanics are working together, in order all parts are mainly in compression. This can be changed from settlement movement or earthquake loadings so activation of interfaces, damages and eventually partial or total collapse are presented. Detailed structural analysis including unilateral interfaces and cracks is, in principle, possible (Leftheris et al., 2006).

Several research efforts have been presented in the last years, focusing on the investigation of the structural response of masonry arches. Different techniques have been developed, ranging from a quick estimation of the ultimate strength to a more refined or exact evaluation of the mechanical response. In more sophisticated numerical models, details of damage like cracks can be observed. In (Motsa et al., 2020), a finite element model with unilateral interfaces is developed to predict failure in Mnajdra megalithic monument. In (Drosopoulos et al., 2008), unilateral contact-friction laws were used to simulate potential failure of a stone arch bridge due to various loads including settlement of supports and concentrated live load. A multi-scale model has been proposed in (Drosopoulos and Stavroulakis, 2018) adopting the extended finite element method to capture arbitrarily oriented cracks and localization phenomena in masonry structures. More efforts on numerical modelling of masonry structures using the finite element method can be found in

* Corresponding author. Technical University of Crete, School of Production Engineering and Management, GR-73100, Chania, Greece.
E-mail address: gestavr@dpem.tuc.gr (G. Stavroulakis).

[1] The research was partially funded by a cooperation project between the Greek Ministry of Culture and Sports, The Region of Crete, The Municipality of Chania and the Technical University of Crete (Contract ID 20SYMV007057887 2020-07-21).

https://doi.org/10.1016/j.dibe.2022.100069
Received 9 November 2021; Received in revised form 31 January 2022; Accepted 17 February 2022
Available online 24 February 2022

Fig. 1. The Neoria monument (Providakis, 2021).

(Betti et al., 2016; Conde et al., 2016; Stavroulaki et al., 2018).

In the present paper, the structural analysis investigation of the Neoria masonry vaulted structure at the Venetian harbor of Chania is presented (Fig. 1). Data related to the structure, the material, the damages and the foundation have been collected during a recent research project (Providakis, 2021). The accurate representation of the geometry of the vaults and the spandrels is necessary in order to model the existing condition including permanent deformations, loose material, cracks (Stavroulaki et al., 2016). This is important for the estimation of the structural strength and dynamic behavior considering the three dimensional, effects of the vaults and the stabilization role of the spandrels (Stavroulaki and Tsinarakis, 2011).

Two different approaches are reported here for the explanation of existing cracks and damages in the Neoria structure. First a classical modal analysis procedure is followed and the areas of higher deformation in the structure are correlated with damage patterns. Furthermore, two- and three-dimensional models with unilateral interfaces are used in a push-over like analysis, to investigate collapse modes and loads. Eigenmodal results are compared to measured data (Providakis, 2021). The procedure has been supported by Python-driven modelling and optimization. Finally, an initial effort is presented, towards the investigation of damage using a three-dimensional non-linear Extended Finite Element Method (XFEM) model. The results indicate the difficulty of this inverse analysis task, in view of the many uncertainties of monuments and must be evaluated carefully, since pushover analysis has been developed mainly for ductile frame structures, while unreinforced masonry has limited, practically zero ductility.

2. Modelling and linear analysis of the structure

2.1. Description of the structure

The Neoria are shipyards built in the 16th century for the repair of the venetian fleet. The front (north) facade was originally open for the entry of the ships. The southern walls were constructed and connected to the lateral walls up until the base of the vaults. Neoria reached about 50 m in length and 9 m of width for each shipyard. The construction of the Neoria is of cut stones up until a height of about 2.5 m and rubblework for the rest of the mass of the walls and the vaults. It is assumed that a destructive earthquake in the 19th century caused serious damages to the structure. The parts of the walls that collapsed, mainly in the southern façade, were filled with smaller rocks. The buttresses were constructed during that period. The walls of the north façade were built in the early 20th century. During the World War II, two vaults were partly destroyed. Last interventions are mainly related to the repair of the two damaged vaults and the application of waterproofing materials (Skoutelis et al., 2021).

2.2. Geometric modelling

Existing drawings have been updated and enriched thorough new measurements (Providakis, 2021). This resulted to a fully three-dimensional model with adequate details able to support structural analysis (Fig. 2 (a) – (e)). Specific areas with different material properties, as shown in Fig. 2(a)–(e), were assumed.

About the material properties, the masonry walls and the vaults have been investigated by using various destructive and non-destructive testing techniques. Additional literature investigation provided us with values for the same or similar monuments in the area (see Table 1).

Rigid constraints have been assumed for the foundation. Foundation settlements have not been observed or reported, apart from possible local influence at the vicinity of newly constructed saw-water installations near the north-west corner of the monument. In addition, the walls of south and north part are based on the soil at the level of the ground. They have been added to the structure after the construction of the vaults and they are no bearing structural elements. Nevertheless during earthquake loading or eventually settlement of supports, they cooperate with the other parts of the structure, acting in some sense like infills. In addition, the bearing parts of the structure that are based on a lower level are also fixed and supported due to the surrounding soil. Therefore this simplified assumption related to the foundation of the walls does not influence the results, at list for the preliminary investigation reported here. Soil-structure interaction will be considered in more details later for detailed analysis.

2.3. Finite element static and modal analysis

Various finite element models have been created. A typical model has 117308 number of nodes and 67766 number of three-dimensional hexahedral elements. Indicative static analysis results are shown in Fig. 3.

Some of the calculated eigenvalues and eigenmodes of the Neoria structure are shown in Fig. 4 (a) – (f).

The eigenmodal participation factors are shown in Fig. 5 (a,b) in the two directions of the structure. From the modal analysis it turns out that there are frequencies where the vaults develop oscillation in the longitudinal direction and that is taken into account in a three-dimensional simulation and analysis of the structure. Specifically in Fig. 4, the oscillation of the vault of the western neorio in the 6th, 24th and 25th eigenmodes, is shown.

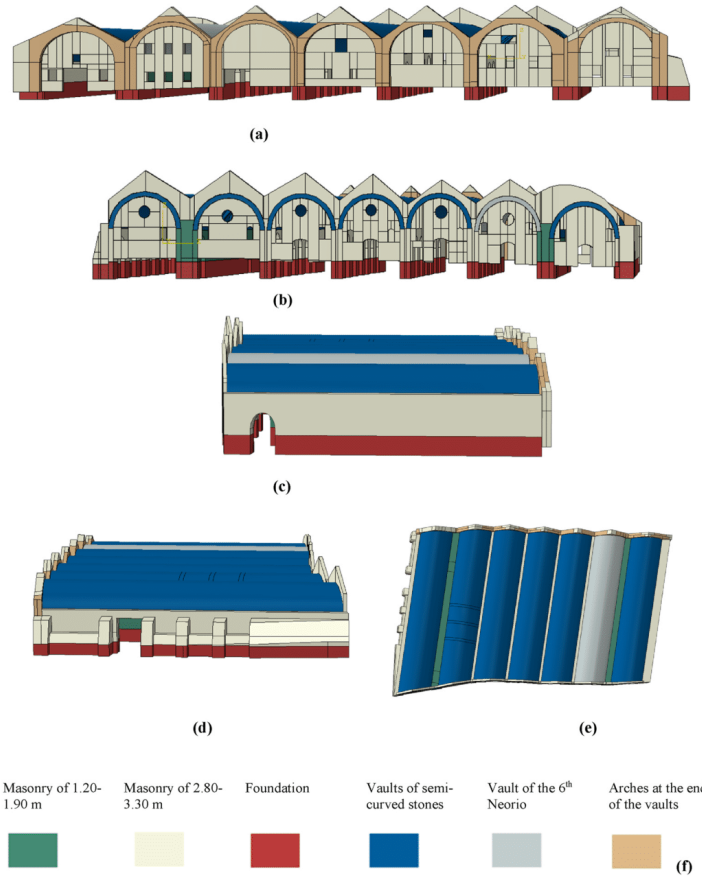

Fig. 2. (a) North view of the model, (b) south, (c) east, (d) west and (e) above view, with colors indicating areas of different material properties. (f) Colors assigned to various structural parts. (For interpretation of the references to color in this figure legend, the reader is referred to the Web version of this article.)

Table 1
Material properties (Evlogimenou).

Parts of the structure	Modulus of Elasticity
Vaults of semi-carved stones, strong mortar and mean thickness of 0.80 m	1860 MPa
Arches of the end of the vaults, in the north, with carved stones, strong mortar and mean thickness of 0.60–0.65 m	2790 MPa
Longitudinal masonry of 1.20–1.90 m thickness, with carved stones in the outer layers and strong mortar	504 MPa
Longitudinal masonry of 2.80–3.30 m thickness, with carved stones in the outer layers and strong mortar	340,2–3000 MPa
6th Neorio vault with shotcrete layer and π shaped hooks.	3280 MPa
Poisson ratio	0.20
Stone weight	21 kN/m3

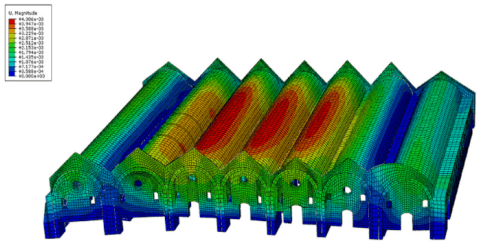

Fig. 3. Displacement for gravity loads (static load).

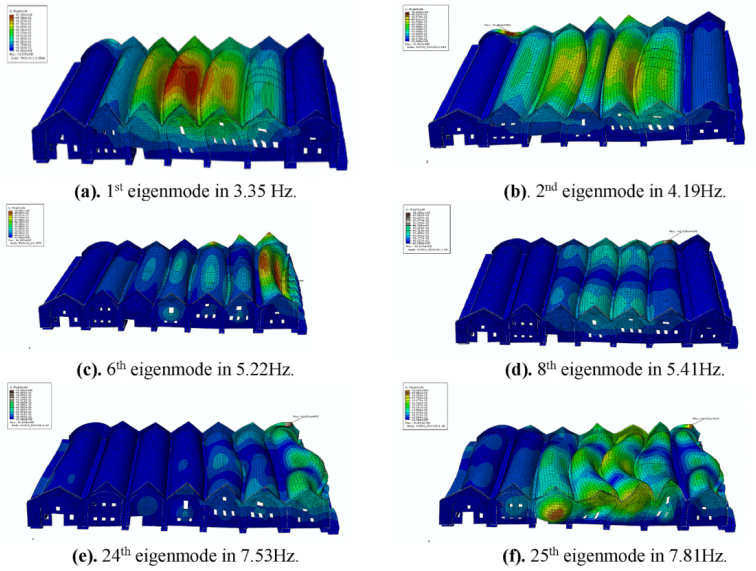

Fig. 4. Selected eigenmodes of the structure.
(a). 1st eigenmode in 3.35 Hz. **(b).** 2nd eigenmode in 4.19Hz.
(c). 6th eigenmode in 5.22Hz. **(d).** 8th eigenmode in 5.41Hz.
(e). 24th eigenmode in 7.53Hz. **(f).** 25th eigenmode in 7.81Hz.

Models in various commercial finite element codes have been prepared (MARC, ABAQUS, NX), with no significant differences.

It must be noted that recent design guidelines KADET 2021 (Regulation for valuation, 2021) require that at least 75% of the active mass must be considered in the modal analysis procedure. For the studied structure this requirement leads to the need of taking into account 142 modes (in X direction) or 197 modes (in Y direction) to the eigenmodal analysis. The first 20 eigenvalues are given in Table 2. From experimental measurements and the picture of existing damages it can be estimated that the structure experienced in the past seismic actions that activated eigenmodes near the value of 15 Hz.

It should be mentioned here that according to the provisions of KADET one observes that in the present structure, which does not have diaphragms, the modal analysis using as many eigenvectors as are required in order to activate the 75% of the total mass requires the inclusion of many eigenmodes. Alternatively, it is recommended to use the time-history analysis, by using a number of characteristic time series representing earthquakes expected in the region (following KANEPE sect. 5.6.3.3). In this paper the dynamic identify of the structure and material/damage identification is performed. For aseismic design and restoration design spectral analysis vs. time-series earthquake loading must be considered and performed. Comparison of the two approaches will be presented in the future.

Further investigation includes the introduction of cracks and soft interfaces at places where such damages have been found (Lakzaeian, 2011). The model with cracks and interfaces and the results are reported in (Charalambidi et al., 2021).

2.4. Parametric modelling and parameter identification

Due to the uncertainty which occurs mainly in material properties and damage patterns, several combinations of inputs must be considered in the mechanical model. The finite element models have been parametrized and driven through a Python script. Eventually, the model will provide the eigenmodes and eigenvalues near to the experimentally measured ones.

The parametrized model has different material properties assigned to different parts of the structure. Theoretically, every combination of elastic material properties can be considered. Based on the reliability of experimental measurements, the final investigation restricted the number of unknown parameters to three, within reasonable intervals for their values (Fig. 6).

The final step is composed of 512 combinations of parameter values and the calculated eigenmodes and eigenvalues. The calculated eigenmodal parameters have been compared with experimental measurements. The first criterion was the deviation between the calculated and the experimental eigenvalues. The Modal Assurance Criterion (MAC) has been supplementary used in order to assure that the compared modes are correctly chosen. MAC values show the convergence between numerical and experimentally measured eigenvalues. The closest this value to one, the better the correlation. This procedure is suitable for massive, monumental structures with complex-shaped eigenmodes and densely placed eigenvalues (Charalambidi et al., 2021) and (Asikoglu et al., 2019). The best combination of material parameters is shown in Table 3. The first row in Table 2 contains the experimentally measured eigenfrequencies (Providakis, 2021). The identification of predominant combinations by MAC is shown in Fig. 7. Different combinations of MAC for values greater than the threshold of 0.3 are presented.

The relation between the experimentally measured eigenfrequencies and the calculated eigenfrequency values is depicted in Fig. 8. The correlation between the MAC coefficient with the numerical eigenfrequencies and the difference between experimental and numerical

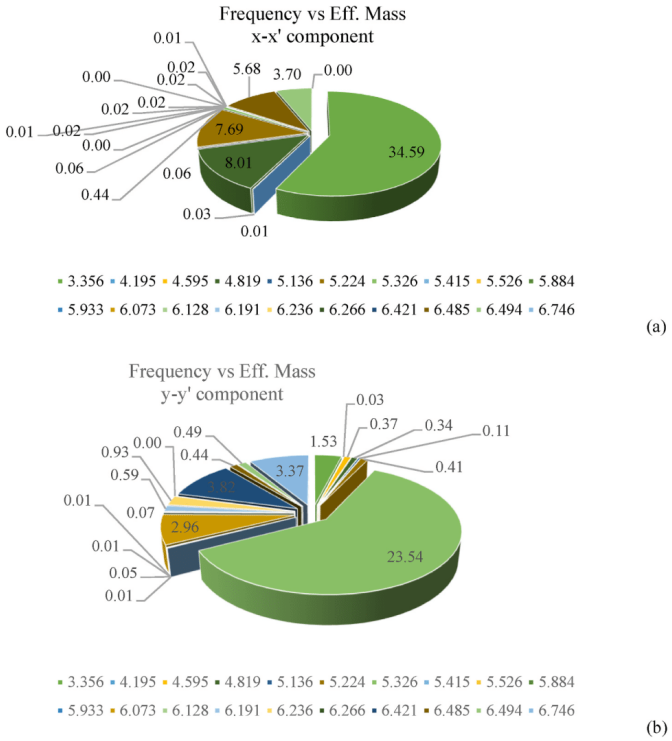

Fig. 5. Eigenmodal participation factors for earthquake in X and Y direction.

eigenfrequencies with the numerical eigenfrequencies is shown in Fig. 9.

In contrast to other works, which consider experimental data from the sterile laboratory environment or study relatively flexible structures (bridges, towers, belltowers, minarets etc), the achieved MAC values are relatively small. For general information and critical appraisal of various MAC factors the reader is referred to (Allemang, 2003) and (Pastor et al., 2012).

3. Pathology of the structure

For the structural model optimization, an analytical investigation of structure's damages was conducted. The purpose of the investigation was to include the existing deteriorations in the finite element model. The identified deteriorations are both biological (perforation, powdering) and mechanical (cracks, previous interventions with incompatible materials). The most important deteriorations of those detected were chosen to be included in the structural model. In Fig. 10, selected areas are illustrated that were simulated as regions of reduced stiffness, that is, three cracks observed in between the buttresses on the west wall, the large width cracks on vaults and the diversity of the width of the southern wall in the 7th Neorio. A longitudinal crack was recorded on the western vault. Because of its small width, it was not included in the analysis.

The structural conditions of the 4th and 6th vault from the west due to poor interventions are also considered as important (Fig. 11 (a)-(b)). They have been imported to the model as material with reduced strength (reduced elastic modulus).

Large width cracks of the inside of the vaults and on the west wall are illustrated in the followed Figures (Fig. 12 (a) – (c))

4. Unilateral crack models and non-linear analysis

4.1. Preliminary structural analysis modelling with cracks

From the in-situ investigation, the crack patterns have been documented. The finite element model of the structure (Ferrari et al., 2019) has been enhanced with weak zones that model, in a simplified way, the existence of cracks and other damages. In Fig. 13, the simulation of the critical cracked region of the structure are illustrated via proper partitioning of the finite element model.

From the analysis and the experimental investigation, it has been shown that higher vibration is accumulated near the frequency of 15 Hz. Therefore, the correlation of existing cracks with the maximum deformation patterns is shown in Fig. 14.

4.2. Classic limit state analysis

A limit state analysis was carried out using LimitState:Ring (Ferrari et al., 2019). Namely, a parametric analysis carried out to check the sensitivity of the ultimate load due to the number of masonry stones that make up one arch, as well as due to the estimated coefficient of friction between the masonry stones. It should be noted that the reason for

Table 2
Eigenvalues for various combinations of materials in the three areas.

Material - Modulus of Elasticity (Pa) (10^9)			7.06 Hz		11.56 Hz		15.75 Hz		17.62 Hz		18.5 Hz		24.62 Hz	
No1	No2	No3	MAC (10^{-4})	f(Hz)	MAC	f(Hz)	MAC	f(Hz)	MAC	f(Hz)	MAC	f(Hz)	MAC	f(Hz)
3,00	2,00	3,75	7,20	7,54	0,21	11,74	0,37	17,20	0,29	17,21	0,34	17,21	0,31	23,71
3,00	2,00	4,00	7,10	7,54	0,22	11,76	0,36	17,24	0,31	17,24	0,33	17,24	0,28	23,23
3,00	3,50	3,50	8,40	7,51	0,26	10,25	0,12	16,60	0,40	18,41	0,40	18,41	0,41	23,82
3,00	3,50	4,00	9,20	7,51	0,26	10,42	0,11	16,63	0,31	18,52	0,30	18,52	0,43	23,88
3,25	2,00	3,75	6,50	7,55	0,21	11,8	0,22	15,86	0,33	19,09	0,33	17,29	0,32	23,6
3,25	3,50	3,00	7,20	7,51	0,29	10,18	0,15	16,67	0,33	18,44	0,34	18,44	0,43	23,77
3,25	3,50	3,25	7,30	7,51	0,29	10,26	0,14	16,70	0,30	18,51	0,31	18,51	0,54	23,87
3,25	3,50	3,75	6,90	7,51	0,27	10,43	0,13	16,73	0,39	18,60	0,40	18,60	0,46	23,98
3,50	2,50	3,50	4,00	7,62	0,2	10,67	0,25	16,94	0,36	16,94	0,32	18,58	0,39	23,27
3,50	3,00	3,00	4,70	7,11	0,08	11,17	0,11	17,17	0,36	17,71	0,32	17,71	0,34	23,37
3,50	3,50	3,00	5,30	7,51	0,3	10,26	0,15	16,77	0,31	18,62	0,24	18,62	0,50	23,87
3,50	3,50	3,50	4,40	7,53	0,28	10,42	0,08	16,83	0,32	18,76	0,31	18,76	0,44	24,01
3,75	2,50	3,50	3,20	7,62	0,19	10,71	0,21	17,13	0,35	17,01	0,30	18,69	0,44	23,35
3,75	2,50	4,00	4,20	7,6	0,2	12,88	0,34	17,24	0,29	17,24	0,34	17,24	0,31	23,69
3,75	3,00	3,00	4,90	7,48	0,1	11,21	0,1	17,24	0,36	17,81	0,30	17,81	0,36	23,4
3,75	3,00	3,75	5,80	7,49	0,27	10,21	0,11	17,20	0,36	18,03	0,34	18,03	0,31	23,5
3,75	3,50	3,00	4,70	7,54	0,32	10,32	0,10	16,86	0,41	18,72	0,36	18,72	0,46	23,94
3,75	3,50	3,25	4,50	7,56	0,29	10,41	0,14	16,9	0,45	18,79	0,40	18,79	0,45	24,01
3,75	3,50	3,50	4,20	7,57	0,28	10,49	0,13	16,93	0,30	18,85	0,32	18,85	0,42	24,08
3,75	3,50	3,75	4,40	7,66	0,27	10,58	0,06	16,92	0,41	18,93	0,34	18,93	0,37	24,14
3,75	3,50	4,00	4,70	7,66	0,19	10,68	0,10	16,95	0,41	19,00	0,35	19,00	0,35	24,19

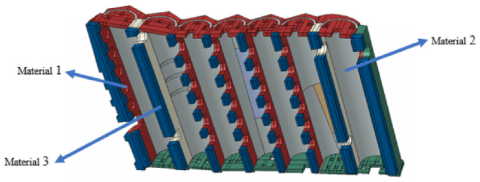

Fig. 6. Identification of parameters in selected areas, according to the instructions of the sensitivity analysis.

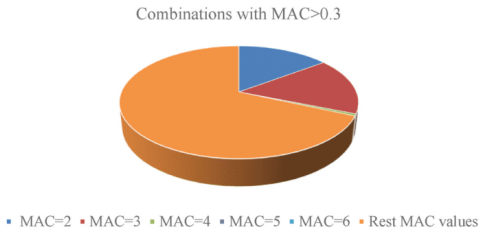

Fig. 7. Identification of predominant combinations by MAC. Percentage of cases with 2,3 etc MAC values greater than the threshold.

Table 3
Geometrical parameters of the damaged arch (west arch).

Shape of intrados	Span (m)	Rise at mid Span (m)	Thickness (mm)	Total Width (m)	Number of units
Segmental	9.39	4.695	727	5.0	20

considering only one arch in these simulations, is primarily to provide an indication for the number of blocks which can be used for each arch in the subsequent cases as well as to suggest a prediction for the friction coefficient. Thus, these simulations are only preliminary and cannot be used for in-depth evaluation of the structural response.

Table 3 shows the geometrical parameters of the arch on the west side which was used for the analysis, since it is the most damaged and it is expected that it will provide a better sense of the condition of the structure.

For the parametric analysis models, a 1 kN load was applied across the span of the arch at 150 mm intervals to identify the critical failure load of the arch and the position it is obtained. The results from the parametric analysis are shown in Figs. 15–16.

From the parametric analysis, it can be observed that failure load increases, until coefficient of friction reaches the value 0.47. The critical load observed is 87.9 kN when the number of segments is set to 10. From previous studies, it has been shown that the assumed coefficient of

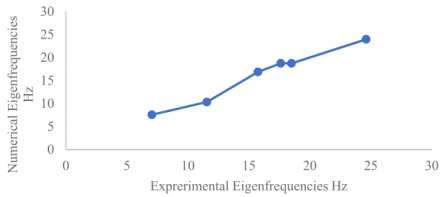

Fig. 8. Correlation between experimentally measured and calculated eigenfrequencies.

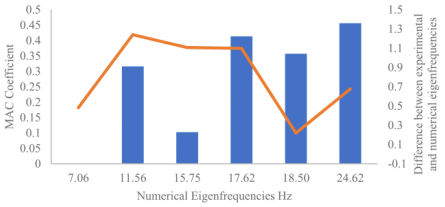

Fig. 9. Correlation between MAC coefficient (blue bar) and difference between experimental and numerical eigenfrequencies (orange line) with numerical eigenfrequencies. (For interpretation of the references to color in this figure legend, the reader is referred to the Web version of this article.)

friction between the masonry blocks tends to give the upper bound of the critical failure load if not coincide with the exact value of failure (Limitstate, 2021). Therefore, for the rest of the models, a 0.5 coefficient of friction has been adopted.

In the next step, the number of masonry blocks that make up the ring were investigated to determine the point at which the number of blocks has no significant effect on the failure load. It can be noted from Fig. 15, that the critical load decreases with the increase in the number of blocks until 10 blocks, whereby the critical load shows a lot of noise. However, when the average of the corresponding critical load from 3 consecutive blocks is plotted, the noise in the critical load becomes insignificant after 20 blocks are used to make up the arch. Therefore, for the rest of the models, each arch is made up of 20 masonry blocks.

It is noted that the failure mechanism obtained from the parametric models, correlates to the longitudinal cracks that were observed on the first arch as mapped on Fig. 10. The mode of collapse is a four-hinge failure mechanism as shown in Fig. 16.

4.2.1. *Two-dimensional analysis*

The mechanical behavior of unreinforced masonry structures is mainly based on compression loads transferred between adjacent parts of it, for instance stones, and secondary on frictional effects. This behavior is also known as unilateral, no-tension behavior. The existence of mortar with unreliable and low tensile strength is neglected. A further simplification for slender structures, like arches or domes, is based on the introduction of unilateral contact interfaces that model the nonlinear behavior. The activation or deactivation of contact, eventually with friction, during loading lead to reduction of the strength of the structure and eventually collapse, due to the formation of collapse mechanisms.

Following this method developed in our previous work (Drosopoulos et al., 2008; Gilbert and Melbourne, 1994) and (Du, 2019) for masonry bridges, a two-dimensional model for one arch as well as for the seven arches of Neoria in the East-West direction has been created. A number of unilateral contact interfaces are included. By applying a horizontal or

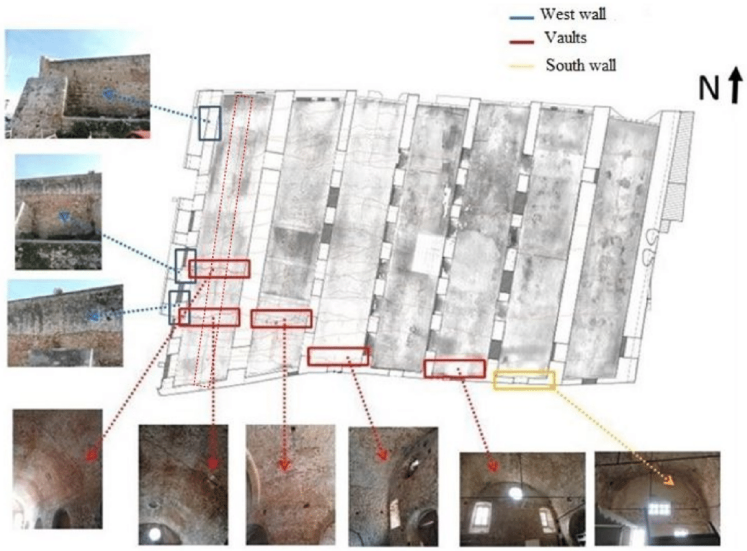

Fig. 10. Areas of reduced ductility on the vaults and on the walls of the structure.

(a) (b)

Fig. 11. Vault (a) inside and (b) outside view.

(a) (b)

(c)

Fig. 12. Crack on vault. (a) Inside and (b) outside view. (c) Biological deterioration on the North Wall.

vertical live load and gradually increasing it, similar to push-over analysis, the unilateral interfaces are activated and eventually collapse is modeled.

Careful application of this procedure, which is recommended by modern design regulations for ductile structures, gave crack patterns that partially explain the measured crack patterns at the outside walls of the structure. A vertical push-down procedure is followed for the estimation of the vertical component of the earthquake on a two-dimensional model of the single, west arch. Thus, the applied load combination consists of the self-weight, assigned in a first load step and an increased by 0.5g vertical gravity load, assigned in a second load step. Activation of cracks at the crown of the vaults can be explained by this procedure. Crack patterns at the west part of the structure can be correlated with the results of the full seven-openings model.

It must be repeated here that the results of pushover analysis have been used to give indicative correlation with existing crack patterns. Due to lack of ductility of the unreinforced masonry structure, they cannot be used for strength evaluation. From the collapse type and the

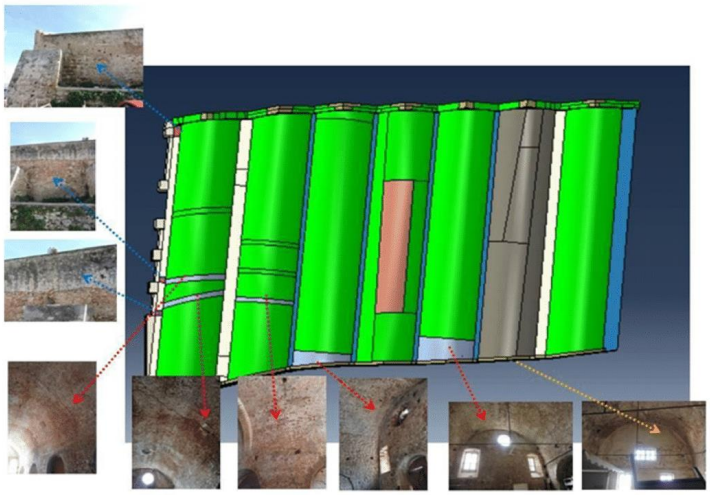

Fig. 13. Simulation of cracked region via partitioning of the F.E. model.

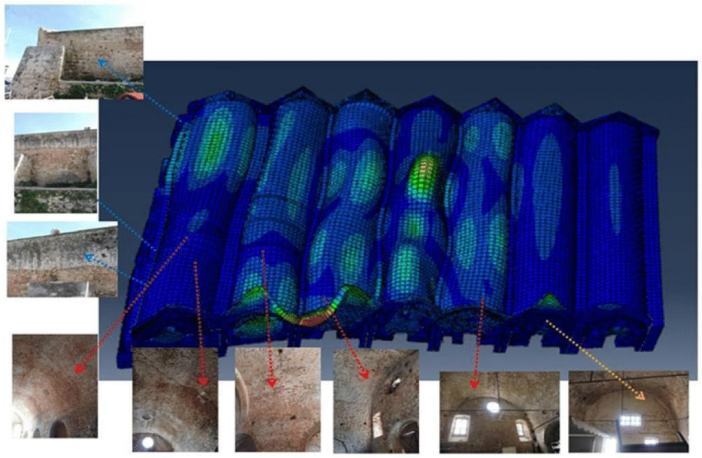

Fig. 14. 15 Hz eigenvalue shape of the structure (cracked model).

performance of the overall two-dimensional model it is observed that the most vulnerable areas are the extreme vaults (Fig. 17). Pathology observation indicates the appearance of longitudinal cracks in the vault of the western and eastern Neorio. These cracks have caused the key vault to break on the north front. It is pointed out that there is no immediate risk of collapse as evidenced by the collapse mechanism which requires the development of cracks in other places of the vault as well as movement of the spandrels (longitudinal walls).

4.2.2. Three-dimensional analysis

Next, a three-dimensional non-linear finite element model is developed in Abaqus (Simulia, 2013). It is noted that comparing to limit analysis, the finite element models can provide more details such as the principal stresses, forces and displacements which can be translated to force-displacement diagrams.

The geometry shown in Table 4 was used to create the numerical models. The longitudinal support provided by masonry walls were also included in the models. The width of the structure is reduced to 3.5 m to simplify the analysis.

The finite element models developed in this paper are solved using the Newton-Raphson incremental-iterative procedure to deal with the nonlinear nature of the problem. The nonlinearity is due to the opening-

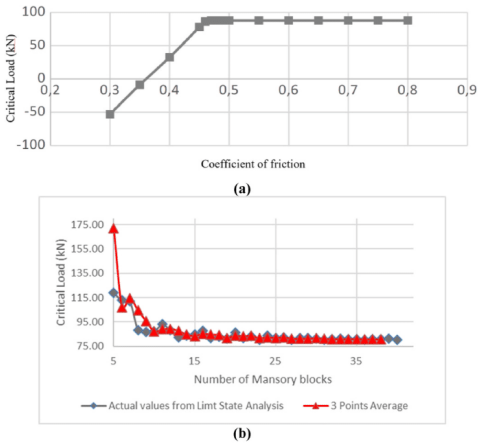

Fig. 15. Parametric analysis showing (a) the critical load vs the coefficient of friction between the masonry blocks and (b) the critical load vs the number of masonry blocks.

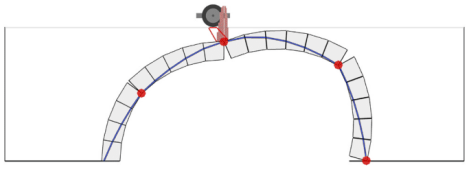

Fig. 16. The limit state failure mechanism of the first arch.

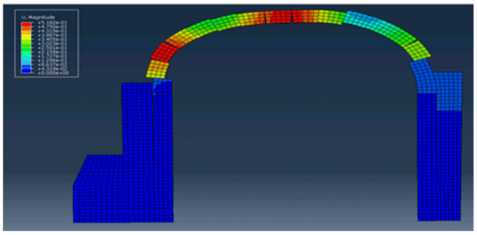

Fig. 17. Collapse mechanism (Western Neorio), where the activation of cracks in the center of the dome is clearly visible, as observed in the building.

closure and sticking-slipping along the masonry stone interfaces. The models were developed with a fixed support and the self-weight was incorporated in the loading condition. Two steps were used to create the models: the first step was a pure gravity load to simulate the state of inertia of the structure and to stabilize the model. The second step has an increased gravity load by 0,5g which was incrementally applied on the

Table 4
Maximum principal stresses (Maxps) used for XFEM model.

Material	Location	Maxps (MPa)
M1	Vaults with semi - carved stones, strong mortar and an average thickness of 0.80 cm	0.774
M2	Arches ending in the north with carved stones and strong mortar (thickness 0.60–0.65 cm)	1.116
M3	Longitudinal masonry 1.20–1.90 m thick with carved stones in the outer layers and strong mortar	0.2016
M4	Longitudinal masonry 2.80–3.30 m thick with stones in the outer layers and strong mortar	0.136
M5	Neoria dome 6 with operation with shotcrete and hooks of shape p.	–

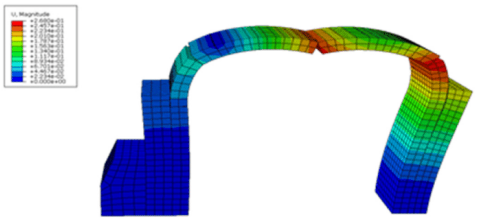

Fig. 18. The failure mechanism of the first arch under gravity loads.

structure. This is used to provide a preliminary indication of the effect of the vertical component of an earthquake to the structural system. The results from these models are shown in Figs. 18–20.

The failure mechanism presented are shown in Figs. 18–20 correlate with the longitudinal cracks observed on the structure in-situ and the damage pattern is similar to the one observed in the limit state analysis. Also, the model with one arch has a similar failure pattern with the full structure of 7 arches, even though the failure pattern is exaggerated on the one arch model. The hinge circled in yellow in Fig. 19 (model with one arch) and Fig. 20 (full structure) shows an outwards opening, respectively. For the model with the full structure, there is an influence of the adjacent arch to the first arch, which acts as a probe which prevents/minimize the lateral movement of the arch. This tends to minimize the overall displacement of the structure making it more stable.

After the first group of models with increased gravity of 0.5g were analyzed, it was noticed that the longitudinal cracks/opening only developed on the first (west) arch while on situ, also mapped on Fig. 10, longitudinal cracks are also visible in spans 2 and 7. In an attempt to understand the cause of the longitudinal cracks, more load cases were investigated:

- (a) Lateral movement of abutment due to a horizontal point load acting on the right-hand side abutment of the structure, as shown in Fig. 21.
- (b) A vertical displacement of supports.

Fig. 22 shows the deformation of the structure after a 100 kN horizontal point load has been applied on the right hand-side abutment. As shown on Fig. 22, multiple hinges (circled in red) are observed on the first span which correlates to the experienced damage. The yellow circles show small hinge opening on fourth, fifth and sixth spans. When the horizontal force is applied to the left hand-side abutment, no correlation

Fig. 19. The displacement contour of the whole structure under gravity loads.

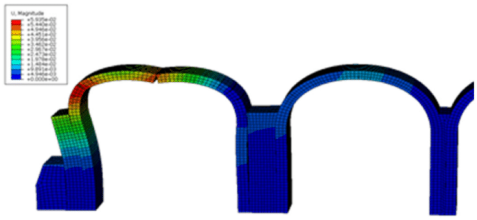

Fig. 20. A close-up view of the failure mechanism of the first arch in whole structure analysis under gravity loads.

Fig. 21. Lateral point load acting on the right-hand side abutment of the structure.

to the experienced damage arises.

Figs. 23–24 show the deformation of the structure after imposing a 100 mm vertical (downwards) settlement of supports 2 and 8, as indicated by the red arrows. This movement of supports may be due to poor ground conditions. Fig. 24 highlights in red circles the hinge openings which might have resulted in the real cracks obtained in situ, as there is a high correlation of the positions of the cracks observed in the numerical model (Fig. 24) and in the real conditions (Fig. 10). The hinge opening on the fifth span (highlighted in yellow) is quite small, similar to the real image. It can be concluded that the longitudinal cracks are most likely to be caused by a vertical displacement of supports 2 and 8.

4.3. Analysis with the extended finite element method

The extended finite element method (XFEM) is an extension of the conventional finite element analysis. It allows for cracks to be modeled independently of the mesh, permitting the propagation of the crack along an arbitrary, solution-based path (Du, 2019). The main concept of this method is to use the partition of unity property and properly enrich the nodal displacement approximation. The enrichment is implemented using appropriate enrichment functions, as provided by equation 2.

Within the XFEM method, a domain containing a discontinuity, is considered. This may involve a discontinuous displacement (strong discontinuity) or a discontinuous displacement gradient (weak discontinuity). A strong discontinuity can be used in numerical modelling to represent a crack, developed in a structure.

For a two-dimensional geometry, a strong discontinuity is depicted by a line located in the finite element mesh. According to the core concept of the XFEM method, the nodes of the elements which are cut by the discontinuity are enriched, using appropriate functions. These enrichment functions are used for the nodes of split elements (thus, elements which are cut by the discontinuity) and for the nodes of tip elements (elements which contain the crack tip). For the enrichment of the split elements, the Heaviside function H is used as given in equation (1). For the tip elements, the branch functions F are introduced.

$$u = \sum_{I=1}^{N} N_I(x) \left[u_I + H(x) a_I + \sum_{a=1}^{4} F_a(x) b_I^a \right] \tag{1}$$

For the structure that is investigated in this article, an XFEM model is

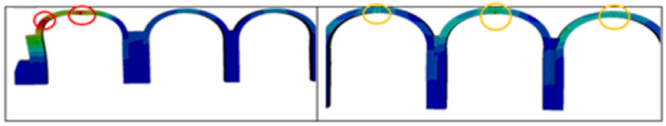

Fig. 22. (a) Deformation shape of first (west) span after a 100 kN horizontal point load has been applied on the right hand-side abutment, (b) Deformation shape of fourth, fifth and sixth spans after a 100 kN horizontal point load has been applied on the right hand-side abutment.

Fig. 23. Deformation shape of the structure after 100 mm vertical settlement of supports 2 and 8.

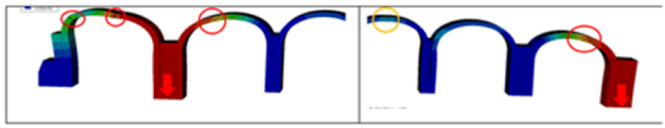

Fig. 24. (a) Deformation shape of 1st and 2nd span after 100 mm vertical settlement of supports 2, 8, (b) Deformation shape of 5th and 7th span after 100 mm vertical settlement of support 1, 8.

developed in Abaqus (Du, 2019) to capture the transverse cracks. A simplified 3-dimensional geometry of the full structure is considered, similar to the full structure in the traditional FEA. A maximum principal stress (Maxps) is adopted to define the traction-separation law which is used to determine the response of the discontinuities. Crack propagation takes place when the stress in the domain of the crack tip reaches this maximum principal stress. Values of the Maxps for different elements of the structure are shown on Table 4. For all the cases, the displacement at failure was considered to be equal to 0.001 m. In this study, the initial cracks were inserted on the first, second, third and seventh spans of the structure as observed on situ. For the mechanical conditions, a 100 mm vertical displacement of the second and eight support was applied together with a 100 kN horizontal force on the left abutment as shown on Fig. 26. The result from this model is shown in Fig. 26 (a)–(d).

Fig. 25(a) shows the initial position of the transverse cracks which are introduced to the model. According to the results of this investigation, the longitudinal cracks, which were observed on the conventional finite element analysis with similar load conditions, are also observed under the extended finite element model. In addition, based on this load case, as well as on more load cases including settlement of supports, analysis results indicate that the existing longitudinal cracks do not propagate. One potential reason for this, is the fact that these transverse cracks may not be considered as critical, since they will not interrupt the structural integrity of the system. Thus, in-between their positions, intact masonry arch parts will still be able to support the structural system.

However, further future investigation needs to be conducted, in order to provide more details for the interaction between longitudinal and transverse cracks and the influence of their interaction on the structural response.

5. Conclusions

Modal analysis results and pushover, limit analysis calculations have been used in order to explain damage and crack patterns found on the structure of the Neoria monument. First a three-dimensional finite element model was used for the classical modal analysis procedure and the areas of higher deformation in the structure were correlated with damage patterns.

The parametrized model has different material properties assigned to different parts of the structure. Theoretically, every combination of elastic material properties can be considered. Based on the reliability of

Fig. 25. Deformation shape of the structure after a 100 kN horizontal point load has been applied on the further left hand-side abutment together with a 100 mm vertical displacement on the 100 mm vertical displacement of the second and eight support.

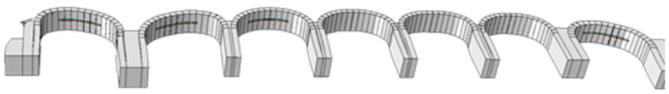

(a)

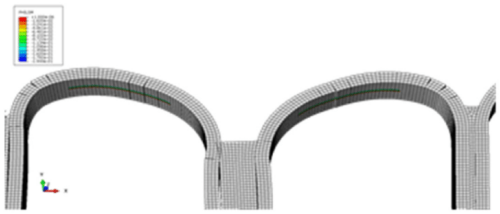

(b)

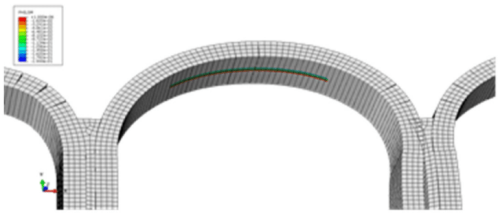

(c)

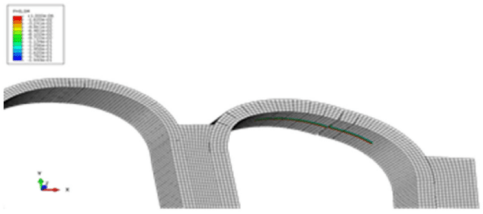

(d)

Fig. 26. (a) Transverse cracks on the different spans of the structure. Close-up (b) on the first and second span, (c) on the third span and (d) on the seventh span of the structure.

experimental measurements, the final investigation restricted the number of unknown parameters to three, within reasonable intervals for their values (Fig. 20). From the reported investigation a fairly satisfactory determination of material parameters has been done, based on a detailed linear finite element model and experimental measurements. Further investigation may include parameter identification using multiple criteria and global optimization techniques. The Python script can support this, provided that sufficient computing time is available.

Furthermore, two- and three-dimensional models with unilateral interfaces were used in a push-over like analysis, in order to investigate collapse modes and loads. It is known that model with contact interfaces can be used in the stability assessment of a large monument (Motsa et al., 2019) and in combination with optimization for the investigation of structures with faults (Conde et al., 2016). Finally, the XFEM method was adopted to provide a further insight of the structural response, by considering transverse discontinuities.

From the analysis results it was concluded the important role of the west wall to the failures of the 1st Neorio vault. Additionally, the isolation of the masonry strength due to lack of maintenance as well as earthquakes are the main causes of existing failures. The understanding the mechanism of construction failure is basic to the next in studying the required interventions.

Due to the complexity of the structure, the uncertainties related to material properties, despite the extensive investigation, more work is needed, towards a further insight on crack propagation and reinforcement suggestions for the monument.

Declaration of competing interest

The authors declare that they have no known competing financial interests or personal relationships that could have appeared to influence the work reported in this paper.

References

Allemang, R.J., 2003. The modal assurance criterion – twenty years of use and abuse. Sound Vib. 37, 14–23. August.

Anastasio, S., 2020. Building between the Two Rivers: an Introduction to the Building Archaeology of Ancient Mesopotamia. Building between the Two Rivers. Archaeopress Archaeology, Oxford.

Asikoglu, A., Avşar, Ö., Lourenço, P.B., Kaplan, O., Karanikoloudis, G., 2019. Finite element modeling and operational modal analysis of a historical masonry mosque. In: Papadrakakis, M., Fragiadakis, M. (Eds.), 7th ECCOMAS Thematic Conference on Computational Methods in Structural Dynamics and Earthquake Engineering Proceedings, Crete, Greece, 24–26 June.

Betti, M., Galano, L., Vignoli, A., 2016. Finite element modelling for seismic assessment of historic masonry buildings. In: D'Amico, S. (Ed.), Earthquakes and Their Impact on Society. Springer, Cham, pp. 377–415.

Charalambidi, B., Motsa, S., Drosopoulos, G., Koutsianitis, P., Kasampali, A., Stavroulaki, M., Stavroulakis, G., 2021. Structural damage investigation of the Neoria monument in Chania. In: 2nd International Conference TMM-CH. Athens.

Chilton, J.C., Isler, H., 2020. Heinz Isler: the Engineer's Contribution to Contemporary Architecture. Thomas Telford Publishing, Telford.

Conde, B., Drosopoulos, G., Stavroulakis, G., Riveiro, B., Stavroulaki, M., 2016. Inverse analysis of masonry arch bridges for damaged condition investigation: application on Kakodiki bridge. Eng. Struct. 127, 388–401.

Drosopoulos, G.A., Stavroulakis, G.E., 2018. A computational homogenization approach for the study of localization of masonry structures using the XFEM. Arch. Appl. Mech. 88, 2135–2152.

Drosopoulos, G., Stavroulakis, G., Massalas, C., 2008. Influence of the geometry and the abutments movement on the collapse of stone arch bridges. Construct. Build. Mater. 22, 200–210.

Du, Z.-Z., 2019. eXtended Finite Element Method (XFEM) in Abaqus. Simulia, Johnston.

Evlogimenou, I., December, 2011. Diploma Thesis. In: Venetian Neoria Chania: Static Solution and Intervention Proposal. NTUA, School of Architecture, D.P.M.S. Protection of Monuments.

Ferrari, R., Froio, D., Rizzi, E., Gentile, C., Chatzi, E.N., 2019. Model updating of a historic concrete bridge by sensitivity- and blobal optimization-based Latin Hypercube Sampling. Eng. Struct. 179, 139–160.

Gilbert, M., Melbourne, C., 1994. Rigid-block analysis of masonry structures. Struct. Eng. 72.

Heyman, J., 1982. The Mansonry Arch. Ellis Horwood Limited, Chichester.

Lakzaeian, F.H., 2011. Ambiend vibration testing and finite element model updating of a concrete footbridge. In: The 4th International Operational Modal Analysis Conference (IOMAC 2011). Istanbul, Turkey, 9-11 May.

Leftheris, B., Sapounaki, A., Stavroulaki, M.E., Stavroulakis, G.E., 2006. Computational Mechanics for Heritage Structures. WIT - Computational Mechanics Publications, Southampton, Boston.

Limitstate. Ring. https://www.limitstate.com/ring. (Accessed 23 October 2021).

Motsa, S.M., Drosopoulos, G.A., Stavroulaki, M.E., Stavroulakis, G.E., Ruben, P., Borg, P., Galea, P., d'Amico, S., 2019. Large-scale contact analysis for the stability estimation of the Mnajdra Monuments. In: Zigoni (Ed.), Advances in Engineering Materials, Structures and Systems: Innovations, Mechanics and Applications. Taylor & Francis, Abingdon, pp. 2160–2164.

Motsa, S.M., Drosopoulos, G.A., Stavroulaki, M.E., Maravelakis, E., Borg, R.P., Galea, P., D'amico, S., Stavroulakis, G.E., 2020. Structural investigation of Mnajdra megalithic monument in Malta. J. Cult. Herit. 41, 96–105.

Pastor, M., Binda, M., Harcarik, T., 2012. Modal assurance criterion. Procedia Eng. 48, 543–548.

Providakis, C., March 2021. Experimental investigation of eigenmodal characteristics. In: Skoutelis, N., et al. (Eds.), Research Investigation for the Restoration of Neoria, Technical University of Crete, Municipality of Chania, Ephorate of Antiquities. Chania.

Regulation for Valuation and Structural Interventions for Masonry (KADET), 2021. Greece.

Simulia, D.S., 2013. Abaqus 6.13 User's Manual. Dassault Systems, Providence, pp. 305–306.

Skoutelis, N., et al. (Eds.), March 2021. Research Investigation for the Restoration of Neoria. Technical University of Crete, Municipality of Chania, Ephorate of Antiquities, Chania.

Stavroulaki, M.E., Tsinarakis, Th, 2011. Finite element analysis of masonry barrel vaults. In: 7th GRACM International Congress on Computational Mechanics. Athens.

Stavroulaki, M.E., Riveiro, B., Drosopoulos, G.A., Solla, M., Koutsianitis, P., Stavroulakis, G.E., 2016. Modelling and strength evaluation of masonry bridges using terrestrial photogrammetry and finite elements. Adv. Eng. Software 101, 136–148.

Stavroulaki, M.E., Drosopoulos, G.A., Tavlopoulou, E., Skoutelis, N., Stavroulakis, G.E., 2018. Investigation of the structural behaviour of a masonry castle by considering the actual damage. Int. J. Mason. Res. 3, 1–33.

Chapter 6 – A data-driven, machine learning scheme used to predict the structural response of masonry arches

Motsa, S.M.[a], Stavroulakis, G.[b*], and Drosopoulos, G [c,a] . A data-driven, machine learning scheme used to predict the structural response of masonry arches. (Submitted for publication and currently under review)

[a] Discipline of Civil Engineering, University of KwaZulu-Natal, Durban, South Africa

[b] Department of Production Engineering and Management, Technical University of Crete, Chania, 73100, Greece

[c] Discipline of Civil Engineering, University of Central Lancashire, Preston, United Kingdom

* Corresponding author.

E-mail address: gestavroulakis@tuc.gr

Abstract

In this article a data-driven, structural analysis methodology is proposed, for the investigation of the ultimate response of masonry arches. The main objective of the study is to adopt machine learning principles, in the form of artificial neural networks, in order to evaluate the structural response of masonry arches. In this framework, numerical metamodels are developed, aiming to predict in a computationally efficient framework, the failure mechanism and the ultimate, collapse load of masonry arches. First, datasets are numerically built, integrating Matlab, Python and commercial finite element software. Heyman's assumptions are adopted within non-linear finite element, incorporating contact-friction laws between adjacent stones/blocks to capture failure in the arch. The artificial neural networks are trained, validated, and tested using the least square minimization technique. It is shown that the proposed scheme can be used to provide a fast and accurate prediction of the deformed geometry, the collapse mechanism and the ultimate, failure load of masonry arches. Cases studies demonstrate the efficiency of the proposed method, by implementing the method to random, new masonry arch geometries, not used for training. All Matlab and Python scripts used to generate the datasets as well as the datasets, are provided with this article. The method can be extended towards structural health monitoring applications and the concept of digital twin.

Keywords: FEM, Machine Learning, Artificial Neural Network, Multi-hinge failure, Damage Prediction, Masonry Arches, Data-driven Mechanics, Digital Twin

1. Introduction

Masonry arches have been used widely during centuries to span and enclose space. The structural benefit of the arch shape is still under investigation even though the technique was first observed in Mesopotamian brick architecture, dating back to the 2nd Millennium BC (Anastasio, 2020). Arches are efficient load-bearing structures, which distribute applied loads through compression in adjacent masonry stones. The arch, as a method of construction, is directly relevant to the material behaviour of masonry. There exists a harmonic relation between the masonry stones and the shape of the arch, to ensure that the structure is mainly under compression. Compression failure of masonry arches is generally unlikely to take place, thus, the typical failure mode of arches is a tensile hinge mechanism (Grillanda et al., 2021).

In particular, the typical mode of failure for masonry arches is the formation of tension hinges in-between the masonry stones, activated when the thrust line falls outside the section of the masonry arch. The change of the structural state, from equilibrium to mechanism, can be caused by settlement of supports due to earthquakes, vertical loads due to vehicles, erosion, or ground bearing failure. This hinge mechanism can result in damage and eventually partial or total collapse.

Several investigations have been conducted, to highlight the structural response of masonry arches. Hooke (1676) has been pioneer for first describing the compression behaviour of masonry arches under their self-weight and for proposing a rational rule to estimate the size of masonry stones and the geometry of masonry arches. This rule is based on the analogy of a hanging chain forming catenary in tension under its self-weight, and on a masonry arch (inverted chain), standing rigid in compression (Heyman, 1982, Heyman, 1998, O'Dwyer, 1999, Block et al., 2006). In (Poleni, 1748), Hooke's hanging chain principle was used to assess the safety of the cracked dome of St. Peter's in Rome. Recently, in (Gáspár et al., 2022) this principle was used in a study which relates the optimal geometry of a masonry arch and the number of concurrent hinges under self-weight, at a limit state quantified by minimum thickness.

In the later years, more advanced techniques have been developed, to evaluate the structural behaviour and ultimate, failure response of masonry arches. Often, the finite element method is the numerical tool used to simulate detailed two and three-dimensional geometries of masonry arches. To capture the failure response, different constitutive descriptions are introduced in these models. The arising computational cost is significant, in particular for bigger models with more structural parts, higher dimensions and complex non-linear material laws.

In (Özmen and Sayın, 2018), three-dimensional finite element models are used to assess the seismic response of an old masonry arch bridge in the framework of the macro modelling approach. In (Charalambidi et al., 2022), a finite element model introducing unilateral interfaces to capture failure between masonry stones, is proposed to identify and predict the cause of the existing structural damage of a masonry monument in Greece. In (Tapkın et al., 2022), various non-linear finite element models were used to simulate the structural response of a three-span masonry arch bridge located in Turkey. In (Drosopoulos and Stavroulakis, 2018), a computational homogenization method is proposed, to investigate localization of damage in masonry walls. Macroscopic, structural scale failure is represented by cohesive cracks in the framework of the extended finite element method, using the effective material properties obtained from microscopic simulations. More efforts on numerical modelling of masonry arches using the finite element method can be found in (Ferrero et al., 2023, Rahimi et al., 2022, Zampieri et al., 2021, Tubaldi et al., 2020, Stavroulaki et al., 2018, Conde et al., 2016, Sarhosis et al., 2016, Milani et al., 2006, Lourenço, 2002).

In the 4th industrial revolution era, machine learning elements, such as artificial intelligence (AI), have been adopted to solve complex non-linear engineering problems. In the recent years, even more machine learning algorithms have been developed to solve engineering problems. In structural engineering, artificial neural networks have been used to assess the strength and performance of concrete structures (Chang and Zheng, 2019, Prakash et al., 2019, Sadowski et al., 2018) and the structural response of steel (Beskopylny et al., 2020, Wołowiec and Kula, 2012). Other available machine learning approaches include non-destructive and vision-based measurement techniques, which are used as a method of structural health monitoring (Yuan et al., 2022, Bekas and Stavroulakis, 2017, Psychas et al., 2016, Cavaleri et. al., 2022, Grandio et al., 2022, Ashrafian et. al., 2023).

The main concept of introducing machine learning approaches in structural engineering, is to use existing data, carrying information for the structural response, in numerical simulations. Thus, databases are developed and used to train a machine learning algorithm. The trained algorithm is then used to assess the response of the structural system. A numerical metamodel is developed within this framework, able to potentially replace or complete existing structural evaluations, due to missing experiments or computationally expensive calculations.

In (Jing et al., 2022), an artificial neural network called BridgeNet is proposed, for automating the segmentation of masonry arch bridge elements obtained from large-scale point clouds. In (Melchiorre et al., 2021), machine learning algorithms are used to structurally optimize the cross-

section of a circular arch by calculating the internal stresses and comparing them against the yield stresses of the material. In (Civera et al., 2022), artificial intelligence and machine learning algorithms are used to interpret operational modal analysis mode shapes, which is normally a computationally expensive task, aiming in the structural health monitoring of masonry arches. In (Drosopoulos and Stavroulakis, 2020), machine learning is introduced in multi-scale computational homogenization to capture the non-linear response of masonry walls. Recent studies emphasize in using image recognition and deep machine learning tools, including for instance computer vision and convolutional neural networks (CNN), to generate geometric digital twins for masonry structures (Dais et al., 2021, Loverdos and Sarhosis, 2023, Loverdos and Sarhosis, 2023).

In this study, a data-driven numerical analysis of masonry arches is proposed, to evaluate their mechanical response considering different arch geometries (span and thickness of the masonry stones). The first step of this investigation is to conduct parametric simulations, in order to develop datasets, using as input and output values geometric and structural parameters of masonry arches. In a subsequent step, these datasets will be used to train artificial neural networks. Therefore, the article proposes a methodology for using machine learning, data-driven techniques, in order to achieve a fast and accurate prediction of the structural response of masonry arches. It is noted that to the authors' best knowledge, only limited works can be found, emphasizing in data-driven, machine learning approaches, for the structural evaluation of masonry arches. Also, the majority of the published research focuses more on the geometric aspects of the data-driven approaches, comparing to the structural response and the failure mode prediction which is the core outcome of this investigation.

In particular, two-dimensional, non-linear finite element models were developed to perform the parametric assessment, considering the following Heyman's assumptions: (i) masonry stones have no tensile strength and, (ii) the compressive strength of the stone is infinite (Heyman, 1966). The results obtained from the finite element models were used to train, validate, and test artificial neural networks. This procedure has been implemented using Python, Matlab and commercial finite element software. The trained neural networks can provide a fast structural evaluation of random masonry arches, with limited computational cost, emphasizing in critical and valid information for the ultimate structure response. Thus, the outputs of the trained neural networks, are, (a) the deformed geometry depicting potential damage under the self-weight, (b) the deformed geometry, also depicting potential damage, under self-weight and a vertical point load applied at ¼ of the span and (c) the ultimate load at collapse.

2. Ultimate (failure) response of masonry arches

Goal of this article is to propose a data-driven methodology for the structural evaluation of masonry arches. According to the overall concept, parametric structural simulations within non-linear finite element analysis are conducted to generate datasets providing the ultimate, failure response of masonry arches of various geometries. Machine learning elements in the form of artificial neural networks are then used to train the set of results obtained from the parametric finite element analysis. The trained neural networks are metamodels able to predict the failure response of randomly chosen masonry arch geometries. The parametric investigations are conducted on circular masonry arches, but any other geometry (e.g. parabolic) or even different structural type, could be adopted using the proposed concept.

In this section, principles of the mechanical response of masonry arches are provided, emphasizing in the ultimate, failure behaviour of these structures. The classical collapse mechanism theory as presented in Heyman (1982), has been widely used to determine the load-bearing capacity of masonry arches. This technique has been adopted by other analytical methods to estimate the thrust line passing through masonry arch stones. For arches to be fully under compression, the thrust line must lie within the core (middle third) of the section (Heyman, 1982). Unreinforced masonry arches form a plastic hinge when the thrust is tangent to the extrados and/or intrados of the arch. When the thrust line is tangent at three extrados and/or intrados points of the arch, three hinges are developed. The introduction of three hinges changes the determinacy of a fixed support arch from statically indeterminate to statically determinate. Then, the development of a fourth hinge triggers a kinematic collapse mechanism, widely known as the four-hinge collapse mechanism (Heyman, 1967).

According to this description, four-hinge collapse mechanism is generally the common cause of structural failure of masonry arches. In addition, this mechanism may not arise when a symmetrical arch is subjected to symmetric loading, like self-weight. Heyman (1967) demonstrated that this response may be obtained on semi-circular arches under their own weight. Under this condition, at least a 5th hinge must form to trigger a kinematic collapse.

To simulate the mentioned hinge mechanism between adjacent stones, principles taken from non-smooth mechanics have been adopted in this article within non-linear finite element analysis (Panagiotopoulos, 1985, Drosopoulos et al., 2006). In particular, a unilateral contact and friction law is used to describe the surface contact conditions. This law introduces a strong nonlinearity, even though the stones are assigned linear material properties. Therefore, nonlinearity is restricted

to the interfaces between the stones, allowing for the opening and/or sliding along these interfaces. This opening and sliding that may appear in an interface, give rise to 8 configurations of deformation between two adjacent stones (Stockdale et al., 2022). These deformation modes include openings, rotations, slips, and slip/rotation combinations, as shown in figure 1. It is noted, that these deformation modes can be predicted by the machine learning, data-driven approach which is proposed in this study.

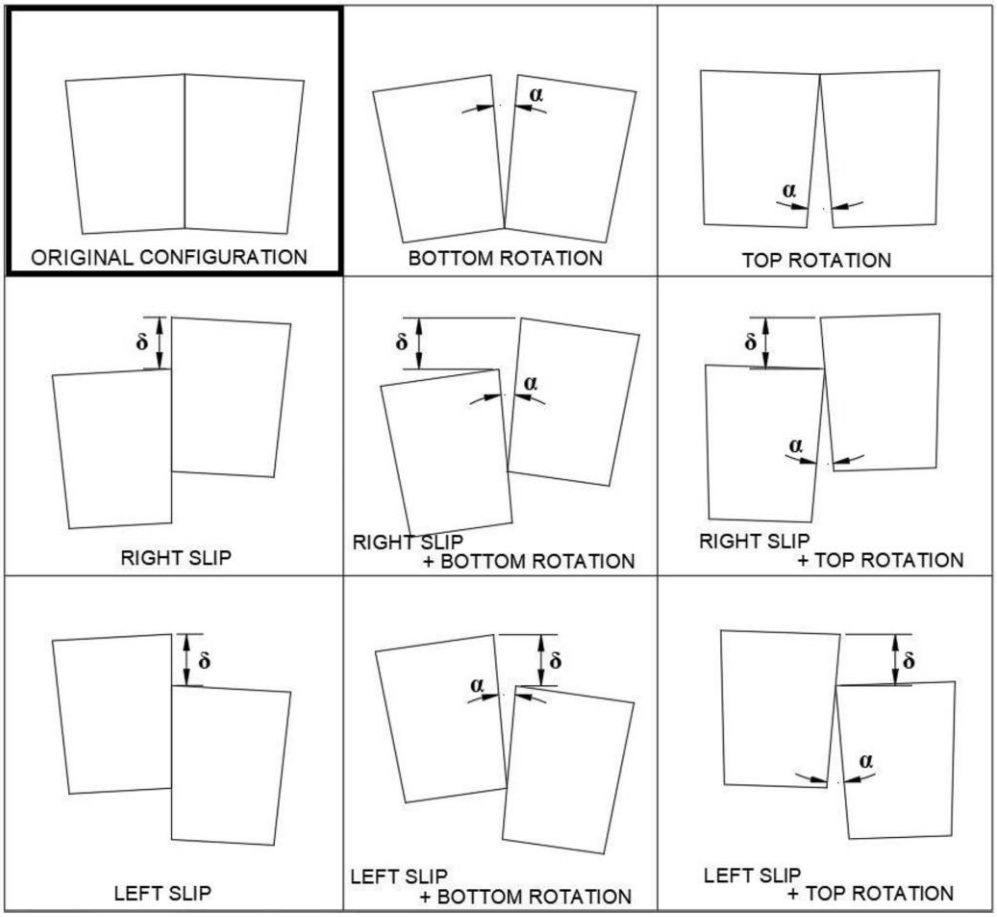

Figure 1: Potential deformation modes between two adjacent blocks of an arch (Stockdale et al., 2022).

3. Machine learning using artificial neural networks

Machine learning is a branch of artificial intelligence which focuses on training computer codes on how to make predictions of systems based on available datasets and algorithms. The ability of machine learning algorithms to recognise patterns from large datasets allows for their usage in various fields of study such as engineering, business, and science.

In (Reich, 1997) it was shown that machine learning was still in its infancy stage due to limitations on machine learning algorithms and computing power, as well as due to the lack of experimental databases to validate the machine learning models. Recently, it has been demonstrated a significant increase of using machine learning tools, to solve complex structural engineering problems (Thai, 2022). In addition, databases like *DataCenterHub*, *DesignSafe* and *Mendeley Data* can now be used to validate machine learning models. The number of machine learning algorithms has been significantly increased and tools like artificial neural networks, decision trees, regression analysis, support vector machine, random forest and boosting algorithms, have been adopted in structural engineering applications (Thai, 2022).

In this article, emphasis is given on using artificial neural networks as the numerical tool which implements data-driven structural assessment. An artificial neural network is developed by biomimicking the human brain structure, thus, how neurons are interconnected to imitate thinking, recognition and decision making (Simon, 1999, Nasrabadi, 2007). It was first invented by (Rosenblatt, 1958) in 1958 and called the *perceptron.* Due to improvements to computational power, various algorithms have been developed such as the feedforward neural network (Ivakhnenko, 1971), the radial basis function neural network (Broomhead and Lowe, 1988), the convolutional neural network (LeCun et al., 1998), the recurrent neural network (Elman, 1990) and the adaptive neuro-fuzzy inference system (Jang, 1993). The feedforward neural network is the most common system, due to its simplicity and robustness to solve multi-variate and nonlinear modelling problems (Mostafa et al., 2022, Thai, 2022).

In this study, a feedforward neural network is adopted to train the datasets which are built by finite element simulations. In figure 2 an example of a neural network represented by x-h-h-y is shown, where x is the number of inputs (variables), h is the number of neurons for one of the two hidden layers, and y is the number of outputs (prediction) (Mostafa et al., 2022). In the hidden layers, the input variables are assigned weights which need to be determined and then used to predict. Activation (sigmoid) functions, such as the nonlinear continuous sigmoid, the tangent sigmoid, and the logarithmic sigmoid, are also introduced (Haykin, 2009). The inputs are

multiplied by weights to provide the values of the output layers, within acceptable accuracy (low error margins). The iterative process of assigning weights is called training. Equation (1) shows a generic neuron j in a hidden layer, where w_{ij}^h is the weight that connects the i^{th} neuron of the current layer to the j^{th} neuron of the following layer, x_i^h is the input variable, b is the bias associated with the j^{th} neuron to adjust the output along with the weighted sum, and f is the activation function (Mostafa et al., 2022). Equations (2) and (3) provide some of the commonly adopted activation functions, the tangent sigmoid and logarithmic sigmoid, respectively.

$$y_j^h = f\left(\sum_{i=1}^{n} w_{ij}^h x_i^h + b_j^k\right) \quad (1)$$

$$f(u) = -1 + \frac{2}{(1+e^{-2u})} \quad (2)$$

$$f(u) = \frac{1}{(1+e^{-u})} \quad (3)$$

In this study, the Levenberg–Marquardt backpropagation algorithm (Hagan and Menhaj, 1994, Marquardt, 1963) is adopted to perform the training. The algorithm consists of two steps: (a) feed-forward weight values are determined to calculate the error by minimizing the least squares error function, and (b) propagating back the error to previous layers and checking if the error value falls outside the acceptable error margin. This iterative process (epoch) of backpropagation is repeated until the errors from the interconnecting weights are within the acceptable error margin. The fixed interconnecting weights now form a neural network which can be used to predict complex problems with certain accuracy. A schematic diagram of the whole training process is shown in figure 3.

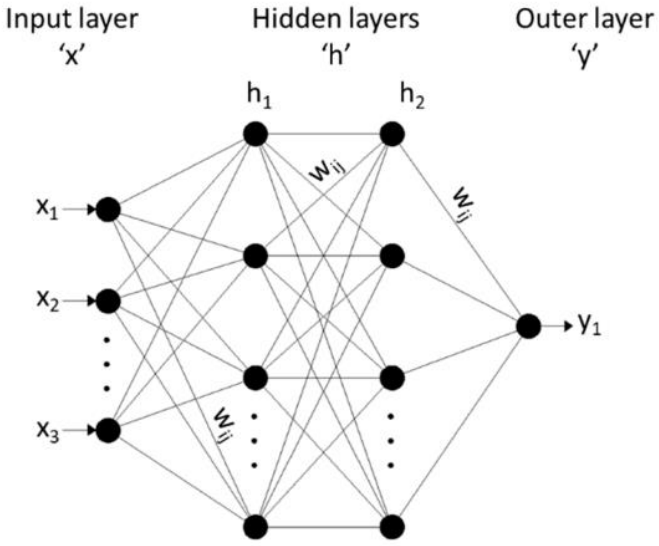

Figure 2: Feed-forward neural network architecture.

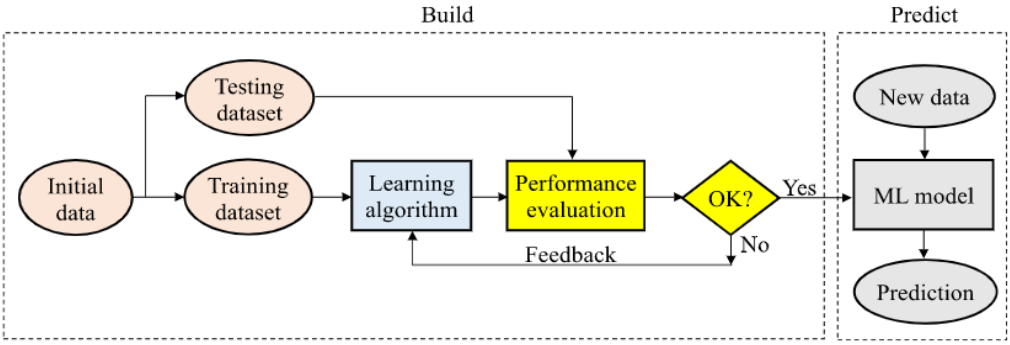

Figure 3: Typical workflow of machine learning (Thai, 2022).

4. The proposed data-driven scheme

The implementation in this article of data-driven structural analysis for masonry arches using machine learning principles, involves the use of a commercial finite element software (Abaqus) and two programming codes, namely, Matlab (Matlab, 2021) and Python. A code developed in Matlab is the pillar of the procedure, since it provides the overall definition of the parameters used by the finite element models, it establishes the connection with the parametric finite element model, and it implements machine learning. In Appendix 9.1 of the article, descriptions for this Matlab code are given.

The finite element software is only used to conduct the parametric structural simulations of masonry arches. A Python script is also introduced within the Matlab code, to call the finite element model without opening the GUI of the finite element software. Descriptions for this Python script are provided in Appendix 9.2 of the article.

The details of the proposed scheme are presented below:

- In the first step, a Matlab script (Appendix 9.1) is developed to define the geometry of the masonry arch and extract the (x) and (y) coordinates of the vertices of the individual stone blocks that make up the structure. The span of the arch and the thickness of the masonry blocks are the parameters introduced to define the geometry and used in the parametric investigation. The extracted coordinates are saved in a text file.
- In the second step, the Matlab script calls a Python script with the finite element model (Appendix 9.2), derived from the commercial finite element software, without the need to open the GUI of the software. The Python script initiates the solution for the discrete finite element model of the masonry arch, which is generated by reading the coordinates

from the text file (previous step). All the details of the non-linear finite element model are included in the Python script, namely, the boundary conditions (fixed supports), the applied loads (step-1: self-weight and, step-2: 100kN vertical point load applied at ¼ of span), the mesh (bilinear quadrilateral elements with size equal to 0.05m), and the unilateral contact/friction laws between the stones.

- In the third step, a second Matlab script (Appendix 9.3) calls the finite element software and runs a second Python script (Appendix 9.4) which extracts results from the finite element analysis solutions. The results extracted, include the (x) and (y) displacements of the four vertices of each stone block after the completion of the first and second loading steps (self-weight only and self-weight plus vertical point load, respectively), and the ultimate load at collapse. It is noted that these (x) and (y) displacements are used to determine the deformed shape of the arch, after the end of each finite element analysis.
- In the fourth step, the results obtained from the finite element models are sorted and stored as mat files (Matlab) to form databases. These databases are trained using an artificial neural network which can then be used to predict the structural response of any masonry arch within the range of the database values.

A flowchart illustrating the steps of the whole process is shown in figure 4. The path marked by the dashed-line (red) arrows in figure 4 shows the workflow/application of the trained neural network.

All the simulations were run on a computer with quad-core Intel® Xeon E5520 at 2.266 GHz and 16 GB RAM. The computational time needed to predict the structural response using the trained neural networks is about 25.5s.

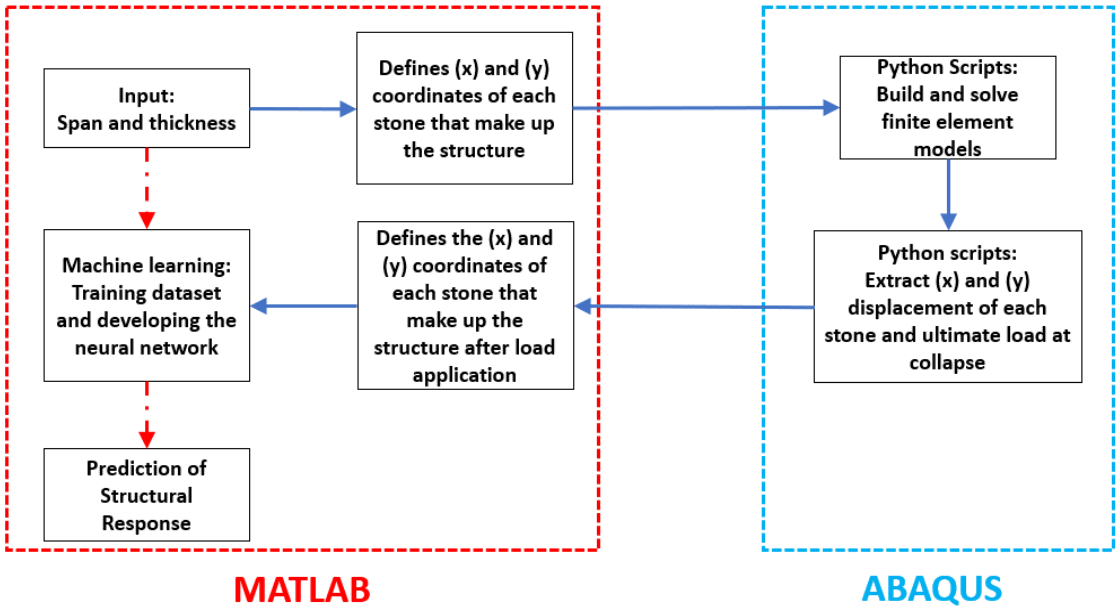

Figure 4: Flowchart of the proposed workflow.

5. Details of the parametric finite element analysis simulations

In this work, unilateral contact-friction interfaces are introduced between adjacent blocks to simulate the failure modes which are shown in figure 1. Sliding and/or opening of these interfaces, lead to the formation of hinges (the thrust line falls outside the section of the stone), depicting failure for two-dimensional masonry arches. To solve this unilateral contact–friction problem, the Lagrange multipliers method is adopted for simulating opening in the normal direction of the interfaces and the penalty method is used for simulating sliding in the tangential direction. In this study, the coefficient of friction is set at 0.5 (Melbourne and Gilbert, 1995). The arches are assigned fixed boundary conditions, the self-weight and a vertical point load, applied at ¼ of the span. Due to the introduction of the unilateral-contact and friction interfaces, the finite element model is non-linear. The Newton-Raphson incremental-iterative procedure is used to solve this problem.

To implement the parametric finite element simulations and generate the datasets, 1862 non-linear finite element models have been developed to provide a holistic insight in the structural response of masonry arches, emphasizing in potential collapse mechanisms. Within the adopted discrete approach, 20 two-dimensional masonry blocks have been used to create each masonry arch. It is noted that in previous studies (Charalambidi et al., 2022, Tapkın et al., 2022), it has been shown

that using more blocks than a chosen number, may not significantly affect the structural response, while it can increase the computational cost.

Due to its low tensile resistance, the mortar is neglected in the models developed for this study. Two steps are used to introduce static loads on the structure: the first step introduces a pure gravity load to simulate the state of inertia of the structure and the second step adds an incrementally applied point load of 100kN at ¼ of the span. The assigned material properties on the finite element models, are as follows: density is equal to 2300kg/m^3, Modulus of elasticity is 30GPa and Poisson's ratio is 0.2.

Concerning the failure response of the masonry arches, as this arises from the used discrete finite element models, it is noticed that the ultimate strength is reached when parts of the structure lose contact and develop rigid body displacements. This happens due to the fact that the defined unilateral contact/friction boundary constraints (assigned between stones) become insufficient to equilibrate the loaded structure. On the numerical model, as collapse is being reached, at least one zero eigenvalue on the tangential stiffness matrix is introduced which makes the analysis unstable.

6. Building the artificial neural networks

In this study, three neural networks have been trained, validated and tested to predict the structural response of masonry arches. Each trained neural network will provide a different insight about the structural behaviour of the arch. The first neural network will be used to predict the deformed geometry of the structure when subjected to self-weight only. The second neural network will predict the deformed geometry when the structure is subjected to self-weight plus a 100kN vertical load applied at ¼ of span. The third neural network will be used to predict the ultimate (failure) load at collapse, when the structure is subjected to self-weight plus a 100kN vertical load applied at ¼ of span.

To train the mentioned artificial neural networks, results derived from the finite element simulations, were extracted and used. In the input layer of each neural network are added the span and thickness of the masonry blocks representing the initial geometry of each arch. Figure 5 shows a Matlab plot of the vertices that make up the intrados and extrados of a 5.0m span arch with 0.25m masonry ring thickness.

In the output layer of the first two neural networks, are included the *x*- and *y*- displacements of each vertex on each of the 20 individual masonry stones, representing the deformed geometry at the end of each loading step of the finite element analysis.

In particular, the *x*- and *y*- displacements values at the end of loading step-1 were used to build the neural network that predicts the deformation of the structure when subjected to self-weight only and the *x*- and *y*- displacements values at the end of loading step-2 were used to build the neural network that predicts the deformation of the structure when subjected to self-weight plus a 100kN vertical point load.

In the third neural network, the output layer was defined by the ultimate load which is obtained at the end of the finite element analysis. Figure 6 shows the deformation of a 5.0m span arch with 0.25m thickness, subjected to self-weight and a 100kN vertical load applied at ¼ of the span. This figure is derived from one of the parametric finite element simulations, developed to create the databases that will be used to train the artificial neural networks. It is noted, that the opening and sliding between the masonry blocks as depicted in figure 6, can also be predicted and shown by the trained neural networks.

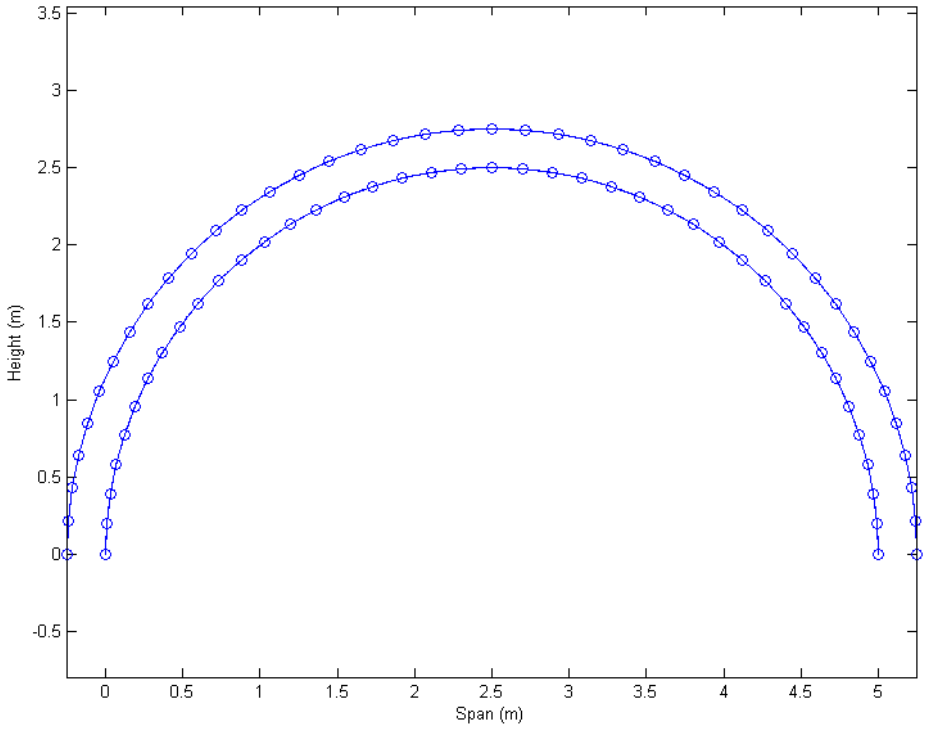

Figure 5: Matlab plot of the vertices that make up the intrados and extrados of a 5m span arch with 0.25m ring thickness.

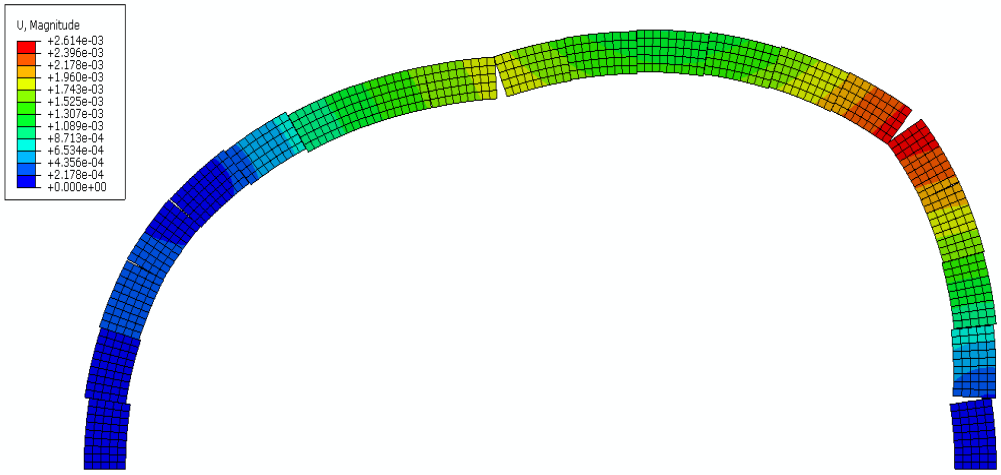

Figure 6: Deformation of 5m span arch with 0.25m thickness subjected to self-weight and a 100kN vertical load applied at 1/4 of the span.

6.1 Methodology and parameters adopted to train the artificial neural networks

In this study, the Levenberg-Marquardt algorithm is adopted to train the neural networks. This is considered as one of the fastest training algorithms (Matlab, 2021) but requires more memory than other techniques available. It uses Jacobian matrix to compute the solution and assumes that the performance function is the mean or sum of square errors. Like the quasi-Newton methods, second-order training speed can be achieved without solving the Hessian matrix (Liu et al., 2021). The Hessian matrix is approximated by equation (4) when the performance function is provided by the sum of squares errors and the gradient can be computed as Jacobian matrix multiplied by the vector of network errors, see equation (5).

Equation (6) shows how the Levenberg-Marquardt algorithms approximate the Hessian matrix (Hagan and Menhaj, 1994, Hagan et al., 1997) by combining the Gradient Descent and Newton-Raphson method. When μ is zero, equation (6) is transformed to Newton's method, using the approximate Hessian matrix. When μ is large, equation (6) forms Gradient Descent with a small step size. The algorithm is faster and more accurate when μ is small since Newton's method is quick when approaching the true value. With each successful iteration (epoch), the performance function is reduced unless the tentative step is not successful thus increasing the performance function. The aim to keep reducing μ makes the algorithm fast.

Table 1 shows the parameters used to train the neural networks. It should be noted that the neural networks were re-trained multiple times to improve the results, since during re-training different

initial conditions and sampling were considered. The 70/15/15 rule was used during the training process, which states that 70% of the dataset is used for training, 15% is used for validating the neural network and the remaining 15% is reserved for testing the neural network.

$$H = J^T J \tag{4}$$

$$g = J^T e \tag{5}$$

$$x_{k+1} = x_k - [J^T J + \mu I]^{-1} J^T e \tag{6}$$

In equations (4)-(6), H is the approximated Hessian matrix, J is the Jacobian matrix, g is the gradient, I is the identity matrix, e is the vector of network errors, and μ. is the adaptive value

Table 1: Parameters used to train the neural networks.

Parameter name	**Value**
Number of neurons in hidden layer	40
Maximum number of epochs to train	1000
Performance goal	0
Maximum validation failures	100
Minimum performance gradient	1e-7
Maximum value for μ	1e10
Initial μ	0.001
Decrease factor for μ	0.1
Increase factor for μ	10

6.2 Using the artificial neural networks

After training, validating, and testing the neural networks, they can be used to predict the structural response. The final deformed geometry of the structure is practically determined using equation (7) where u_o is the vector of coordinates of the vertices of the masonry blocks depicting the undeformed geometry before any load is applied, u_i is the vector of the displacements of the vertices of the masonry blocks after the load application and C is a user defined scale factor to ensure the deformation of the structure is easily visible. The vector u_i is predicted by the neural network and is dependent on the geometry of the structure and the load application.

Figure 7 shows the deformation of a 5.0m span arch with 0.25m thickness, subjected to self-weight and a 100kN vertical load applied at ¼ of the span, as derived by using the equation (7). A scale factor of 100 is used in this example so that the hinge formation can easily be seen. It should be emphasized that figure 7 indicates the capacity of the proposed approach to predict the deformed shape and the collapse mechanism of a masonry arch for a random geometry, using the proposed data-driven scheme. The Matlab code which is used to generate the deformed geometry, with inputs the vectors of the initial coordinates of the vertices of the masonry blocks u_o and the vector u_i of the displacements of the vertices of the masonry blocks after the load application, is given in Appendix 9.5.

$$u_j = u_o + C.u_i \tag{7}$$

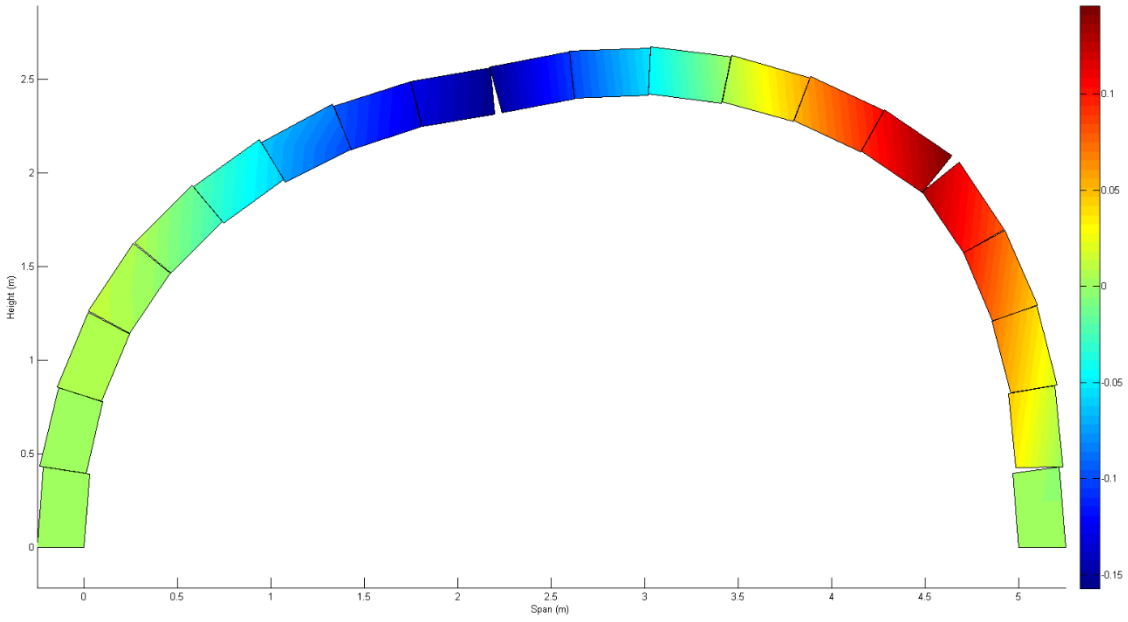

Figure 7: Deformation of 5m span arch with 0.25m thickness subjected to self-weight and a 100kN vertical load applied at 1/4 of the span, as derived by using equation (7).

7. Results and discussions

In this section, the performance and training accuracy of the developed neural networks are discussed. Then, it is shown how the trained neural networks can be used to predict the structural response of masonry arches of random geometry. Relevant results are provided and compared with existing output from literature.

7.1 Performance of the trained artificial neural networks

Three neural networks, namely, A, B and C, were trained by using 1304 data points, validated by 279, and tested by 279 data points respectively. In all neural networks, 2 input variables were used, namely, the span and the thickness of the masonry blocks that represent the arch geometry. In the first 2 neural networks (A and B) which are used to predict the deformed geometry under self-weight or self-weight and vertical loading, 160 output variables were used, namely, the displacements of the vertices of each of the 20 individual blocks making up the arches: 20 blocks x 4 vertices per block x 2 displacements per vertex. The deformed geometry of the arches can then be determined using theses 160 output variables, according to relation (7). In the third neural network (C), 1 output variable is considered, namely, the ultimate load.

In table 2, are provided details related to the training of the three neural networks. The neural network A in table 2 refers to the neural network that predicts the deformation due to self-weight only, the neural network B refers to the one predicting the deformation due to self-weight and a 100kN vertical point load and the neural network C refers to the neural network that predicts the ultimate load at collapse.

Regarding the training times given in table 2, neural network C depicted a shorter training time as compared to the other two networks, since the output layer of network C had only one variable, the ultimate load at collapse, comparing to the 160 variables of the output layer of the neural networks A and B of table 2.

As shown in table 2, the training, validation, and testing of the neural networks are accurate, with neural networks A and C showing more than 98% accuracy and with neural network B showing more than 95% accuracy. The neural networks were trained four times to increase accuracy, with each proceeding training done from the previously trained neural network without reinitializing and starting weights from zero. In addition, the mean squared error obtained from the training of the networks is very small.

Table 2: Summary information from the training process of the three neural networks.

	Neural Network A	**Neural Network B**	**Neural Network C**
Training time	1hr:10min:04sec	2hr:26min:41sec	15min:12sec
Iterations of train(epoch)	19	126	218
Training accuracy	98.63%	95.92%	99.23%
Validation accuracy	99.91%	96.14%	99.15%
Testing accuracy	99.86%	94.91%	99.26%
Mean Squared Error (MSE)	0.0001%	0.039%	0.0005%

Figures 8-10, show the regression plots for the training, validation and testing of the neural networks and how the trained neural network fit the dataset. From these figures, it is observed that the regression for training, validation and testing of the neural networks is almost 1, with 1 representing zero error in the trained neural network.

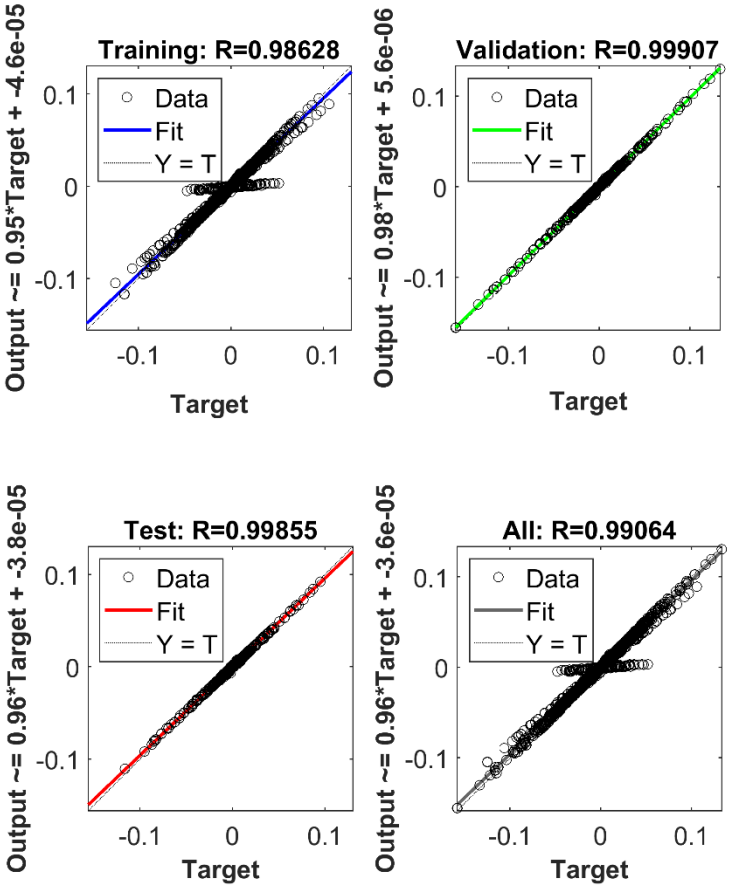

Figure 8: Regression plot for neural network A.

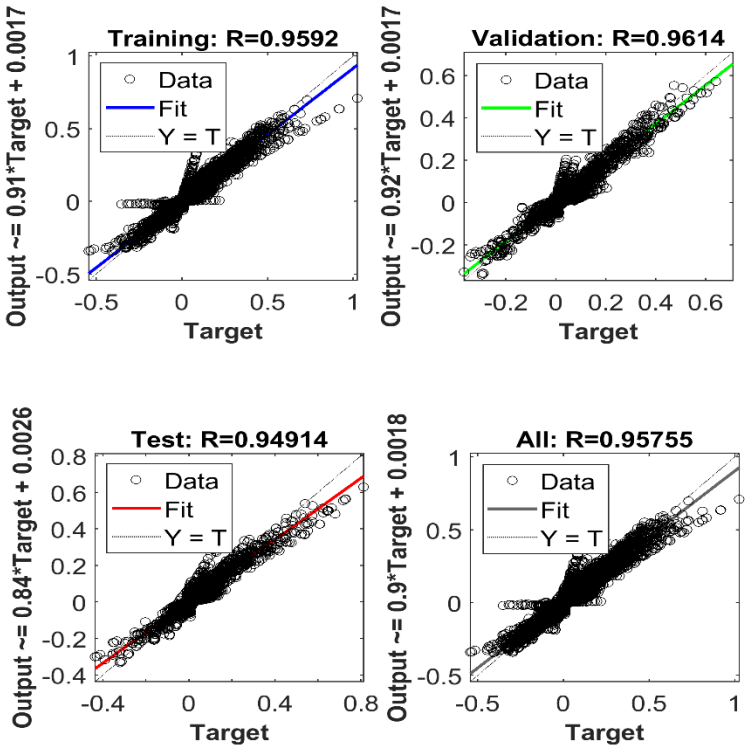

Figure 9: Regression plot for neural network B.

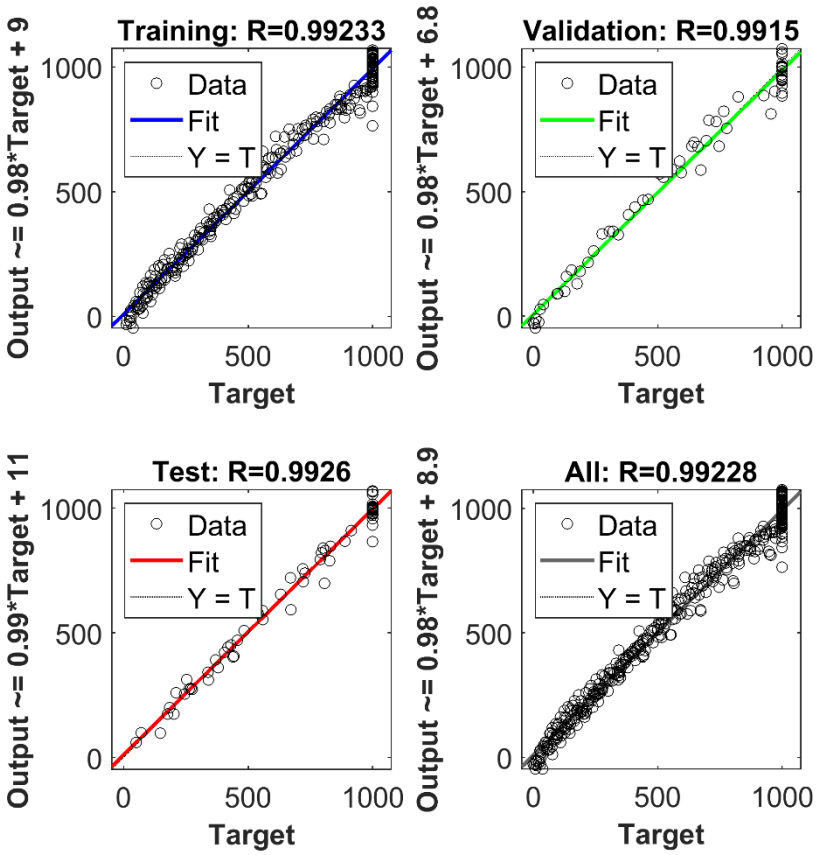

Figure 10: Regression plot for neural network C.

7.2 Predicting the response of random masonry arches using the proposed data-driven scheme

This section investigates the structural behaviour of six masonry arches as predicted by the trained neural networks. The dimensions of the six selected structures are within the range of the dataset values (1.5m-to-50m span, and 0.1m-to-1m masonry ring thickness). For the last two masonry arch geometries shown in table 3 (arches 5 and 6), the predicted by the proposed metamodel collapse mechanism and ultimate load, are compared with the results obtained from finite element analysis using commercial software.

In addition, arches 1 and 3 in table 3 are based on the minimum stone thickness for a circular arch to maintain stability under self-weight as proposed by (Couplet, 1729) and (Milankovitch, 1904, Milankovitch, 1907), respectively. (Couplet, 1729) proposed that the theoretical minimum thickness, t, of a circular masonry arch with radius, R, should be t/R=0.1075. Several years later, (Milankovitch, 1904, Milankovitch, 1907) proposed that the theoretical minimum thickness for a monolith arch should is t/R=0.10748.

In table 3 below, are provided the geometry of the selected arches as well as the ultimate load at collapse, which is predicted from the neural networks, when a vertical point load is applied at the quarter span.

Table 3: Geometry of masonry arches tested on neural networks and predicted ultimate load.

Name	**Span (m)**	**Height (m)**	**Stone thickness (m)**	**Ultimate Load (kN)**	**Source**
Arch 1	2.3	1.15	0.12	0	(Couplet, 1729)
Arch 2	16.0	8.0	1.0	100	-
Arch 3	6.0	3.0	0.32	13.4	(Milankovitch, 1904, Milankovitch, 1907)
Arch 4	12.0	6.0	0.5	9.1	-
Arch 5	20.2	10.1	0.84	35.9	-
Arch 6	10.4	5.2	0.45	8.8	-

The deformed shape of the arch 1 which is presented in figure 11, shows that the arch is highly unstable, since it collapses under its self-weight. It is noted that the deformation of this arch is derived using the neural network which predicts the deformation due to the self-weight loading (neural network A of table 2). Then, once the neural network which predicts the ultimate load is

used (neural network C of table 2), a zero load is obtained. A classical hinge failure mechanism of 5 hinges is obtained due to self-weight loading. This is a potential type of collapse, as found in literature when a symmetric, circular arch is subjected to symmetrical loading, e.g. self-weight (Cocchetti et al., 2012, Foce and Huerta, 2005, Heyman, 1995). A similar, five-hinge collapse mechanism is depicted in Figure 12 for a circular arch with the theoretical minimum thickness, as proposed in (Milankovitch, 1904, Milankovitch, 1907, Couplet, 1729).

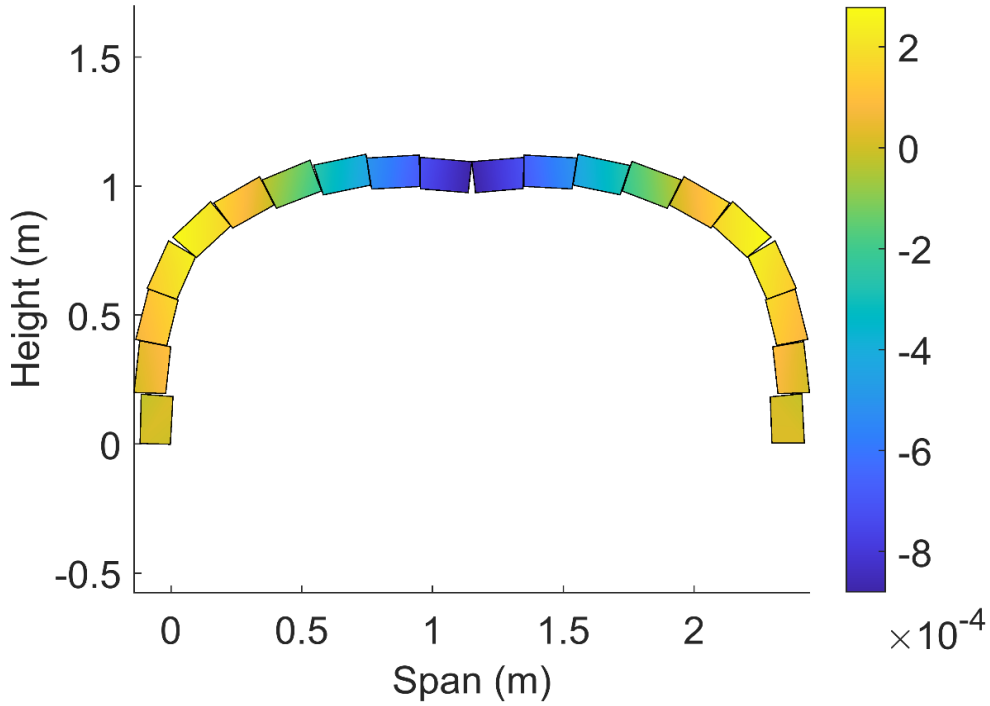

Figure 11: Deformation (m) of the arch 1 of table 3 (2.3m span, 0.12m thickness) due to self-weight only, when scale factor = 200.

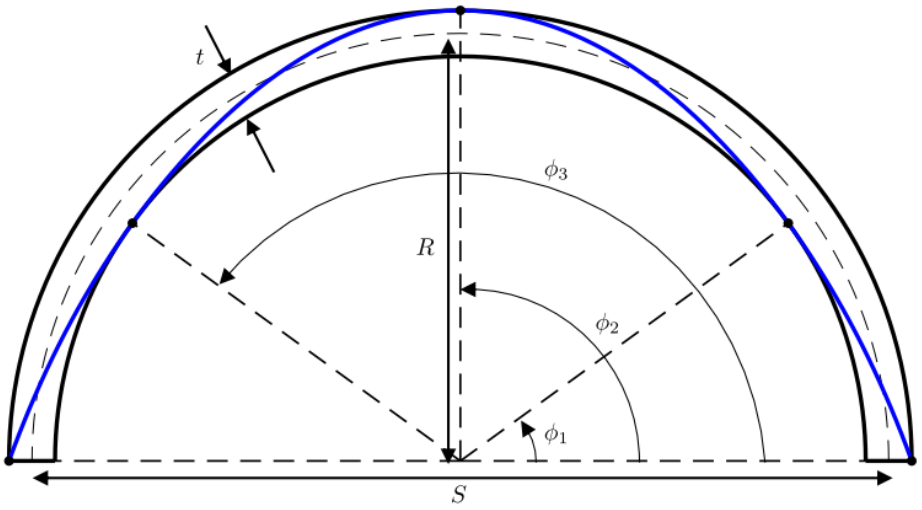

Figure 12: Five hinge mechanism for a circular masonry arch under self-weight based on literature. (McLean et al., 2021).

In figures 13-14, the deformed geometries of the arch 2 of table 3 due to self-weight only, as well as due to self-weight and a vertical point load, are shown. From the deformed shape due to self-weight (figure 13), is noticed that no hinge formation can be seen. According to figure 14, though some hinges have been developed in the arch, the four hinges mechanism is not fully developed at this load level, indicating that the arch is able to fully support the total applied load.

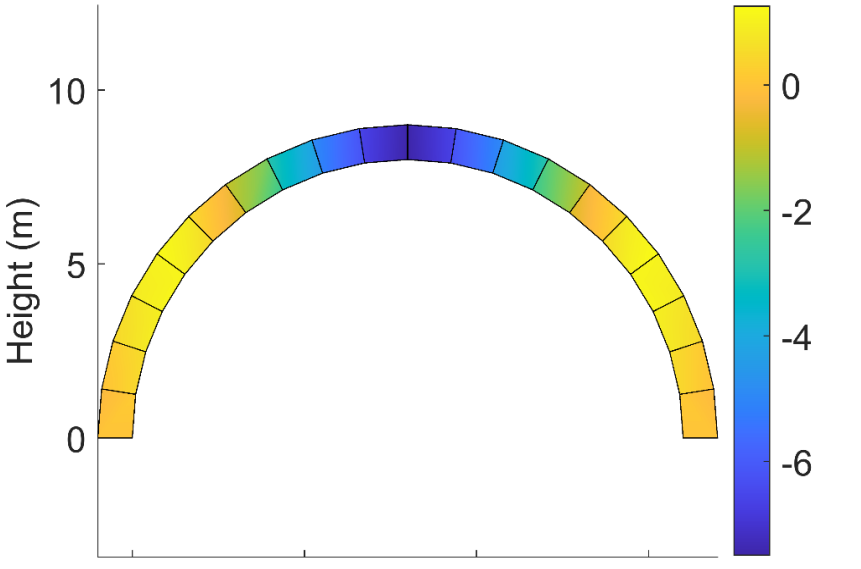

Figure 13: Deformation (m) of the arch 2 of table 3 (16m span, 1.0m thickness) due to self-weight only, when scale factor = 1.

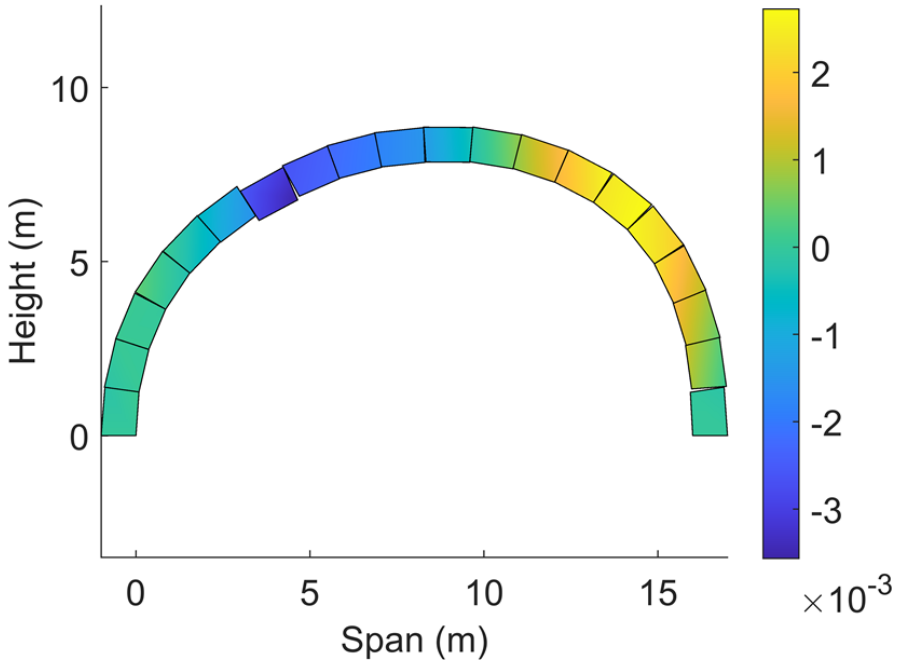

Figure 14: Deformation (m) of the arch 2 of table 3 (16m span, 1.0m thickness) due to self-weight and vertical load, when scale factor = 100.

In figures 15 and 17, the deformed geometries of arches 3 and 4 due to self-weight only are shown. These are followed by figures 16 and 18 depicting the deformed geometry of the same arches, due to self-weight and the vertical point load. When arches 3 and 4 are subjected to self-weight and a vertical point load, the deformed shapes of both arches as shown in figures 16 and 18, indicate that the four-hinge mechanism is developed. Thus, the arches fail to support the overall vertical load. The predicted ultimate loads at collapse, as obtained by the neural network C of table 2, are 13.4kN and 9.1kN for arches 3 and 4, respectively.

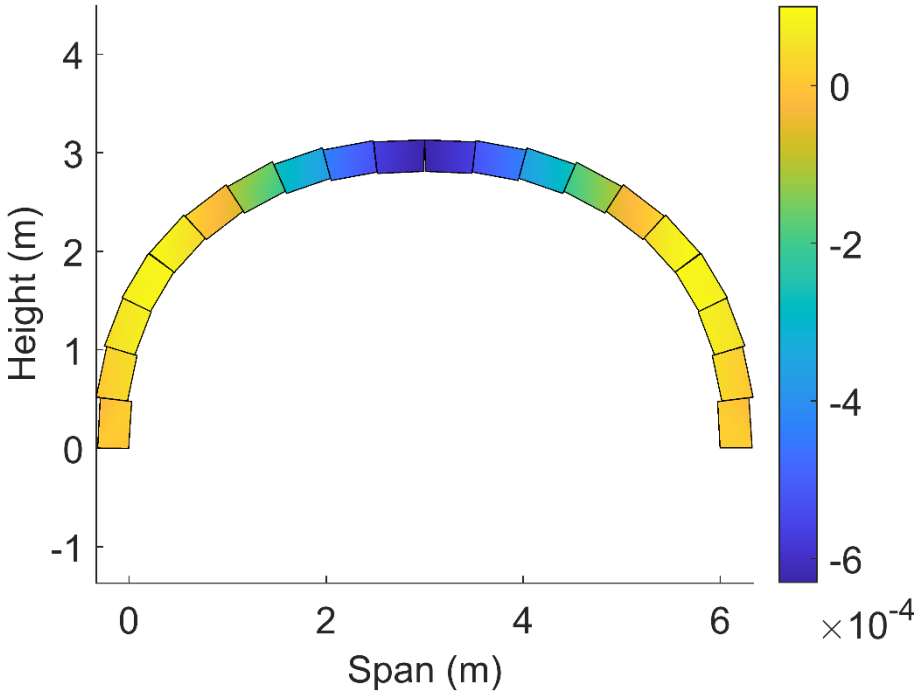

Figure 15: Deformation (m) of the arch 3 of table 3 (6m span, 0.32m thickness) due to self-weight only, when scale factor = 300.

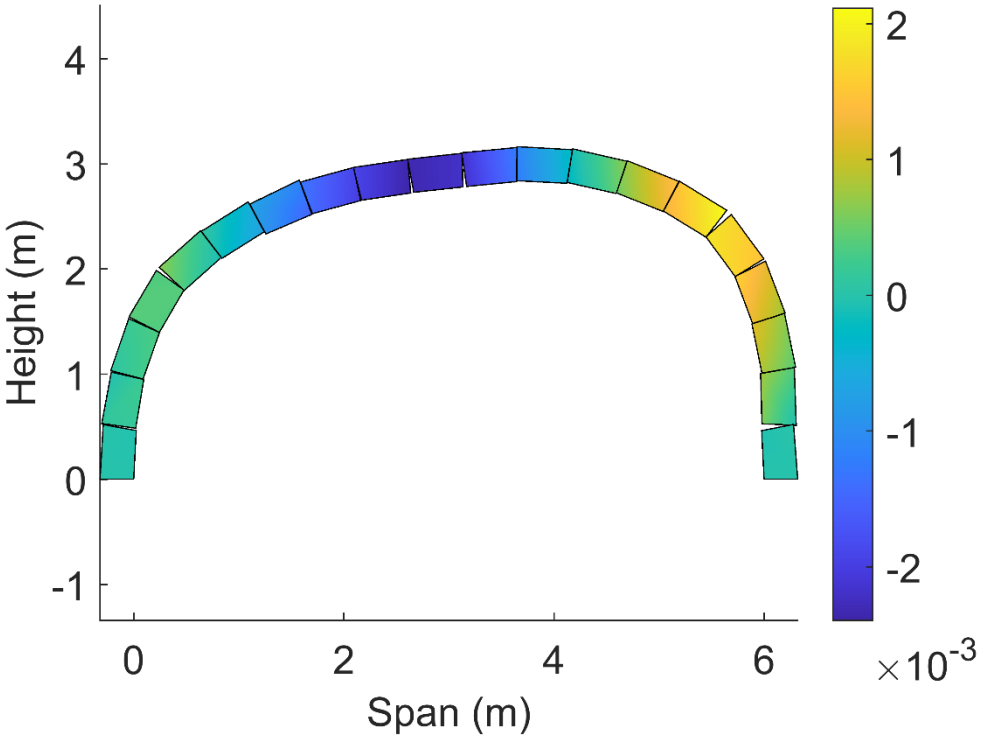

Figure 16: Deformation (m) of the arch 3 of table 3 (6m span, 0.32m thickness) due to self-weight and vertical load, when scale factor = 100.

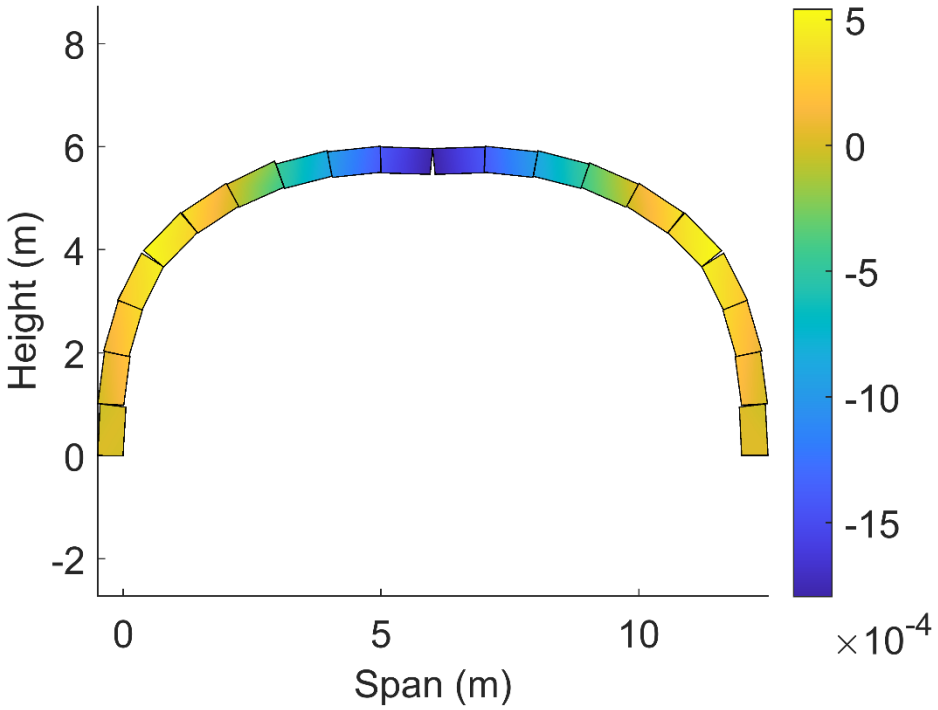

Figure 17: Deformation (m) of the arch 4 of table 3 (12.0m span, 0.5m thickness) due to self-weight only, when scale factor = 300.

In figures 19-20, the deformed geometries of the arch 5 of table 3 due to self-weight only, as well as due to self-weight and the vertical point load, are shown, as obtained from the trained neural networks. To provide a comparison of the results which are derived by the predictions of the trained neural networks, the same arch has been simulated using finite element analysis implemented by the commercial software. Figures 21 and 22 show the deformed geometry of the arch 5 due to self-weight as well as due to self-weight and the point load, as obtained by finite element analysis.

The geometry of the arch is stable under its self-weight as a symmetrical 3-hinge formation can be observed in figures 19 and 21. When the arch is subjected to self-weight and a vertical point load, the classical four-hinge collapse mechanism can be observed in figures 20 and 22. The predicted ultimate load (35.9kN, table 3) at collapse is comparable with the ultimate load (34.1kN) obtained from finite element analysis. It is noted that the ultimate load predicted by the neural network C of table 2 is slightly overestimated by 5.3%. The position of hinges, which are depicted in the neural network prediction and in the finite element analysis results, is also similar.

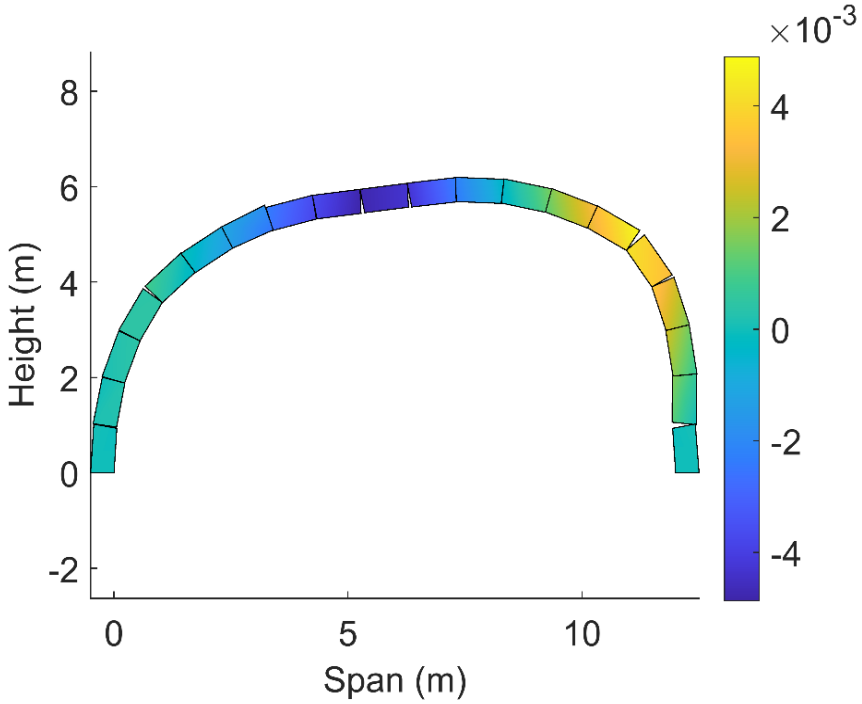

Figure 18: Deformation (m) of the arch 4 of table 3(12.0m span, 0.5m thickness) due to self-weight and vertical load, when scale factor = 100.

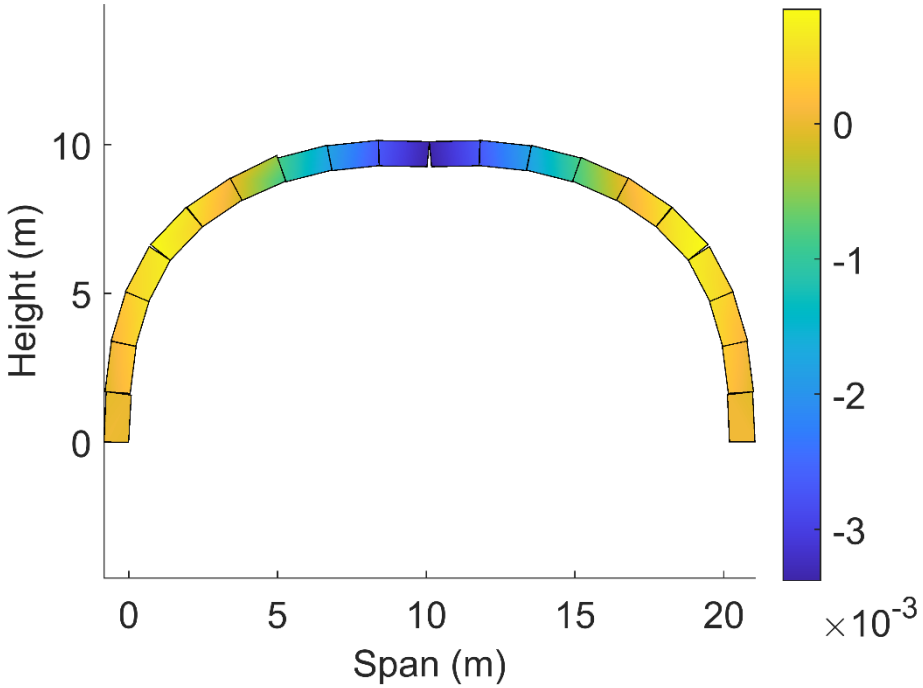

Figure 19: Deformation (m) of the arch 5 of table 3 (20.2m span, 0.84m thickness) due to self-weight only, when scale factor = 250.

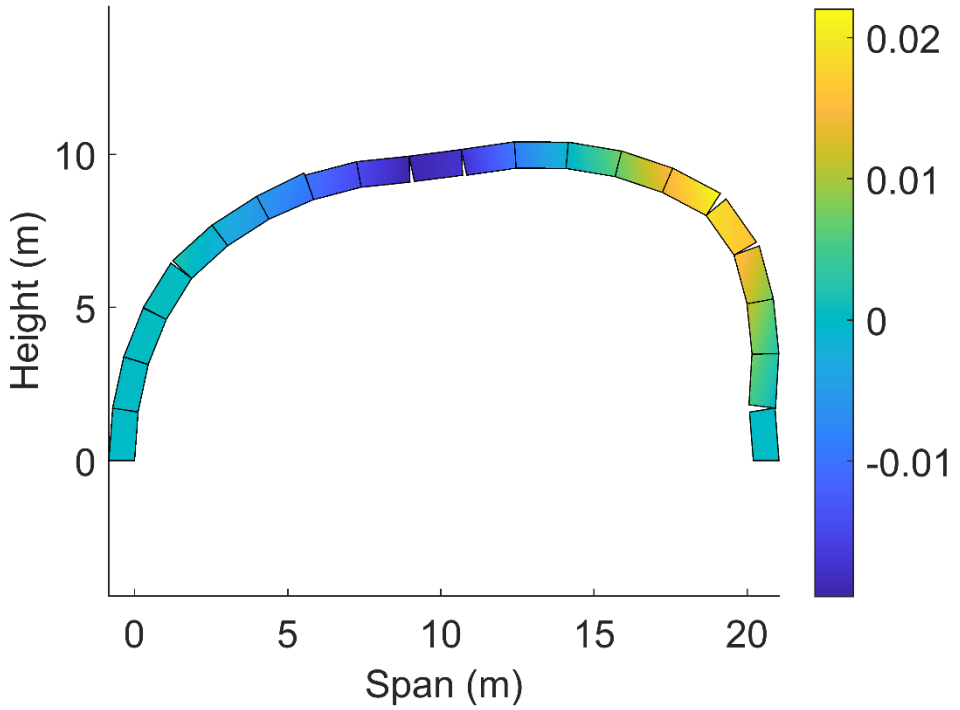

Figure 20: Deformation (m) of the arch 5 of table 3(20.2m span, 0.84m thickness) due to self-weight and vertical load, when scale factor = 45.

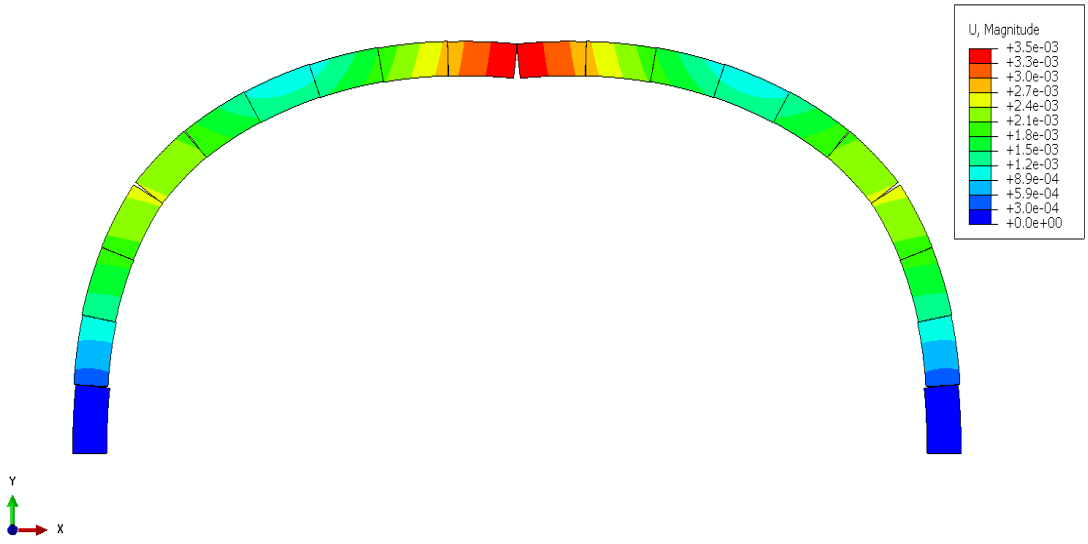

Figure 21: Deformation (m) of the arch 5 of table 3 (20.2m span, 0.84m thickness) due to self-weight only as obtained from finite element analysis. Figure is scaled by a deformation factor of 250.

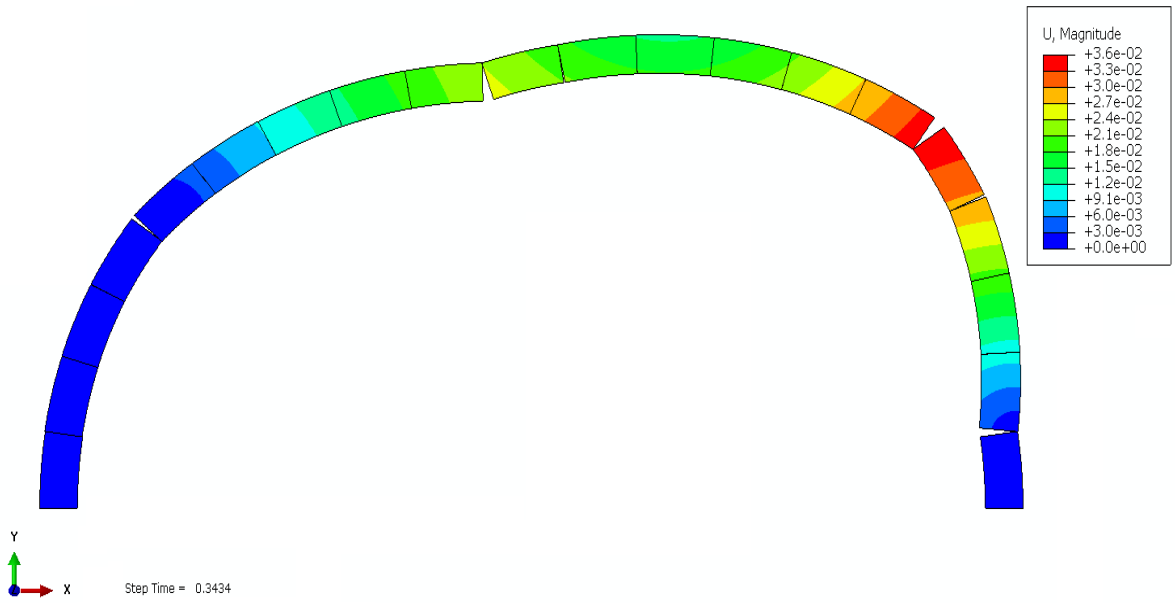

Figure 22: Deformation (m) of the arch 5 of table 3 (20.2m span, 0.84m thickness) due to self-weight and vertical load as obtained from finite element analysis. Figure is scaled by a deformation factor of 45.

Another example is presented, providing a comparison of the ultimate failure load and collapse mechanism obtained from finite element analysis and the proposed metamodel. Figures 23 and 24 show the deformed geometry of arch 6 due to self-weight and vertical point load as obtained from finite element analysis and as predicted by neural network B of table 2, respectively. It can be noted that in both figures 23 and 24, the classical four-hinge collapse mechanism can be observed. The predicted ultimate load (8.8kN) at collapse is comparable with the ultimate load (10.4kN) obtained from the finite element model. It is noted that the ultimate load predicted by the neural network C of table 2 is conservative.

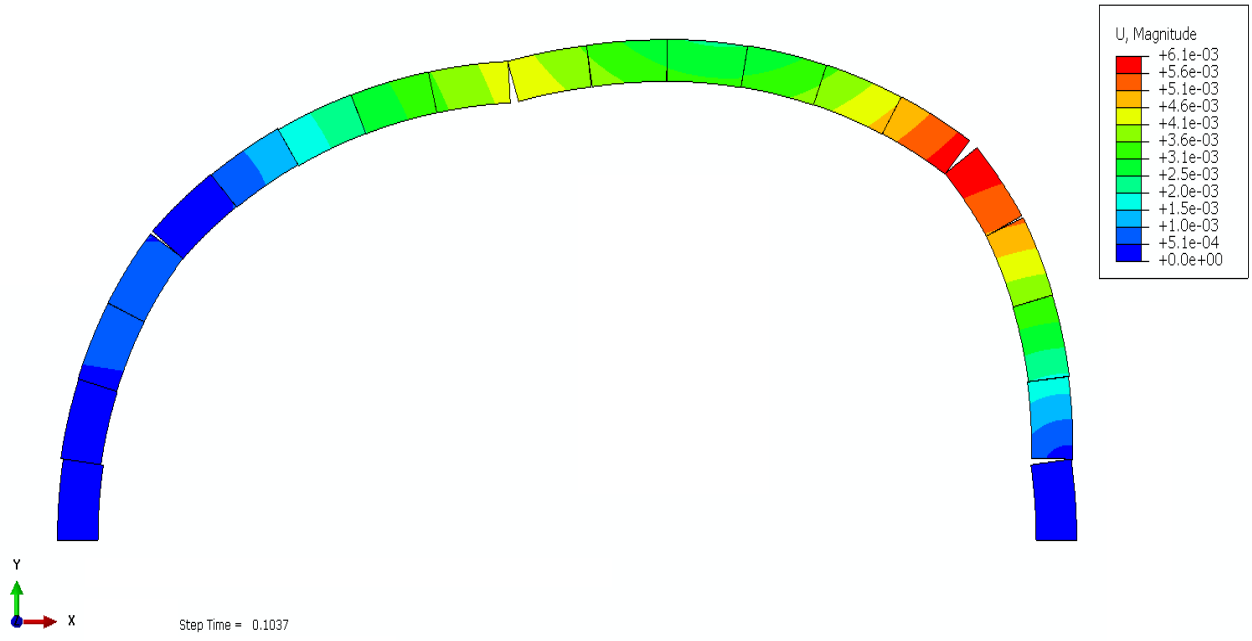

Figure 23: Deformation (m) of the arch 6 of table 3 (10.4m span, 0.45m thickness) due to self-weight and vertical load as obtained from finite element analysis. Figure is scaled by a deformation factor of 100.

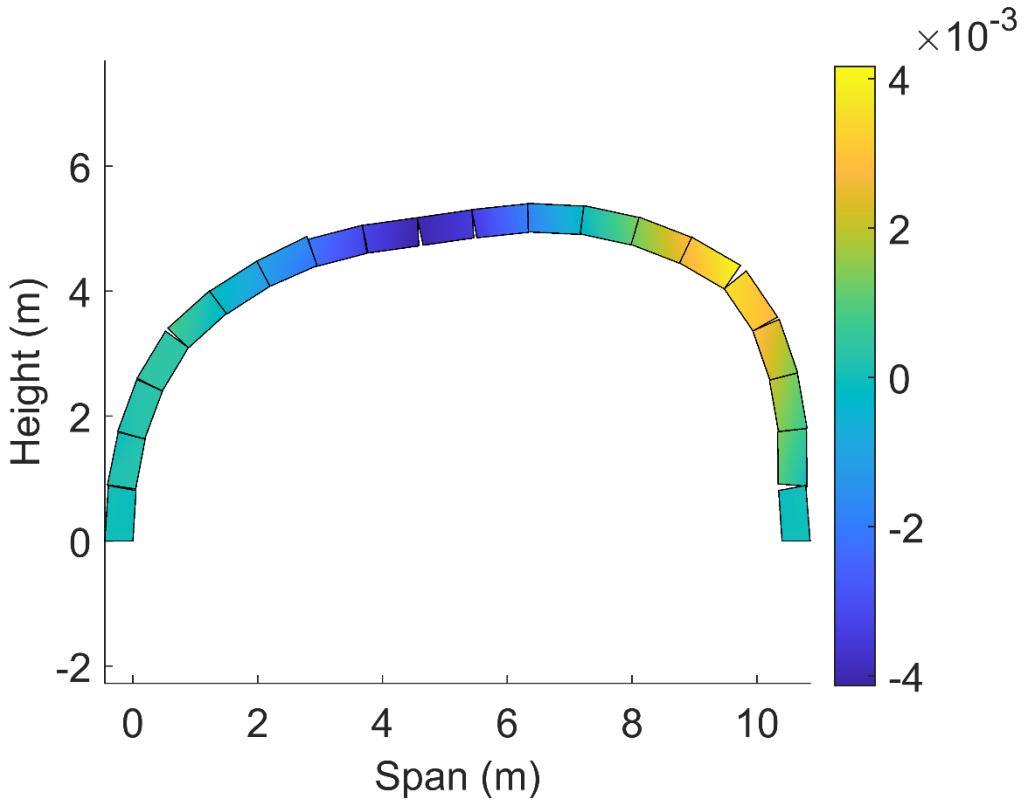

Figure 24: Deformation (m) of the arch 6 of table 3 (10.4m span, 0.45m thickness) due to self-weight and vertical load, when scale factor = 100

7.3 Summary of the results and datasets output

Finally, an effort to summarize the results provided in the datasets, reflecting holistically the structural response of masonry arches, is made here. In particular, it was observed that the structural response of a masonry arch varies with the span and masonry ring thickness. Therefore, both the span and the ring thickness values, which have been tested in the parametric simulations and included in the datasets, are provided in figures 25 and 26. In both figures, unstable and stable masonry arch geometries are denoted. The unstable geometries correspond to arches which fail under their self-weight and thus, cannot support any vertical loading. Stable geometries are the ones which support their self-weight and potentially fail under the vertical loading.

In figure 25, masonry ring thickness versus span values are provided for unstable and stable geometries. It is shown that for higher spans, ring thicknesses significantly increase in order to provide a stable geometry. For example, for a span of 20m, ring thicknesses higher than 0.75m lead to stable arches.

In figure 26, thickness/span ratio versus the number of dataset points, called dataset node values in the graph, are provided for unstable and stable geometries. According to this graph, 400 dataset points from the parametric simulations (approximately) lead to stable masonry geometries, while more than 1300 dataset points lead to unstable geometries. In addition, for a masonry ring thickness to span ratio lower than 0.0383, as indicated by the average line in figure 26, unstable masonry arch geometries arise. For higher values of this ratio, depicting a dispersion of increased thicknesses (or reduced spans), stable masonry arches arise. It is noted that the datasets for stable and unstable masonry arch geometries, providing also the ultimate loads, accompany this article. Relevant descriptions can be found in Appendix 9.6

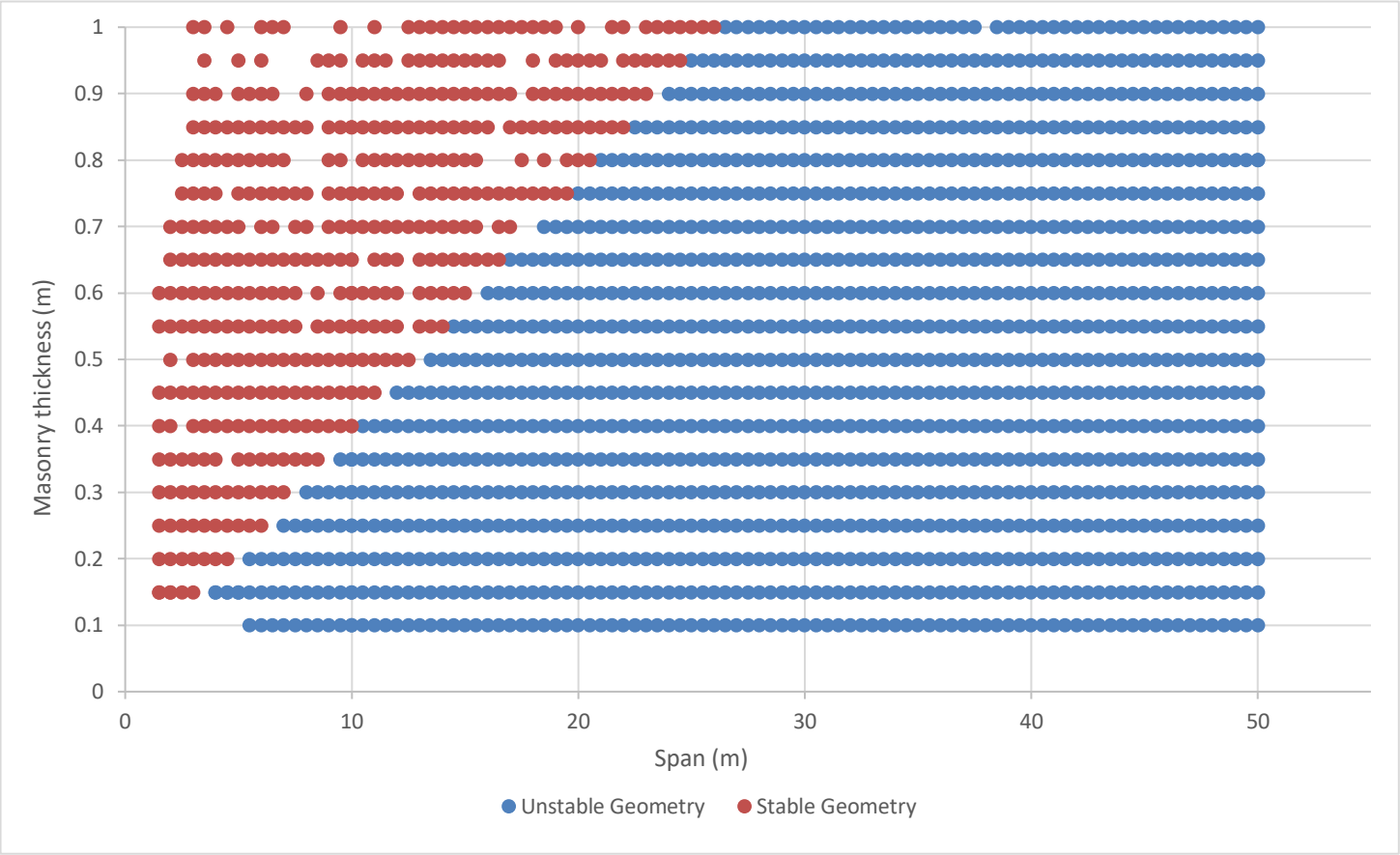

Figure 25: Plot of masonry thickness against span for stable and unstable masonry arch geometry.

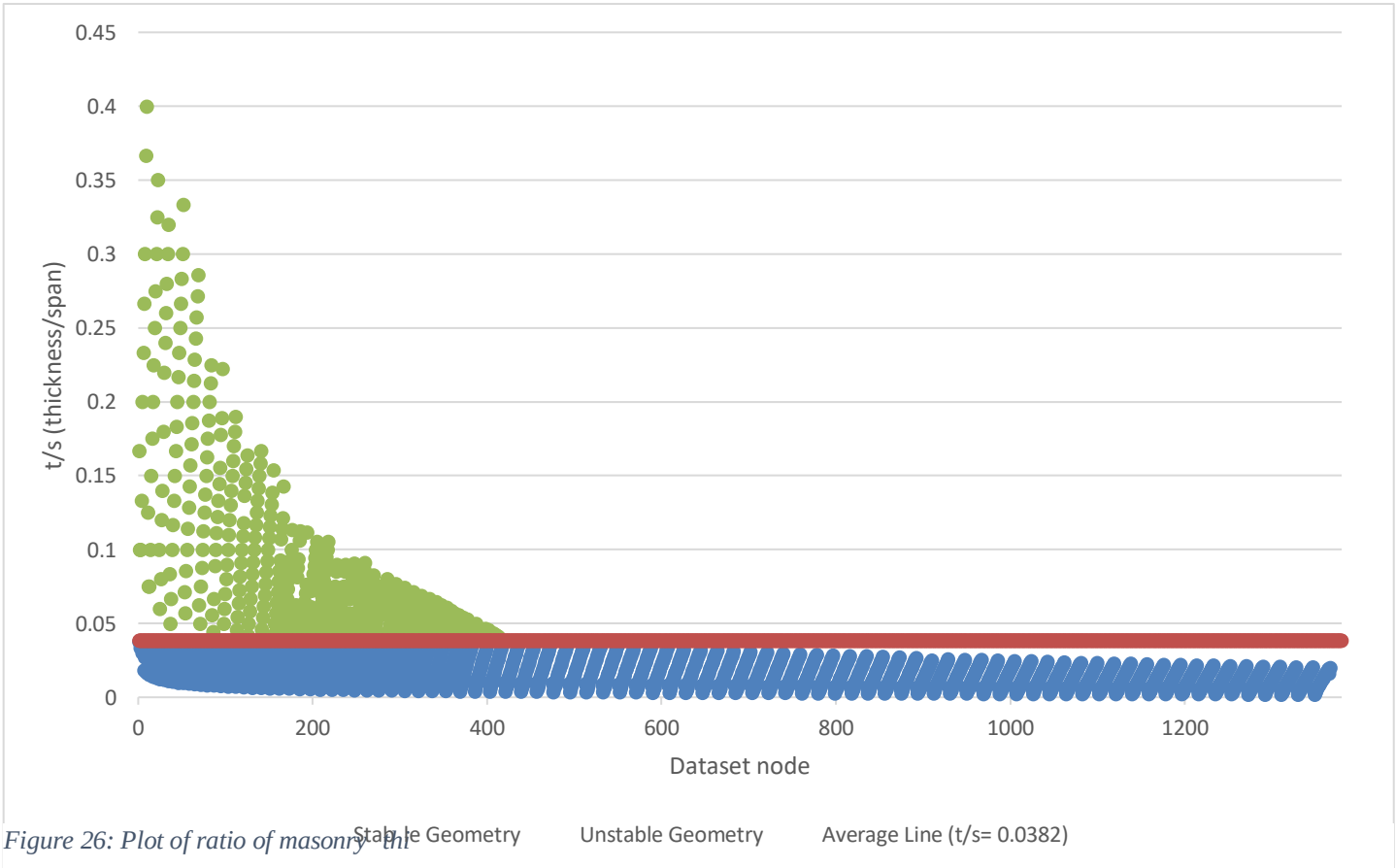

Figure 26: Plot of ratio of masonry thi

8. Conclusions

A data-driven methodology, relying on machine learning and finite element analysis is proposed in this article, to investigate the structural behaviour of masonry arches. The structures are subjected to two loading steps, the self-weight and the self-weight plus a vertical point load applied at the quarter span. Parametric, non-linear finite element simulations were conducted to generate datasets providing the ultimate response. These datasets were then used to train artificial neural networks which stand as metamodels, providing the ultimate load and the collapse mechanism of random masonry arches.

Two-dimensional geometries of masonry arches were developed using a Matlab script, where the coordinates of each of the vertices of the masonry stones is extracted. The structural, finite element models were created using Python scripts called within Matlab to drive, a commercial finite-element software. The Python scripts provide the geometry of the structure by reading the extracted coordinates of the masonry stones vertices. The script also adds the mechanical boundary conditions, the subjected loads, and a unilateral law, used to simulate potential damage due to opening/sliding (contact-friction) between the masonry stones. Due to the nonlinearity of the models, the Newton–Raphson incremental–iterative process was used to solve the numerical problem. Python scripts within Matlab were also used to extract the results from the models. A total of 1862 dataset points were used to train the neural networks. The training, validation and testing of the network neural networks were within acceptable tolerance.

The investigation shows that the proposed data-driven structural analysis of masonry arches can be used to provide accurate representation of the ultimate, failure response. The developed metamodel, can be used to predict the response of random masonry arches. The methodology can be extended to more complex three-dimensional geometries.

The article also proposes a numerical scheme to generate numerical datasets using Matlab and Python scripts as well as commercial finite element software. A complete set of relevant codes accompanies the article. Relevant descriptions can be found in the Appendix of the article.

The following conclusions can also be drawn:

- Machine learning can be a useful structural tool, in solving highly complex structural problems within a few seconds.

- The deformed geometries of the arches, which are predicted from the proposed process, are comparable with literature as well as with results obtained from finite element analysis.
- The developed structural tool can be used to investigate the structural behaviour of masonry arches without the need for extensive computational cost. Once the metamodel is built, predictions of the structural response can be provided in few seconds. Little or no structural knowledge is required since inputs of the metamodels are the span and the ring thickness of the structure. Thus, the proposed methodology can be extended and used for a first, fast and accurate representation of the ultimate response of similar structural systems.

Future work may involve the incorporation of image identification algorithms to the developed neural networks. With an image identification algorithm added, a photograph of a masonry arch can simply be supplied, read the geometry of the structure and feed it to the developed machine learning tool to predict the structural response. This would make the proposed methodology useful in structural health monitoring and site assessment for masonry arches. A system that quickly evaluates the remaining strength using these concepts could be helpful for the maintenance of these structures or during emergency situations after earthquakes or other disasters.

9. Appendices

In this section are provided descriptions of the source codes which have been developed to generate the dataset points. The interested reader can use, as well as extend the codes, for instance to generate more sophisticated (e.g. three-dimensional) geometries. All the source Matlab and Python files that have been used to create the parametric finite element simulations, as well as the datasets which have been used to train the artificial neural networks, accompany this article.

9.1 Central Matlab script

The central code in Matlab, which is used to create the parametric investigation of several geometries of masonry arches, is included in the Matlab script: *Appendix-1.m*.
Within this script, the commercial finite element software (Abaqus) is called, using a Python script (*Appendix-2.py*), to run a non-linear finite element simulation, for each arch geometry. The coordinates of the four vertices of each masonry block of each arch, are generated in *Appendix-1.m* script and saved in .txt files.

9.2 Python script implementing non-linear finite element analysis

The Python code, which is used to implement the non-linear finite element analysis of each parametric masonry arch geometry, is provided in the Python script: *Appendix-2.py*. Each parametric geometry, defined in *Appendix-1.m* script, is imported in *Appendix-2.py* script. In this script, all the steps of a finite element model can also be identified, including the material properties, the mesh, the loading and boundary conditions, as well as the unilateral contact-friction interfaces between the masonry blocks.

9.3 Matlab script generating results

The Matlab code which is used to generate results, is provided in the Matlab script: *Appendix-3.m*. Within this script, the commercial finite element software (Abaqus) is called via a Python script (*Appendix-4.py*), to provide the solution of the finite element analysis.

9.4 Python script generating results

The Python code, which is used to extract the results from the finite element simulations, is included in the Python script: *Appendix-4.py*. The extracted results are the displacements at the four vertices of each masonry block and the ultimate load.

9.5 Matlab script generating the deformed geometry of each masonry arch

The Matlab code, which is used to generate the deformed geometry of each masonry arch, is included in the Matlab script: *Appendix-5.m.* Inputs to generate one geometry, are the initial coordinates of the four vertices of each masonry block, as well as the displacements of the vertices of the masonry blocks at the end of each finite element simulation.

9.6 Datasets

The generated datasets, which have been used to train the artificial neural networks are also attached to this article in the form of an Excel spreadsheet: *DataSet.xlsx*. Within the datasets, stable and unstable geometries are identified.

At each column of the Excel spreadsheet, the following dataset points, derived from each parametric simulation, are provided: span of the masonry arch, thickness, ultimate load,

thickness/span ratio, deformed geometry of the arch due to self-weight, deformed of the arch due to point load (for the stable geometries).

Acknowledgments

Siphesihle Mpho Motsa has been supported by **Erasmus+ Program** within the framework of action "**International Credit Mobility**" between the Technical University of Crete, School of Production Engineering and Management and the University of KwaZulu-Natal, department of Civil engineering under Structural Engineering & Computational Mechanics (SECM) Group.

References

Anastasio, S. 2020. Building between the two rivers: an introduction to the building archaeology of ancient Mesopotamia. *Building between the Two Rivers*, 1-220.

Ashrafian, A., Panahi, E., Salehi, S., Karoglou, M., Asteris, P.G. 2023. Mapping the strength of agro-ecological lightweight concrete containing oil palm by-product using artificial intelligence techniques. *Structures*, 48, 1209-1229.

Beskopylny, A., Lyapin, A., Anysz, H., Meskhi, B., Veremeenko, A. & Mozgovoy, A. 2020. Artificial Neural Networks in Classification of Steel Grades Based on Non-Destructive Tests. *Materials (Basel)*, 13.

Bekas, G.K. & Stavroulakis, G.E. 2017. Machine learning and optimality in multi storey reinforced concrete frames. *Infrastructures*, 2, 6.

Block, P., DeJong, M. & Ochsendorf, J. 2006. As Hangs the Flexible Line: Equilibrium of Masonry Arches. *Nexus Network Journal*, 8, 13-24.

Broomhead, D. S. & Lowe, D. 1988. Radial basis functions, multi-variable functional interpolation and adaptive networks. Royal Signals and Radar Establishment Malvern (United Kingdom).

Cavaleri, L., Barkhordari, M.S., Repapis, C.C., Armaghani, D.J., Ulrikh, D.V., Asteris, P.G. 2022. Convolution-based ensemble learning algorithms to estimate the bond strength of the corroded reinforced concrete. *Construction and Building Materials*, 359, 129504.

Chang, W. & Zheng, W. 2019. Estimation of compressive strength of stirrup-confined circular columns using artificial neural networks. *Structural Concrete*, 20, 1328-1339.

Charalambidi, B., Koutsianitis, P., Motsa, S. M., Tairidis, G., Kasampali, A., Drosopoulos, G., Stavroulaki, M. & Stavroulakis, G. 2022. Modelling, identification and structural damage investigation of the Neoria monument in Chania. *Developments in the Built Environment*, 10, 100069.

Civera, M., Mugnaini, V. & Zanotti Fragonara, L. 2022. Machine learning-based automatic operational modal analysis: A structural health monitoring application to masonry arch bridges. *Structural Control and Health Monitoring*, 29, e3028.

Cocchetti, G., Colasante, G. & Rizzi, E. 2012. On the Analysis of Minimum Thickness in Circular Masonry Arches. *Applied Mechanics Reviews*, 64.

Conde, B., Drosopoulos, G., Stavroulakis, G., Riveiro, B. & Stavroulaki, M. 2016. Inverse analysis of masonry arch bridges for damaged condition investigation: Application on Kakodiki bridge. *Engineering Structures*, 127, 388-401.

Couplet, P. 1729. De la poussée des voûtes. *Histoire de l'Académie royale des sciences*, 79, 117-141.

Dais, D., Bal, I. E., Smyrou, E., Sarhosis, V. 2021. Automatic crack classification and segmentation on masonry surfaces using convolutional neural networks and transfer learning. *Automation in Construction*, 125, 103606.

Drosopoulos, G., Stavroulakis, G. & Massalas, C. 2006. Limit analysis of a single span masonry bridge with unilateral frictional contact interfaces. *Engineering Structures*, 28, 1864-1873.

Drosopoulos, G. A. & Stavroulakis, G. E. 2018. A computational homogenization approach for the study of localization of masonry structures using the XFEM. *Archive of Applied Mechanics*, 88, 2135-2152.

Drosopoulos, G. A. & Stavroulakis, G. E. 2020. Data-driven computational homogenization using Neural Networks, *Journal on Computing and Cultural Heritage*, 14, 1-19.

Elman, J. L. 1990. Finding structure in time. *Cognitive Science*, 14, 179-211.

Ferrero, C., Calderini, C. & Roca, P. 2023. Effect of joint deformability on the experimental and numerical response of dry-joint masonry arches subjected to large support displacements. *Engineering Structures*, 275, 115236.

Foce, F. & Huerta, S. 2005. On the safety of the masonry arch. Different formulations from the history of structural mechanics. *Essays in the History of Theory of Structures*, 117-142.

Gáspár, O., Sajtos, I. & Sipos, A. A. 2022. Multi-Hinge Failure Mechanisms of Masonry Arches Subject to Self-Weight as Derived from Minimum Thickness Analysis. *International Journal of Architectural Heritage*, 1-29.

Grandio, J., Riveiro, B., Soilán, M., Arias, P. 2022. Point cloud semantic segmentation of complex railway environments using deep learning. *Automation in Construction*, 141, 104425.

Grillanda, N., Milani, G., Ghosh, S., Halani, B. & Varma, M. 2021. SHM of a severely cracked masonry arch bridge in India: Experimental campaign and adaptive NURBS limit analysis numerical investigation. *Construction and Building Materials*, 280, 122490.

Hagan, M. T., Demuth, H. B. & Beale, M. 1997. Neural network design, PWS Publishing Co.

Hagan, M. T. & Menhaj, M. B. 1994. Training feedforward networks with the Marquardt algorithm. *IEEE transactions on Neural Networks*, 5, 989-993.

Haykin, S. 2009. *Neural networks and learning machines*, 3/E, Pearson Education India.

Heyman, J. 1966. The stone skeleton. *International Journal of solids and structures*, 2, 249-279.

Heyman, J. 1967. On shell solutions for masonry domes. *International Journal of Solids and Structures*, 3, 227-241.

Heyman, J. 1982. *The Mansonry Arch*, Chichester, UK: Ellis Horwood.

Heyman, J. 1995. The stone skeleton: structural engineering of masonry structures. Cambridge University Press, Cambridge, UK.

Heyman, J. 1998. *Structural analysis: a historical approach*, Cambridge University Press.

Hooke, R. 1676. A description of helioscopes, and some other instruments, London, printed by T.R. for John Martyn.

Ivakhnenko, A. G. 1971. Polynomial theory of complex systems. *IEEE transactions on Systems, Man, and Cybernetics*, 364-378.

Jang, J.-S. 1993. ANFIS: adaptive-network-based fuzzy inference system. *IEEE transactions on systems, man, and cybernetics*, 23, 665-685.

Jing, Y., Sheil, B. & Acikgoz, S. 2022. Segmentation of large-scale masonry arch bridge point clouds with a synthetic simulator and the BridgeNet neural network. *Automation in Construction*, 142, 104459.

LeCun, Y., Bottou, L., Bengio, Y. & Haffner, P. 1998. Gradient-based learning applied to document recognition. *Proceedings of the IEEE*, 86, 2278-2324.

Liu, D., Tang, Z., Bao, Y. & Li, H. 2021. Machine-learning-based methods for output-only structural modal identification. *Structural Control and Health Monitoring*, 28, e2843.

Lourenço, P. B. 2002. Computations on historic masonry structures. *Progress in Structural Engineering and Materials*, 4, 301-319.

Loverdos, D., Sarhosis, V. 2022. Automatic image-based brick segmentation and crack detection of masonry walls using machine learning. *Automation in Construction*, 140, 104389.

Loverdos, D., Sarhosis, V. 2023. Geometrical digital twins of masonry structures for documentation and structural assessment using machine learning. *Engineering Structures*, 275, Part A, 115256.

Marquardt, D. W. 1963. An algorithm for least-squares estimation of nonlinear parameters. *Journal of the society for Industrial and Applied Mathematics*, 11, 431-441.

Matlab 2021. release R2021a. Natick, Massachusetts: The MathWorks Inc.

McLean, T., Málaga-Chuquitaype, C., Kalapodis, N. & Kampas, G. 2021. OpenArch: An open-source package for determining the minimum-thickness of arches under seismic loads. *SoftwareX*, 15, 100731.

Melbourne, C. & Gilbert, M. 1995. The behaviour of multiring brickwork arch bridges. *Structural Engineer*, 73.

Melchiorre, J., Manuello, A. & Marano, G. 2021. Application of a Machine Learning Algorithm for the Structural Optimization of Circular Arches with Different Cross-Sections. *Journal of Applied Mathematics and Physics*, 09, 1159-1170.

Milani, G., Lourenco, P. & Tralli, A. 2006. Homogenization Approach for the Limit Analysis of Out-of-Plane Loaded Masonry Walls. *Journal of Structural Engineering-asce - J STRUCT ENG-ASCE*, 132.

Milankovitch, M. 1904. Beitrag zur Theorie der Druckkurven. Dissertation zur Erlangung der Doktorwürde, KK Technische Hochschule Vienna.

Milankovitch, M. 1907. Theorie der druckkurven, éditeur inconnu.

Mostafa, K., Zisis, I. & Moustafa, M. A. 2022. Machine Learning Techniques in Structural Wind Engineering: A State-of-the-Art Review. *Applied Sciences*, 12, 5232.

Nasrabadi, N. M. 2007. Book Review: Pattern Recognition and Machine Learning. *SPIE*.

O'Dwyer, D. 1999. Funicular analysis of masonry vaults. *Computers & Structures*, 73, 187-197.

Özmen, A. & Sayın, E. 2018. Linear dynamic analysis of a masonry arch bridge.

Panagiotopoulos, P. D. 1985. Inequality Problems in Mechanics and Applications: Convex and nonconvex energy functions, *Springer Science & Business Media*.

Poleni, G. 1748. Memorie istoriche della Gran Cupola del Tempio Vaticano, *Padua: Nella Stamperia del seminario*.

Prakash, M., Manikandan, S., Surenther, I., Aswin Kumar, M., Ilakkiya, S. & Menaka, D. 2019. Speculation of compressive strength of concrete in real-time. *International Journal of Recent Technology and Engineering*, 7, 988-992.

Psychas, I.D., Schauer, M., Böhrnsen, J.U., Marinaki, M., Marinakis, Y., Langer, S.C., Stavroulakis G.E. 2016. Detection of defective pile geometries using a coupled FEM/SBFEM approach and an ant colony classification algorithm. *Acta Mechanica 227*, 1279–1291.

Rahimi, A., Aval, S. B. B., Noori, M., Sarhosis, V., Wu, Z., Nikkhoo, A. & Altabey, W. A. 2022. A simplified beam model for the numerical analysis of masonry arch bridges –A case study of the Veresk railway bridge. *Structures*, 45, 1253-1266.

Reich, Y. 1997. Machine learning techniques for civil engineering problems. *Computer-Aided Civil and Infrastructure Engineering*, 12, 295-310.

Rosenblatt, F. 1958. The perceptron: a probabilistic model for information storage and organization in the brain. *Psychological review*, 65, 386.

Sadowski, Ł., Nikoo, M. & Nikoo, M. 2018. Concrete compressive strength prediction using the imperialist competitive algorithm. *Computers and Concrete, An International Journal*, 22, 355-363.

Sarhosis, V., Bagi, K., Lemos, J. V. & Milani, G. Computational Modeling of Masonry Structures Using the Discrete Element Method. 2016.

Simon, H. 1999. Neural networks: a comprehensive foundation, Prentice hall.

Simulia, D. S. 2013. ABAQUS 6.13 User's manual. Dassault Systems, *Providence, RI*, 305, 306.

Stavroulaki, M. E., Drosopoulos, G. A., Tavlopoulou, E., Skoutelis, N. & Stavroulakis, G. E. 2018. Investigation of the structural behaviour of a masonry castle by considering the actual damage. *International Journal of Masonry Research and Innovation*, 3, 1-33.

Stockdale, G., Yuan, Y. & Milani, G. 2022. The behavior mapping of masonry arches subjected to lumped deformations. *Construction and Building Materials*, 319, 126069.

Tapkın, S., Tercan, E., Motsa, S. M., Drosopoulos, G., Stavroulaki, M., Maravelakis, E. & Stavroulakis, G. 2022. Structural Investigation of Masonry Arch Bridges Using Various Nonlinear Finite-Element Models. *Journal of Bridge Engineering*, 27.

Thai, H.-T. 2022. Machine learning for structural engineering: A state-of-the-art review. *Structures*, 38, 448-491.

Tubaldi, E., Minga, E., Macorini, L. & Izzuddin, B. A. 2020. Mesoscale analysis of multi-span masonry arch bridges. *Engineering Structures*, 225, 111137.

Wołowiec, E. & Kula, P. Practical Application of Artificial Neural Networks in Designing Parameters of Steel Heat Treatment Processes. In: RUTKOWSKI, L., KORYTKOWSKI, M., SCHERER, R., TADEUSIEWICZ, R., ZADEH, L. A. & ZURADA, J. M., eds. Artificial Intelligence and Soft Computing, 2012// 2012 Berlin, Heidelberg. *Springer Berlin Heidelberg*, 196-203.

Yuan, Y., Stockdale, G. & Milani, G. A novel fast and low-cost masonry monitoring strategy for masonry arches. 2022 IEEE International Workshop on Metrology for Living Environment (MetroLivEn), 2022. *IEEE*, 149-153.

Zampieri, P., Tetougueni, C. D. & Pellegrino, C. 2021. Nonlinear seismic analysis of masonry bridges under multiple geometric and material considerations: Application to an existing seven-span arch bridge. *Structures*, 34, 78-94.

Chapter 7 – Conclusion and Future work

7.1 Conclusion

This chapter summarises the findings of this study and presents recommendations for future work. Detailed outcomes of the investigations which are conducted in this thesis, can also be found at the end of Chapters 4-6. The main aim of the present study was to provide more insight in the structural response of masonry systems using nonlinear finite element analysis.

In Chapter 4, a methodology to investigate multi-span masonry arches is proposed, starting from laser scanning, and building numerical models towards the structural response. The geometry of the arch bridge was obtained in-situ using terrestrial laser scanning, to collect a point cloud describing the geometry, which is then converted to a 3D solid geometry using AutoCAD. Numerical models were developed considering two modelling approaches, namely, the discrete and the continuum. Within this framework, continuum damage laws were introduced to capture compressive/tensile failure and a discrete model consisting of unilateral contact–friction interfaces were developed to simulate the potential opening of interfaces in adjacent masonry blocks. The discrete models were strongly nonlinear due to the presence of unilateral contact–friction interfaces. The Newton–Raphson incremental–iterative process was used to solve the numerical problem.

In this study, it was proved that the presence of fill above the arch barrel reduces the load dispersion to the arch thus increasing the ultimate load. The numerical modelling of out-of-plane loads, for instance the movement of supports in the direction of the waterway is highly unstable and computationally expensive. It was noted that the critical failure mode pattern observed is the hinge-mechanism which can be seen on both in-plane and out-of-plane loads. The classical four-hinge failure mechanism can be observed when a vertical point load is applied at middle arch, which has been depicted in classical studies for single-span arch masonry bridges. It is also shown that the three-hinge mechanism, which has been depicted in literature for single-span arch masonry bridges under a horizontal settlement of supports, may also be obtained for multi-arch bridges.

In addition, it was shown that the continuum approach model results in easy modelling and is computationally inexpensive. Tensile plastic strain distribution is the dominant failure pattern depicted by this approach. From the two continuum constitutive descriptions, the smeared cracking law results in convergence difficulties attributed to the brittle nature of this description. The failure patterns that are obtained from the continuum concrete damage plasticity law are

similar to the ones derived from the discrete approach. The discrete approach may lead to numerical instabilities and increased computational cost due to the presence of multiple unilateral contact–friction.

In Chapter 5, a methodology for the investigation and identification of the structural damage on masonry buildings is provided, using as a case-study the Neoria monument in Chania. The geometry of the structure is based on detailed geometric data, collected from sources and in-situ measurements. A detailed 3D geometric model of the structure was created with computer aided design (CAD) tools. A three-dimensional finite element model was then used to provide modal analysis. The goal of the modal analysis was to identify the different material properties assigned to different parts of the structure.

In this investigation, two- and three-dimensional models with unilateral contact–friction interfaces were used in a modified push-over analysis. Various numerical models with different loads were developed to investigate the cracks which are present on the different parts of the structure. In particular, to understand the influence of longitudinal cracks on the different sections of the monument, the following loads were considered in the framework of modified push-over analysis: (a) Lateral movement of the abutment due to a horizontal point load, and (b) a vertical displacement of supports. It was concluded that the longitudinal cracks are most likely caused by a vertical displacement of supports 2 and 8.

Lastly, an XFEM method was adopted to provide a further insight on the transverse discontinuities which are present on the structure. From the developed numerical models, it is observed that the existing longitudinal cracks do not propagate with the chosen load application. One potential reason for this, is the fact that these transverse cracks may not be considered as critical, since they will not interrupt the structural integrity of the system. Thus, in-between their positions, intact masonry arch parts will still be able to support the structural system.

In Chapter 6, a data-driven procedure for the investigation of the structural response of circular masonry arches using machine learning is proposed. To build the artificial neural networks that predict the structural response, 1862 nonlinear finite element models were developed and solved providing databases for training. The proposed data-driven procedure can predict the structural response when the masonry arches are subjected to two load cases: (a) self-weight only and (b) self-weight and a 100kN vertical point load applied at quarter span.

The development of the database required the integration of MATLAB scripts, Python scripts and a finite element software (ABAQUS). Two-dimensional geometries of masonry arches were

created using a MATLAB script, where the coordinates of each of the vertices of the masonry stones were extracted. The structural, finite element models were created using Python scripts within MATLAB to drive the commercial finite-element software. The Python scripts ran within MATLAB and the finite element software and created the geometry of the model by reading the extracted coordinates of the masonry stones vertices. The script also adds the mechanical boundary conditions, the subjected loads, and a unilateral law, used to simulate the contact-friction between the masonry stones. Due to the nonlinearity of the models, the Newton–Raphson incremental–iterative process was used to solve the numerical problem.

The neural networks used to predict the structural behaviour were built in MATLAB using the Levenberg-Marquardt training algorithm. The 70/15/15 rule was adopted to train the neural networks and 10 hidden layers were used. A total of 1862 data points were used to train the neural networks with each data points consists of 160 variables expect for the target layer for neural network C which had only one variable (the ultimate load).

The developed structural tool can be used to understand and investigate the structural behaviour of circular masonry arch structures without the need for extensive computational cost. This can be implemented within 26s and little or no structural knowledge is required since the inputs is just the span and thickness of the structure. Thus, the proposed methodology can be extended and used for a first, fast and accurate representation of the ultimate response of similar structural systems. Structural health monitoring applications can also use the proposed methodology.

7.2 Recommendations for further research

Following the comprehensive structural investigation on the response of masonry structures presented in this thesis, there is scope for future work.

From Chapter 4, where a methodology to investigate multi-span masonry arches is proposed, the influence of the spandrel walls on the mechanical response of masonry arch bridges can be investigated. The role of the spandrel walls is to contain the fill material from spilling out. Advanced numerical tools can used to model the cohesive behaviour of joint mortar even though it is computationally expensive.

From Chapter 5, there is scope to advance the methodology highlighted in the investigation of the structural damage on the Neoria monument. One of the future works can be attributed to the complexity of a massive, monumental structure, where there are uncertainties in the material properties. Currently there are efforts to implement nonlinear time history analysis, in order to evaluate the ultimate response of the building under real earthquakes. A plan to reinforce the monument will also be considered.

From Chapter 6, future work may involve the incorporation of photo identification algorithm to the developed neural networks. This would make the proposed methodology useful in structural health monitoring and site assessment of masonry arch structures. This system that can quickly evaluate the remaining strength of structures following emergency situations, like earthquakes.

Acknowledgements

Siphesihle Mpho Motsa has been supported by **Erasmus+ Program** within the framework of action "**International Credit Mobility**" between the Technical University of Crete, School of Production Engineering and Management and the University of KwaZulu-Natal, department of Civil engineering under Structural Engineering & Computational Mechanics (SECM) Group.

Appendix

PUBLICATION ACKNOWLEDGEMENTS

Authorship contribution statement of article presented in Chapter 4:

Tapkın, S., Tercan, E., **Motsa, S.M.**, Drosopoulos, G., Stavroulaki, M., Maravelakis, E. and Stavroulakis, G., (2022). Structural Investigation of Masonry Arch Bridges Using Various Nonlinear Finite-Element Models. Journal of Bridge Engineering, 27(7), p.04022053. (https://doi.org/10.1061/(ASCE)BE.1943-5592.0001870)

Authorship contribution statement

24th November, 2020

The following statement provides the contribution of each author on the following article and refers to the examination committee of the PhD thesis of the third co-author, Mr. M. Motsa. The only purpose of this document is to provide evidence for the contribution of Mr. Motsa on the conducted research and support his PhD thesis. The document will be submitted to the research office of UKZN, South Africa once the PhD thesis of Mr. Motsa is submitted. No other usage for this document is suggested.

Tapkın, S., Tercan, E., **Motsa, S.M.***, Drosopoulos, G., Stavroulaki, M., Maravelakis, E. and Stavroulakis, G., (2022). Structural Investigation of Masonry Arch Bridges Using Various Nonlinear Finite-Element Models. Journal of Bridge Engineering, 27(7), p.04022053. (https://doi.org/10.1061/(ASCE)BE.1943-5592.0001870)

*Corresponding Author

The contribution of each author is summarized below:

- S. Tapkin: Provided data for the laser scanning, needed for the representation of the geometry of the masonry arch bridge under investigation. He also participated in the revision of the initial version of the article.

- E. Tercan: Provided data for the laser scanning, needed for the representation of the geometry of the masonry arch bridge under investigation. He also participated in the revision of the initial version of the article.

- M. Motsa (Corresponding Author): Mr. Motsa is the PhD student at UKZN, who conducted the study for this article. In particular: he developed the numerical models needed for the structural investigation of the masonry arch using commercial software, he run all the simulations and he produced the results. Mr. Motsa also wrote and provided the first version of the article and participated in the revision of the article until the final version.

- G. Drosopoulos: Supervisor of Mpho Motsa, he assisted Mr. Motsa in the numerical simulations by providing instructions where needed.

- M. Stavroulaki: Provided ideas for the conducted research and the type of numerical simulations.

- E. Maravelakis: He transformed the format of the geometry of the masonry arch bridge under investigation, from point cloud (provided by the first two authors) to an appropriate format for the structural analysis software which was used (by Mr. Motsa) to simulate the structural response of the bridge.

- G. Stavroulakis: Provided ideas for the conducted research and the type of numerical simulations. He also provided access for Mr. Motsa to a computer server with the necessary capacity for the demanding numerical simulations of this work as well as to the software used for the numerical simulations.

Signature of all authors:

S. Tapkın:

E. Tercan:

M. Motsa:

G. Drosopoulos:

M. Stavroulaki: ΜΑΡΙΑ ΣΤΑΥΡΟΥΛΑΚΗ 2020.12.01 15:37:31 +02'00'

E. Maravelakis:

G. Stavroulakis: Georgios Stavroulakis Digitally signed by Georgios Stavroulakis Date: 2020.11.24 09:46:32 +02'00'

Authorship contribution statement of article presented in Chapter 5:

Charalambidi, B., Koutsianitis, P., **Motsa, S.M**., Tairidis, G., Kasampali, A., Drosopoulos, G., Stavroulaki, M. and Stavroulakis, G., (2022). Modelling, identification and structural damage investigation of the Neoria monument in Chania. *Developments in the Built Environment, 10*, p.100069. (https://doi.org/10.1016/j.dibe.2022.100069)

This publication is a result of a collection of three conference articles which were presented at the second international conference of *Transdisciplinary Multispectral Modeling and Cooperation for the Preservation of Cultural Heritage,* 13-15 December 2021 Athens, Greece (https://www.tmm-ch.com/tmm_ch2021). The references to these three conference papers are listed below. Copies of the two conference articles where the author (**Motsa S.M.)** had direct contribution on their preparation are presented in the Appendix section of this thesis.

1. Charalambidi, B., Koutsianitis, P., **Motsa, S.M**., Drosopoulos, G., Koutsianitis, P., Kasampali, A., Stavroulaki, M. and Stavroulakis,G. (2021). Structural Damage Investigation of the Neoria Monument in Chania. *Transdisciplinary Multispectral Modeling and Cooperation for the Preservation of Cultural Heritage: Second International Conference, TMM_CH 2021, Athens, Greece, December 13–15, 2021.* (https://www.tmm-ch.com/tmm_ch2021)

2. **Motsa, S.M.,** Drosopoulos, G., Charalambidi, B., Koutsianitis, P., Kasampali, A., Stavroulaki, M. and Stavroulakis, G., (2021). Discrete and XFEM Analysis for Crack Interpretation of the Neoria Monument in Chania. *Transdisciplinary Multispectral Modeling and Cooperation for the Preservation of Cultural Heritage: Second International Conference, TMM_CH 2021, Athens, Greece, December 13–15, 2021.* (https://www.tmm-ch.com/tmm_ch2021)

3. Koutsianitis, P., Charalambidi, B., Kasampali, A., Stavroulaki, M. and Stavroulakis, G., (2021). FEM Structural Modelling and Identification of the Neoria Monument in Chania. *Transdisciplinary Multispectral Modeling and Cooperation for the Preservation of Cultural Heritage: Second International Conference, TMM_CH 2021, Athens, Greece, December 13–15, 2021*. (https://www.tmm-ch.com/tmm_ch2021)

Authorship contribution statement of article presented in Chapter 6:

Chapter 6 of this thesis is prepared in the form of an article which has been submitted for publication in an international journal and is currently under review.

> **Motsa, S.M.**, Stavroulakis, G., and Drosopoulos, G. A data-driven, machine learning scheme used to predict the structural response of masonry arches. (Submitted for publication and currently under review)

Siphesihle Mpho Motsa conducted the research.

Georgios A. Drosopoulos is the supervisor of this PhD. Georgios Stavroulakis has contributed to the research by several discussions on the topic.

The main aspects of this chapter were conceptualised and developed at the Technical University of Crete in Greece by Siphesihle Mpho Motsa over a period of 3 months during his "**International Credit Mobility**" visit under the **Erasmus+ Program**.

CONFERENCE PAPERS

Paper 1: Structural Damage Investigation of the Neoria Monument in Chania

Structural Damage Investigation of the Neoria Monument in Chania

Barbara Charalambidi[1[0000-0001-9153-4611]], Siphesihle Motsa[2[0000-0003-4990-5225]], Georgios Drosopoulos[3[0000-0002-4252-6321]], Panagiotis Koutsianitis[1[0000-0002-4252-6321]], Amalia Kasampali[1[0000-0001-5627-3831]], Maria Stavroulaki[1[0000-0003-0882-5763]], Georgios Stavroulakis[1[0000-0001-9199-2110]]

[1] Technical University of Crete, Chania 73100, Greece
[2] University of Kwazulu-Natal, Durban, South Africa
[3] University of Central Lancashire, Preston, United Kingdom

Abstract. The structural investigation of Neoria masonry monument (venetian arsenal of the 16th century) includes an explanation of the existing damages and evaluation of their importance for further restoration and usage studies. Damages have been recorded and materials at different parts of the structure have been identified with several experimental techniques. A detailed geometric model of the structure and a parametrized finite element model has been created. Existing cracks and other defects have been collected during the experimental investigation and the site inspections. They have been included in the model with several simplification assumptions. A comparison of collapse predictions based on modified pushover analysis on a model with cracks and more classical modal analysis has been performed. An explanation of existing damages is attempted, based on the predictions of the numerical models.

Keywords: Finite Element Analysis, Monuments, Pushover Analysis, Damage Evaluation, Performance Prediction.

1 Introduction

Masonry structures have a peculiar mechanical behavior due to their no-tension characteristics. Form of the structure and mechanics are working together, trying to form a structure where all parts are mainly in compression, a loading that can be accommodated even by raw stones without mortar. Settlement movement or earthquake loadings disturb this picture and lead to activation of interfaces, damages and eventually partial or total collapse. Detailed structural analysis including unilateral interfaces and cracks is, in principle, possible [1].

Specific to study of historical masonry structures with vaults an accurate geometry of the vaults and the spandrels is necessary in order to model the existing condition including permanent deformations, weak material, cracks [2]. This is important for the estimation of the structural strength and dynamic behavior considering the three dimensional, effects of the vaults and the stabilization role of the spandrels [3].

Two different approaches are reported here for the explanation of existing cracks and damages in the Neoria structure (Fig. 1). First a classical modal analysis procedure is followed and the areas of higher deformation in the structure are correlated with damage patterns. Furthermore, a simplified two-dimensional model with unilateral interfaces is used in a push-over like analysis, to investigate collapse modes and loads. The results must be evaluated carefully, since pushover analysis has been developed mainly for ductile structures, while unreinforced masonry has limited, practically zero ductility.

Fig. 1. Neoria monument [Skoutelis et al. Intermediate Report, March 2021]

2 Pathology of Structure

For the structural model optimization, an analytical investigation of structure's damages was conducted. The purpose of the investigation was to include the existing deteriorations in the finite element model. The identified deteriorations are both biological (perforation, powdering) and mechanical (cracks, previous interventions with incompatible materials). The most important deteriorations of those detected were chosen to be included in the structural model. In Figure 2a all the cracks of the vaults, a plan view of which is illustrated in Figure 2b, can be shown. Five cracks on the vaults have been characterized as critical due to their depth and length as well as, three cracks on the west wall are considered as important (Fig. 3).

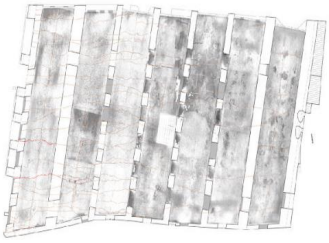

Fig. 2a. Plan View - Cracks Pattern on Structure's Roof (vaults) [4]

Fig. 2b. Plan view – Vaults (via Google Earth)

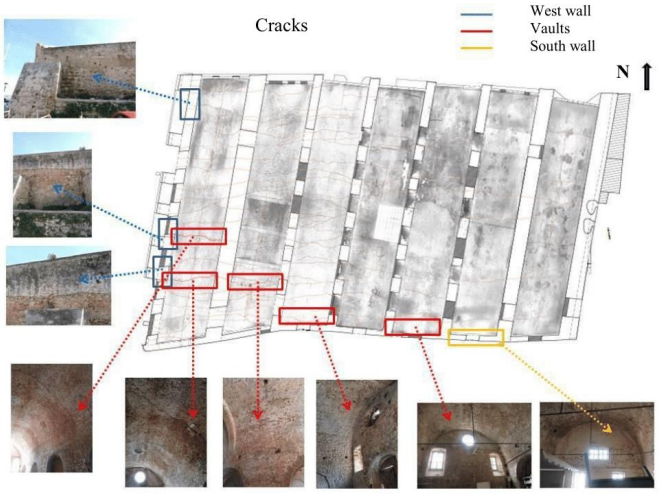

Fig. 3. Critical cracks (red and yellow annotation) on the vault and three critical cracks (annotated in blue) on the west wall of the structure

The structural conditions of the 4th and 6th vault from the west due to poor interventions are also considered as important (Fig. 4a, 4b). They have been imported to the model as material with reduced strength (reduced elastic modulus).

Fig. 4a. 4th vault – inside view

Fig.4b. 6th vault outside view

Characteristic cracks of the inside of the vaults and on the west wall are illustrated in the followed Figures (Fig. 5a, 5b, 5c)

Fig. 5a. Crack on vault – inside view

Fig. 5b. Crack on wall – West view

Fig. 5c. Biological Deterioration on the North Wall

3 Structural analysis modeling with cracks

From the in-situ investigation, the crack patterns have been documented. The finite element model of the structure [5] has been enhanced with weak zones that model, in a simplified way, the existence of cracks and other damages. In Figure 6, the simulation of the critical cracked region of the structure are illustrated via proper partitioning of the finite element model.

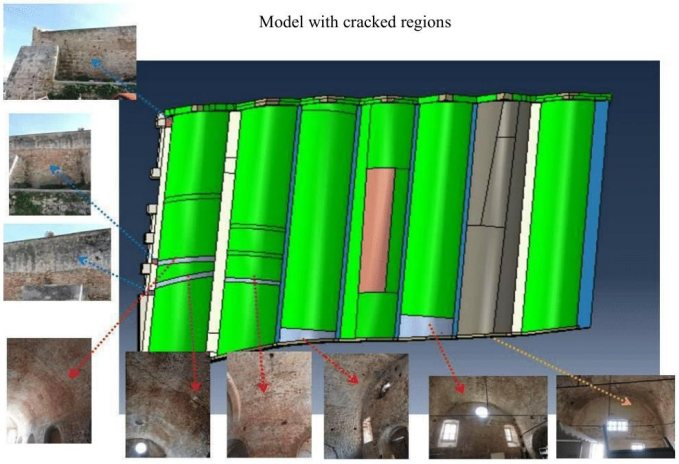

Fig. 6. Simulation of cracked region via partitioning of the F.E. model

From the analysis and the experimental investigation, it has been shown that higher vibration is accumulated near the frequency of 15 Hz. Therefore, the correlation of existing cracks with the maximum deformation patterns is shown in Figure 7.

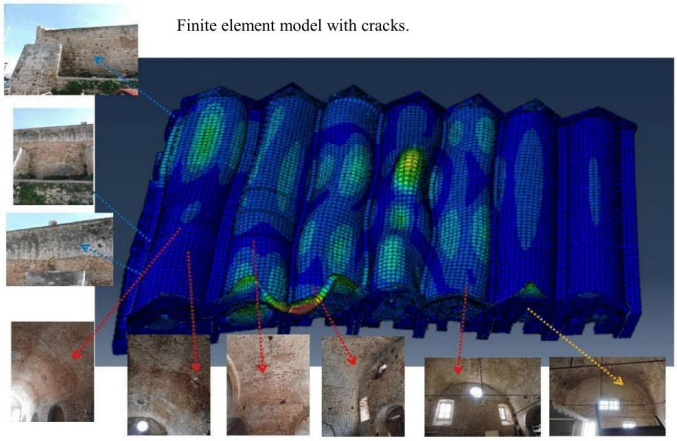

Fig. 7. 15 Hz eigenvalue shape of the structure (cracked model)

4 Unilateral crack models and push-over analysis

The mechanical behavior of unreinforced masonry structures is mainly based on compression loads transferred between adjacent parts of it, for instance stones, and secondary on frictional effects. This behavior is also known as unilateral, no-tension behavior. The existence of mortar with unreliable and low tensile strength is neglected. A further simplification for slender structures, like arches or domes, is based on the introduction of unilateral contact interfaces that model the nonlinear behavior. The activation or deactivation of contact, eventually with friction, during loading lead to reduction of the strength of the structure and eventually collapse, due to the formation of collapse mechanisms.

Following this method developed in our previous work [6-8] for masonry bridges, a two-dimensional model for one and for the seven Arsenals in the East-West direction has been created. A number of unilateral contact interfaces are included. By applying a horizontal or vertical life load and gradually increasing it, similarly, to push-over analysis, the unilateral interfaces are activated and eventually collapse is modeled.

Careful application of this procedure, which is recommended by modern design regulations for ductile structures, gave crack patterns that partially explain the measured crack patterns at the outside walls of the structure. A vertical push-down procedure is followed for the estimation of the vertical component of the earthquake. Activation of cracks at the crown of the vaults can be explained by this procedure. Crack patterns at the west part of the structure can be correlated with the results of the full seven- openings model.

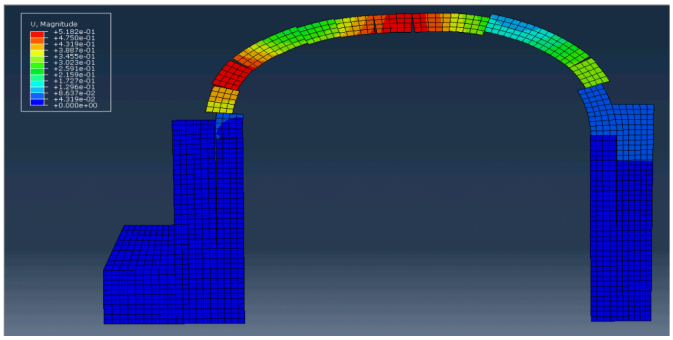

Fig. 8. Collapse mechanism (Western Neorio), where the activation of cracks in the center of the dome is clearly visible, as observed in the building.

Fig. 9. Indicative results from the whole two-dimensional model.

It must be repeated here that the results of pushover analysis have been used to give indicative correlation with existing crack patterns. Due to lack of ductility of the unreinforced masonry structure, they cannot be used for strength evaluation. From the collapse type and the performance of the overall two-dimensional model it is observed

that the most vulnerable areas are the extreme vaults. Pathology observation indicates the appearance of longitudinal cracks in the vault of the western and eastern Neorio. These cracks have caused the key vault to break on the north front. It is pointed out that there is no immediate risk of collapse as evidenced by the collapse mechanism which requires the development of cracks in other places of the vault as well as movement of the spandrels (longitudinal walls). More analytical results of usage of unilateral contact-friction interfaces integrated in limit analysis as developed within non-linear finite element analysis of Neoria are presented in [9].

5 Conclusion

Limit analysis calculations and modal analysis results have been used in order to explain damage and crack patterns found on the structure of the Neoria monument. First a three-dimensional finite element model were used for the classical modal analysis procedure and the areas of higher deformation in the structure were correlated with damage patterns.

Furthermore, a simplified two-dimensional model with unilateral interfaces was used in a push-over like analysis, in order to investigate collapse modes and loads. It is known that model with contact interfaces can be used in the stability assessment of a large monument [10] and in combination with optimization for the investigation of structures with faults [11].

Form the analysis results it was concluded the important role of the west wall to the failures of the 1st Neorio vault. Additionally, the isolation of the masonry strength due to lack of maintenance as well as earthquakes are the main causes of existing failures. The understanding the mechanism of construction failure is basic to the next in studying the required interventions.

References

1. Leftheris B., Sapounaki A., Stavroulaki M.E., Stavroulakis G.E.: Computational Mechanics for Heritage Structures. WIT - Computational Mechanics Publications, Southampton, Boston. (2006)
2. Stavroulaki, M.E., Riveiro, B., Drosopoulos, G. A., Solla, M., Koutsianitis, P., & Stavroulakis, G. E.: Modelling and strength evaluation of masonry bridges using terrestrial photogrammetry and finite elements. Advances in Engineering Software, 101, 136–148(2016).
3. Stavroulaki M.E., Tsinarakis Th.: Finite element analysis of masonry barrel vaults, 7th GRACM International Congress on Computational Mechanics, Athens (2011).
4. Skoutelis et al. Research Project on Rehabilitation of the Neoria Monument. Intermediate Report, Technical University of Crete, Municipality of Chania, Ministry of Culture, March 2021
5. Koutsianitis P., Charalambidi B., Kasampali A., Stavroulaki M., Stavroulakis G.: Finite Element Structural Modelling and Identification of the Neoria Monument in Chania. 2nd International Conference TMM-CH, Athens(2021)
6. Drosopoulos G.A., Stavroulakis G.E., Massalas C.V.: Limit analysis of a single span masonry bridge with unilateral frictional contact interfaces. Engineering Structures, 28, 1864-1873(2006).

7. Drosopoulos G.A., Stavroulakis G.E., Massalas C.V.: Influence of the geometry and the abutments movement on the collapse of stone arch bridges. Construction and Building Materials, 22(3), 200-210(2008)
8. Stavroulakis G.E., Menemenis I., Stavroulaki M.E., Drosopoulos G.A.: Collapse Prediction and Safety of Masonry Arches. In: Gocić M., Aronica G., Stavroulakis G., Trajković S. (eds) Natural Risk Management and Engineering. Springer Tracts in Civil Engineering. Springer, Cham. (2020)
9. Motsa S.M., Drosopoulos G.A., Charalambidi B., Koutsianitis P., Kasampali A., Stavroulaki M., Stavroulakis G.: Discrete and XFEM Analysis for Crack Interpretation of the Neoria Monument in Chania. 2nd International Conference TMM-CH, Athens(2021)
10. Motsa S.M., Drosopoulos G.A., Stavroulaki M.E., Stavroulakis G.E., Ruben P. Borg, P. Galea S d'Amico: Large-scale contact analysis for the stability estimation of the Mnajdra Monuments. Advances in Engineering Materials, Structures and Systems: Innovations, Mechanics and Applications. Zigoni (Ed.), Taylor & Francis, 2160-2164(2019).
11. Conde, B., Drosopoulos, G.A., Stavroulakis, G.E., Riveiro, B., Stavroulaki, M.E.: Inverse analysis of masonry arch bridges for damaged condition investigation: Application on Kakodiki bridge. Engineering Structures, 127, 388-401(2016).

Paper 2: Discrete and XFEM Analysis for Crack Interpretation of the Neoria Monument in Chania

Discrete and XFEM Analysis for Crack Interpretation of the Neoria Monument in Chania

Siphesihle Mpho Motsa[1(0000-0003-4990-5225)], Georgios Drosopoulos[1,2(0000-0002-4252-6321)], Barbara Charalambidi[3(0000-0001-9153-4611)], Panagiotis Koutsianitis[3(0000-0002-4252-6321)], Amalia Kasampali[3(0000-0001-5627-3831)], Maria Stavroulaki[3(0000-0003-0882-5763)], Georgios Stavroulakis[3(0000-0001-9199-2110)]

[1] University of Kwazulu-Natal, Durban, South Africa
[2] University of Central Lancashire, Preston, United Kingdom
[3] Technical University of Crete, Chania 73100, Greece

Abstract. In this article, a structural investigation of Venetian Neoria masonry monument is presented. A comprehensive study of the current conditions of the structure is conducted, adopting a combination of visual assessment and usage of different numerical techniques. Previous experimental research has revealed existing damage patterns in the form of cracks, that have been developed on the structure over the post construction years. Goal of the article is to highlight the different structural analysis techniques that can be used to provide a satisfactory prediction of the structural behaviour of the monument. The numerical tools which are used in the study, include usage of unilateral contact-friction interfaces integrated in limit analysis framework as well as developed within nonlinear finite element analysis. An initial effort is also presented, to simulate the propagation of existing cracks using the Extended Finite Element method (XFEM). In this framework, a parametric analysis is conducted to provide the sensitivity of the number of masonry blocks used in the arches of the structure, and the values of friction coefficient between the unilateral contact-friction interface. The study exploits the possibility of adopting the mentioned numerical tools, in order to provide an insight description of the existing damage pattern of the monument.

Keywords: Masonry Arch, XFEM, Limit Analysis, Unilateral Contact-friction, Damage identification.

1 Introduction

Masonry arches are among the oldest structural systems in the world. The technique of building masonry arches was first seen in the 2nd millennium BC in Mesopotamian brick architecture [1]. Arches develop their strength by transferring the applied load into compressive forces, in a thrust line along adjacent masonry blocks [3]. When the thrust line is found out of the section of the masonry blocks, opening of the interfaces between the blocks takes place which can result in a hinge collapse mechanism [11]. Furthermore, compressive failure is unlikely on masonry arch structures.

Several research efforts have been presented in the last years, focusing on the investigation of the structural response of masonry arches. Different techniques have

been developed, ranging from a quick estimation of the ultimate strength to a more refined or exact evaluation of the ultimate strength. In more sophisticated numerical models, details of damage like cracks can be observed. In [13], a finite element model with unilateral interfaces is developed to predict failure in Mnajdra megalithic monument. In [6], unilateral contact-friction laws were used to simulate potential failure of stone arch bridge due to various loads including settlement of supports and concentrated live load. A multi-scale model has been proposed in [7] adopting the extended finite element method to capture arbitrarily oriented cracks and localization phenomena in masonry structures. More efforts on numerical modelling of masonry structures using the finite element method can be found in [2], [4], [15].

In this article, three numerical analysis techniques are explored for the evaluation of the structural response of the Neoria structure. First, classical limit analysis is adopted to perform a parametric investigation, aiming in calibrating the following numerical models. The second technique relies on a 3-dimensional non-linear finite element model which incorporates unilateral contact-friction interfaces to provide the collapse mechanism and potential cracks. Finally, an initial effort is presented, towards the investigation of damage using a 3-dimensional non-linear XFEM model.

2 In-situ structural investigation

The Venetian Neoria structure is one of the masonry monuments that can be found at the Old Port of Chania in Greece. Results of the in-situ structural investigation, including material properties based on various experimental techniques as well as mapping of existing cracks and damages are given in references [5], [9].

These cracks may have developed due to ground movement, caused by the settlement of the supports, or earthquake activities. In subsequent pages they are called “transverse” cracks. In Fig. 1 some “longitudinal” cracks can also be identified, which appear in the north to south direction and highlighted by green rectangles.

The first arch on the west side of the structure is severely affected by cracks. These cracks may have been developed due to several openings on the west wall, as most of the transverse cracks lead to the area where the openings appeared in the past. The openings were later covered by walls, in an attempt to preserve the structure. The covered openings are highlighted in blue on Fig. 1.

3 Structural numerical models

3.1 Classical limit state analysis

A limit state analysis was carried out using LimitState:Ring [12]. Namely, a parametric analysis carried out to check the sensitivity of the ultimate load due to the estimated coefficient of friction between the masonry stones and the number of masonry stones that make up one arch. Table 1 show the geometrical parameters of the arch on the west side which was used for the analysis, since it is the most damaged and it is expected that it will provide a better sense of the condition of the structure.

Table 1. Geometrical parameters of the damaged arch (west arch).

Shape of intrados	Span (m)	Rise at mid Span (m)	Thickness (mm)	Total Width (m)	Number of units
Segmental	9.39	4.695	727	5.0	20

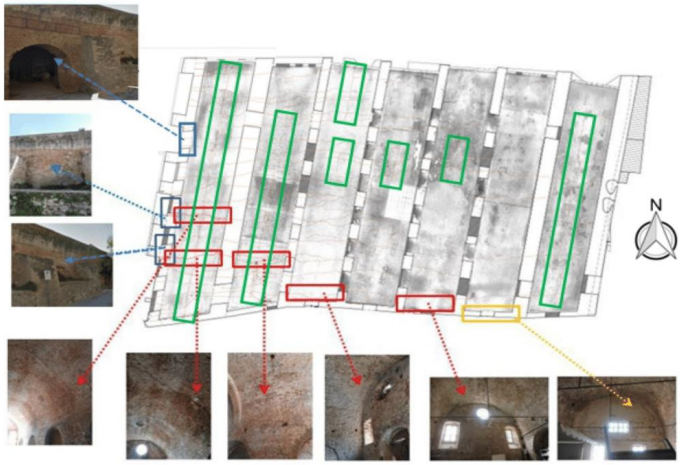

Fig. 1. Repairs and damages recorded from the in-situ investigation [5].

For the parametric analysis models, a 1 kN load was applied across the span of the arch at 150mm intervals to identify the critical failure load of the arch and the position it is obtained. The results from the parametric analysis are shown in Figs. 2 - 4.

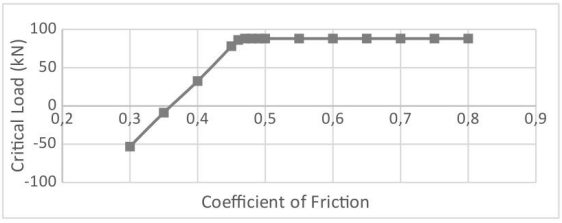

Fig. 1. Parametric analysis showing the critical load vs the coefficient of friction between the masonry blocks.

From the parametric analysis, it can be observed that failure load increases, until coefficient of friction reaches the value 0.47. The critical load observed is 87.9 kN when the number of segments is set to 10. From previous studies, it has been shown that the assumed coefficient of friction between the masonry blocks tends to give the upper bound of the critical failure load if not coincide with the exact value of failure[10]. Therefore, for the rest of the models, a 0.5 coefficient of friction has been adopted.

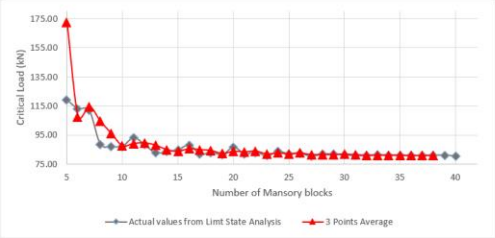

Fig. 1. Parametric analysis showing the critical load vs the number of masonry blocks

Fig. 1. The limit state failure mechanism of the first arch

In the next step, the number of masonry blocks that make up the ring were investigated to determine the point at which the number of blocks has no significant effect on the failure load. It can be noted from Fig. 3, that the critical load decreases with the increase in the number of blocks until 10 blocks, whereby the critical load shows a lot of noise. However, when the average of the corresponding critical load from 3 consecutive blocks is plotted, the noise in the critical load becomes insignificant after 20 blocks are used to make up the arch. Therefore, for the rest of the models, each arch is made up of 20 masonry blocks.

It is noted that the failure mechanism obtained from the parametric models, correlates to the longitudinal cracks that were observed on the first arch as mapped on Fig. 1. The mode of collapse is a four-hinge failure mechanism as shown in Fig. 4.

3.2 Finite element analysis

For the finite element analysis, a simplified 3-dimensional non-linear finite element model is developed in Abaqus [14]. It is noted that comparing to limit analysis, the finite element models can provide more details such as the principal stresses, forces and displacements which can be translated to force-displacement diagrams.

The geometry shown in table 1 was used to create the numerical models. The longitudinal support provided by masonry walls were also included in the models. The width of the structure is reduced to 3.5 m to simplify the analysis. The width of the structure was chosen in such a way that it is not less than the effective width to ensure that the width is not a limiting factor to the structural behavior. The effective width is a function of the contact load area and how the load is redistributed in the arch as defined by equation 1.

$$\underset{width}{effective} = \underset{or\ load\ contact\ area}{specified\ axle} + \underset{the\ loaded\ axle\ or\ contact\ area}{amount\ of\ load\ spread\ at} + \underset{distribution\ within\ the\ arch}{extra\ distance\ to\ account\ for} \quad (1)$$

The finite element models developed in this paper are solved using the Newton-Raphson incremental-iterative procedure to deal with the nonlinear nature of the problem. The nonlinearity is due to the opening-closure and sticking-slipping along the masonry stone interfaces. The models were developed with a fixed support and the self-weight was incorporated in the loading condition. Two steps were used to create the models: the first step was a pure gravity load to simulate the state of inertia of the structure and to stabilize the model. The second step has an increased gravity load by 0,5g which was incrementally applied on the structure. The results from these models are shown in Figs. 5 to 7.

The failure mechanism presented are shown in Figs. 5 - 7 correlate with the longitudinal cracks observed on the structure in-situ and the damage pattern is similar to the one observed in the limit state analysis. Also, the model with one arch has a similar failure pattern with the full structure of 7 arches, even though the failure pattern is exaggerated on the one arch model. The hinge circled in yellow in Fig. 5 (model with one arch) and Fig. 7 (full structure) shows an outwards opening, respectively. For the model with the full structure, there is an influence of the adjacent arch to the first arch, which acts as a probe which prevents/minimize the lateral movement of the arch. This tends to minimize the overall displacement of the structure making it more stable.

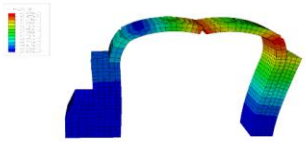

Fig. 1. The failure mechanism of the first arch under finite element analysis.

Fig. 1. The displacement contour of the whole structure under finite element analysis.

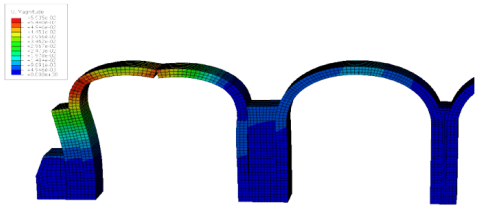

Fig. 1. A close-up view of the failure mechanism of the first arch in whole structure analysis under finite element analysis.

After the first group of models with increased gravity of 0.5g were analysed, it was noticed that the longitudinal cracks/opening only developed on the first (west) arch while on situ, also mapped on Fig. 1, longitudinal cracks are also visible in spans 2 and 7. In an attempt to understand the cause of the longitudinal cracks, more load cases were investigated:

- (a) Lateral movement of abutment due to a horizontal point load
- (b) A vertical displacement of supports.

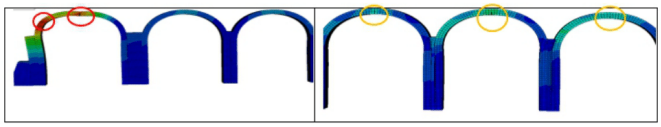

Fig. 1. (a) Deformation shape of first (west) span after a 100 kN horizontal point load has been applied on the right hand-side abutment, (b) Deformation shape of fourth, fifth and sixth spans after a 100 kN horizontal point load has been applied on the right hand-side abutment.

Fig. 8 shows the deformation of the structure after a 100 kN horizontal point load has been applied on the right hand-side abutment. As shown on Fig. 8, multiple hinges (circled in red) are observed on the first span which correlates to the experienced

damage. The yellow circles show small hinge opening on fourth, fifth and sixth spans. When the horizontal force is applied to the left hand-side abutment, no correlation to the experienced damage arises.

Fig. 1. Deformation shape of the structure after 100 mm vertical settlement of supports 2 and 8.

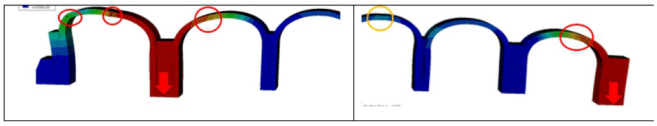

Fig. 1. (a) Deformation shape of 1st and 2nd span after 100 mm vertical settlement of supports 2, 8, (b) Deformation shape of 5th and 7th span after 100 mm vertical settlement of support 1, 8.

Figs. 9-10 show the deformation of the structure after imposing a 100 mm vertical (downwards) settlement of supports 2 and 8, as indicated by the red arrows. This movement of supports may be due to poor ground conditions. Fig. 10 highlights in red circles the hinge openings which might have resulted in the real cracks obtained in situ, as there is a high correlation of the positions of the cracks observed in the numerical model (Fig. 10) and in the real conditions (Fig. 1). The hinge opening on the fifth span (highlighted in yellow) is quite small, similar to the real image. It can be concluded that the longitudinal cracks are most likely to be caused by a vertical displacement of supports 2 and 8.

3.3 Analysis within the extended finite element method

The extended finite element method (XFEM) is an extension of the conventional finite element analysis. It allows for cracks to be modelled independently of the mesh, permitting the propagation of the crack along an arbitrary, solution-based path [8]. The main concept of this method is to use the partition of unity property and properly enrich the nodal displacement approximation. The enrichment is implemented using appropriate enrichment functions, as provided by relation (2).

Within the XFEM method, a domain containing a discontinuity, is considered. This may involve a discontinuous displacement (strong discontinuity) or a discontinuous displacement gradient (weak discontinuity). A strong discontinuity can be used in numerical modelling to represent a crack, developed in a structure.

For a 2-dimensional geometry, a strong discontinuity is depicted by a line located in the finite element mesh. According to the core concept of the XFEM method, the nodes of the elements which are cut by the discontinuity are enriched, using appropri-

ate functions. These enrichment functions are used for the nodes of split elements (thus, elements which are cut by the discontinuity) and for the nodes of tip elements (elements which contain the crack tip). For the enrichment of the split elements, the Heaviside function H is used as given in relation (2). For the tip elements, the branch functions F are introduced.

$$u=\sum_{I=1}^{N} N_I(x)\left[u_I+H(x)a_I+\sum_{a=1}^{4} F_a(x)b_I^a\right] \quad (2)$$

For the structure which is investigated in this article, an XFEM model is developed in Abaqus [14] to capture the transverse cracks. A simplified 3-dimensional geometry of the full structure is considered, similar to the full structure in the traditional FEA. A maximum principal stress (Maxps) is adopted to define the traction-separation law which is used to determine the response of the discontinuities. Crack propagation takes place when the stress in the domain of the crack tip reaches this maximum principal stress. Values of The Maxps for different elements of the structure are shown on table 2. For all the cases, the displacement at failure was considered to be equal to 0.001 m. In this study, the initial cracks were inserted on the first, second, third and seventh spans of the structure as observed on situ. For the mechanical conditions, a 100 mm vertical displacement of the second and eight support was applied together with a 100 kN horizontal force on the left abutment as shown on Fig. 11. The result from this model is shown in Figs. 12 - 15.

Fig. 1. Deformation shape of the structure after a 100 kN horizontal point load has been applied on the further left hand-side abutment together with a 100 mm vertical displacement on the 100 mm vertical displacement of the second and eight support.

Table 1. Maximum principal stress (Maxps) used for XFEM model.

Material	Location	Maxps (MPa)
M1	Domes with semi - carved stones, strong mortar and an average thickness of 0.80 cm	0.774
M2	Arches ending in the north with carved stones and strong mortar (thickness 0.60-0.65 cm)	1.116
M3	Longitudinal masonry 1.20 -1.90 m thick with carved stones in the outer layers and strong mortar	0.2016
M4	Longitudinal masonry 2.80 - 3.30 m thick with stones in the outer layers and strong mortar	0.136
M5	Neoria dome 6 with operation with shotcrete and hooks of shape p.	-

Fig. 12 shows the initial position of the transverse cracks which are introduced on the model. According to the results of this investigation, the longitudinal cracks which were observed on the conventional finite element analysis with similar load conditions, are also observed under the extended finite element model. Further investigation needs to be conducted, in order to provide more details for the interaction between longitudinal and transverse cracks and the influence of their interaction on the structural response.

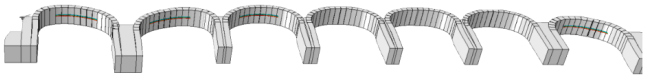

Fig. 1. Transverse cracks on the different spans of the structure.

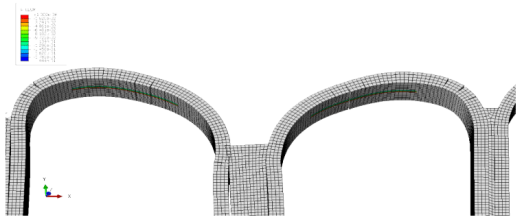

Fig. 1. Close-up cracks on the first span and second span after the analysis.

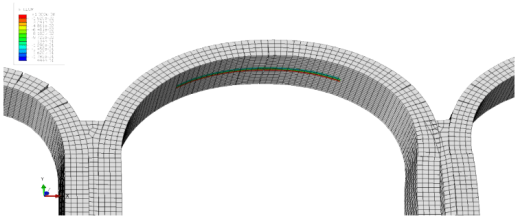

Fig. 1. Close-up crack on the third span of the structure after the analysis.

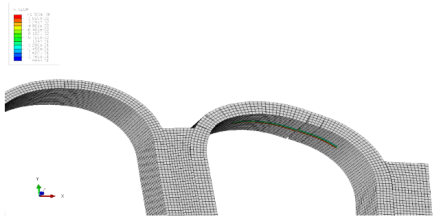

Fig. 1. Close-up crack on the seventh Span on the structure after the analysis.

4 Conclusion

Three numerical approaches are used in this article, for the structural evaluation of an ancient masonry structure consisting of arches. First, limit analysis is adopted and parametric investigations are conducted, providing necessary information for the subsequent finite element analysis. This investigation focuses on appropriate values of the friction coefficient and on the number of blocks which are considered to simulate the arch. A 3-dimensional non-linear finite element model is also developed, using unilateral contact-friction interfaces, to simulate the contact condition and potential damage between the stones of the arches. Finally, the XFEM method is adopted to provide a further insight of the structural response, by considering transverse discontinuities.

The developed models can represent the existing failure pattern. Results of the investigation indicate that vertical settlement in some of the supports may have caused the existing damage pattern of the structure. The concurrent consideration of transverse cracks by using the XFEM method and longitudinal cracks by using unilateral contact-friction interfaces has been tested and it needs to be further investigated. More work is needed, towards a further insight on crack propagation and reinforcement suggestions for the monument.

References

1. Anastasio, S.: Building between the two rivers: an introduction to the building archaeology of ancient Mesopotamia. Building between the Two Rivers, 1-220 (2020).
2. Betti, M., Galano, L., Vignoli, A.: Finite element modelling for seismic assessment of historic masonry buildings. Earthquakes and their impact on society. Springer (2016).
3. Chilton, J. C., Isler, H.: Heinz Isler: the engineer's contribution to contemporary architecture, Telford (2020).
4. Conde, B., Drosopoulos, G., Stavroulakis, G., Riveiro, B., Stavroulaki, M.: Inverse analysis of masonry arch bridges for damaged condition investigation: Application on Kakodiki bridge. Engineering Structures, 127, 388-401 (2016).

5. Charalambidi, B., Motsa, S., Drosopoulos, G., Koutsianitis, P., Kassampali, A., Stavroulaki, M., Stavroulakis, G.: Structural investigation of the Neoria Monument in Chania. 2nd International Conference TMM-CH (2021).
6. Drosopoulos, G., Stavroulakis, G., Massalas, C.: Influence of the geometry and the abutments movement on the collapse of stone arch bridges. Construction and Building Materials, 22, 200-210 (2008).
7. Drosopoulos, G. A., Stavroulakis, G. E.: A computational homogenization approach for the study of localization of masonry structures using the XFEM. Archive of Applied Mechanics, 88, 2135-2152 (2018).
8. Du, Z.-Z.: eXtended Finite Element Method (XFEM) in Abaqus. Simulia: Johnston, RI, USA (2019).
9. Editorial, V. C.: Venetian Neoria, https://visitchania.gr/en/places-to-visit/venetian-neoria, last accessed 2021/07/06.
10. Gilbert, M., Melbourne, C.: Rigid-block analysis of masonry structures. Structural engineer, 72 (1994).
11. Heyman, J.: The Mansonry Arch, England, Ellis Horwood Limted (1982).
12. Limitstate:Ring.: https://www.limitstate.com/ring, last accessed 2021/07/07.
13. Motsa, S. M., Drosopoulos, G. A., Stavroulaki, M. E., Maravelakis, E., Borg, R. P., Galea, P., D'amico, S., Stavroulakis, G. E.: Structural investigation of Mnajdra megalithic monument in Malta. Journal of Cultural Heritage, 41, 96-105 (2020).
14. Simulia, D. S.: Abaqus 6.13 User's manual. Dassault Systems, Providence, RI, 305, 306 (2013).
15. Stavroulaki, M. E., Drosopoulos, G. A., Tavlopoulou, E., Skoutelis, N., Stavroulakis, G. E.: Investigation of the structural behaviour of a masonry castle by considering the actual damage. International Journal of Masonry Research and Innovation, 3, 1-33 (2018).